MYOCARDIAL ENERGY UTILISATION IN RELATION TO CANINE CIRCULATORY CONTROL, STUDIED BY MULTIVARIATE ANALYSIS AND COMPUTER SIMULATION

A thesis submitted for the Degree of

Doctor of Philosophy

in the University of London

by

Bruce Smaill

June 1975

Engineering in Medicine Laboratory
Department of Electrical Engineering
Imperial College of Science and Technology
London, S.W.7

ABSTRACT

A systems analysis approach was applied to the study of cardiac function. The pumping capacity of the heart is determined by four important parameters: end-diastolic volume, hydraulic input impedance, contractile state and heart rate; thus an imposed circulatory load can be met in many different ways. If the relative "costs" of these different responses are not the same, conditions for possible optimization may exist. The applicability of an optimization approach was investigated first by a simple model study and then with a series of physiological experiments.

The aim of the experiments was to obtain a rigorous multi-variate characterization of several indices of cardiac performance and nonlinear regression surfaces were used to describe these indices as functions of heart rate and mean arterial pressure. It was found that for a fixed left ventricular output and mean arterial pressure myocardial oxygen consumption did not monotonically decrease with reduced heart rate, but exhibited a shallow minimum. From the results it was inferred that at rest or in moderate exercise the naturally occurring heart rate is consistent with efficient hydraulic energy transfer and a favourable myocardial oxygen consumption. It was also shown that, under normal conditions, the balance of myocardial oxygen supply and demand is made worse by increasing heart rate or reducing mean arterial pressure. The way in which underlying factors determine these relationships is discussed. Changes due to variations in contractile state were also considered.

To investigate whether the regional balance of myocardial oxygen supply

and demand is adequately reflected by the balance for the left ventricle as a whole, a realistic structural and geometrical model was set up for the analysis of left ventricular stresses. This included variable fibre orientation and fibre anisotropy, together with nonlinear and nonhomogenous elastic properties. It was found that mean stresses could be estimated using simple expressions. However, the regional distribution of stresses was strongly influenced by structural properties, with maximum circumferential and fibre stress located between the subendocardium and midwall.

The significance of these experimental and theoretical results is discussed and possible clinical applications are considered. It was concluded that optimization was relevant to studies of cardiac function and that further investigation along these lines would be warranted.

INDEX

ACKNOWLEDGMENTS

A joint grant from the New Zealand University Grants Committee and the New Zealand Medical Research Council enabled me to study at Imperial College and I am grateful for their generous support.

I wish to thank my supervisor Professor B. McA. Sayers for the advice and guidance which he has given me throughout this project.

I have also received considerable help and co-operation from the staff of the Engineering in Medicine Laboratory and from others who have been associated with the Laboratory. My thanks are due to Dick Kitney who introduced me to the concept of optimal control with respect to biological systems. During the early stages of this project I collaborated with Dr. C. Borst, Jan Swammerdam Instituut, Amsterdam. I am particularly grateful to Kees for communicating to me some of his enthusiasm for the subject of physiology and for his continued interest in this work. Dr. R. S. Clist and Dr. D. T. Stagg are also acknowledged both for their advice on the processing of experimental data and for their contribution of computer programs. I would like to thank Dr. D. M. Munro for the use of his program ADC. My thanks go to Bill Cutler also, for his technical assistance.

The experimental work was performed in collaboration with Dr. J. H. Chamberlain and the results presented here could not have been obtained without his personal commitment. I would also like to thank Rick Challis for his advice and for his contributions to these experiments. The assistance of Julie Lloyd, Heather Milburn and Phillip Swan is gratefully acknowledged.

This thesis was typed by Valerie Collins and the diagrams and equations were prepared by Janet Edwards. I wish to thank them both for their care and effort.

Finally, my sincere thanks are due to my wife, Barbara, for her generosity and companionship throughout the preparation of this thesis.

1. INTRODUCTION

1. INTRODUCTION

The optimization of a multi-variate system with respect to some index of cost or efficiency is now an established concept widely used in the synthesis of technological control systems. It may also be relevant to certain biological systems. Cardiac function, for instance, depends on several different factors and the heart can meet an imposed circulatory load in a variety of ways. It is unlikely that the relative "costs "of these different responses will be the same and thus conditions for possible optimization may exist.

Like most biological organisms the cardiovascular system has a multi-level or hierarchical structure. Such organization reflects the existence of integrated and characteristic responses to system requirements and it can be argued from the law of natural selection that these responses will be optimal in the sense that they maximize the probability of survival. Optimal criteria involving the minimization of energy "costs" appear to operate at many levels in biological systems and this provides some insight into the mechanisms which control these systems. It is interesting, therefore, to consider if any such criteria govern normal cardiovascular responses.

The concepts of optimality and cardiac "cost" are also relevant to specific clinical problems. Myocardial ischaemia occurs when the supply of oxygen to a region of the ventricular wall is not sufficient to meet the demands of oxidative metabolism. If the regional balance of myocardial oxygen supply and demand is not restored, sources of anaerobic metabolism are rapidly exhausted and irreversible cell damage - myocardial infarction, takes place.

The normal heart never becomes ischaemic. A precise autoregulation mechanism matches coronary blood supply to myocardial oxygen demand and arterial oxygen content is almost completely extracted by the myocardium. Any increase in oxygen demand must therefore be satisfied entirely by increased coronary flow. The reserve capacity of the coronary circulation is such that extremely large demands for coronary flow can be met by peripheral vasodilation. However, if myocardial oxygen consumption is abnormally large, or coronary flow is obstructed, conditions may occur in which coronary peripheral vasodilation is maximal and supply no longer matches demand. The resultant myocardial ischaemia is generally associated with a characteristic precordial pain, which disappears with rest - angina pectoris.

The sudden occlusion of a coronary artery cuts off the blood supply to a region of the myocardium. Ischaemia and infarction follow rapidly. If the resultant loss of ventricular function is significant, the regions of ischaemia and myocardial infarction may be progressively extended until the heart fails completely and unless this process is reversed, or at least limited, it will result in death due to cardiogenic shock.

Angina pectoris and acute myocardial infarction must be distinguished; while acute myocardial infarction is associated with the failing heart, this is not, in general, true of angina. The aim of clinical intervention in both cases, however, must be to improve the regional balance of myocardial oxygen supply and demand. A number of haemodynamic and pharmocological stimuli are used for this purpose and their effect on the oxygen supply and demand balance is broadly understood. However, myocardial oxygen consumption and coronary flow reflect the interactions of a complex system. For this reason, it is difficult

to predict and accurately assess the results of such interventions.

While it is pointless to oversimplify clinical problems such as these, it appears that conditions for possible optimization may exist here. Indeed, current thought on the treatment of acute myocardial infarction; Braunwald and Maroko (1974), emphasizes the need to improve the balance of myocardial oxygen supply and demand, while taking note of the multi-factorial nature of this problem. To date, however, no formal systems approach has emerged.

We have considered aspects of both normal and pathological cardiac function. It is quite possible that concepts of optimality which might be relevant to the treatment of myocardial ischaemia may have no significance in normal cardiovascular responses. Any approach to the clinical problem, however, must be based on a thorough understanding of the factors which determine myocardial oxygen consumption and the regional balance of myocardial oxygen supply and demand. From this, it can be argued that rigorous multi-variate descriptions of these aspects of cardiac function should first be obtained for the normal case.

The basic premise of this discussion has been that the techniques of multi-variate systems analysis may provide a practical and quantitative approach to the problems outlined. In this study, we will consider the feasibility of such an approach.

2. A SYSTEMS ANALYSIS OF LEFT VENTRICULAR FUNCTION

2. A SYSTEMS ANALYSIS OF LEFT VENTRICULAR FUNCTION

2.1 INTRODUCTION

The possibility of applying multi-variate optimization theory to specific aspects of cardiac function has been considered. We will attempt here to set up a general systems framework on which such an approach might be based; left ventricular function only is considered.

Control theory and systems analysis have been extensively used in studies of the cardiovascular system. However, most of this work has been concentrated on the analysis of cardiovascular reflexes and control mechanisms using the techniques of classical control theory. The study by Scher and Young (1963) of the baroreceptor reflex and the control of arterial blood pressure is a typical example of the classical approach.

Recently, more sophisticated concepts of systems analysis have been applied. Sagawa (1967), Herndon and Sagawa (1969), have presented multi-variate analyses of cardiac pumping capacity. Multi-variate optimization theory has been successfully used in studies of respiratory function, but despite this few attempts have been made to characterize cardiac function in this way. Some simple conditions for the existence of an optimal balance of coronary flow and myocardial oxygen consumption were considered by Taylor (1964) and Borst (1972) presented a model study on the optimization of left ventricular performance in angina pectoris. What follows is an attempt to extend and develop this general optimal systems approach.

2.2 ASPECTS OF SYSTEMS ANALYSIS

The primary object of control theory and systems analysis is the improvement of system performance. A clear-cut definition of goal or goals is therefore central to the systems approach.

We have already used the terms multi-variate optimization, classical control theory and multi-level hierarchical system. It is essential that these and other terms commonly applied to biological systems should be clearly defined and understood before going any further.

OPTIMIZATION OF A MULTI-VARIATE SYSTEM

Consider a process the output of which depends on three independent variables. We can write

$$y = y(x_1, x_2, x_3) \qquad 2.2.1$$

where y is the dependent or output variable and x_1, x_2, x_3 are the independent or input variables.

Assume that the process conforms to the conditions

$$\begin{aligned} Y &= y \\ X_1 \leq x_1 &\leq X_2 \\ X_3 \leq x_2 &\leq X_4 \end{aligned} \qquad 2.2.2$$

A requirement imposed on the output variable is defined as a constraint, while limitations on the input variables are defined as restraints. In general, a constraint can be satisfied by a variety of combinations of the input variables

(subject to the restraints). The "cost" of each of these combinations of input variables may not, however, be the same. An obvious example is the case in which different economic costs are associated with each of the input parameters. A combination of independent variables which satisfied the constraint and minimized total economic cost would probably be considered optimal here.

We define a generalized performance index or cost function

$$p = p(x_1, x_2, x_3) \qquad 2.2.3$$

Using the constraint 2.2.2. it is possible to derive a modified version of the performance index.

$$p' = p'(x_1, x_2) \qquad 2.2.4$$

The optimal values of x_1 and x_2 can be obtained by minimizing the modified performance index using conventional numerical or analytical techniques. The corresponding value of x_3 can be obtained from 2.2.1.

In any optimal systems analysis, the essential steps are :

- process identification
- choice of performance index

Process identification involves the determination of the relationship between dependent and independent system variables. Identification of the independent variables is an obvious and necessary precondition here. Clearly, the choice of performance index is an essentially subjective exercise, since it depends on the relative weighting of sometimes dissimilar components of cost.

CONTROL THEORY AND SYSTEMS ANALYSIS

Historically, both control theory and systems analysis developed from the problem of controlling simple mechanical processes. In the classical closed loop system the controlled variable is sensed and negative feedback used to reduce the error between the actual and required values of this variable. Typically, the design goal here is to achieve a good dynamic response without the instability which is inherent in the closed loop configuration. In general, frequency domain analysis is used for this purpose and most simple linear control systems can be decomposed into the classical closed loop form.

With the extension of control theory to deal with more complex control problems new concepts of performance became relevant and the development of optimal control is one application of these concepts. The theory of multi-variate optimization relates most directly to static or quasi-static systems. However, by introducing functions of time into the performance index it is possible to apply the concept of optimality to the control of dynamic processes.

Adaptive control represents a further refinement of optimal control theory. In a time-varying system the dynamic properties of the controlled process are sometimes radically altered by environmental disturbance and it may be necessary to change the performance index in order to reach a truly optimal state. An adaptive control system continuously re-evaluates its control strategy in order to approach optimal conditions of at all times.

The organization of most large systems falls naturally into a pyramidal chain of command. Such hierarchical systems are characterized by the existence of discrete levels of function and at each level control can be divided into

intrinsic and extrinsic components. The intrinsic components represent the regulation of local function, while the extrinsic components represent the intervention in these local control processes by higher levels of function. This structure is repeated at every level in the hierarchy and while no level has direct control over all others the degree of influence on the over-all system increases with hierarchical rank.

In Fig. 2.1 we present an example of the hierarchical organization typical of most biological control systems. It appears that such organization leads to an efficient and stable co-ordination of competing levels of function and, in general, hierarchical systems combine elements of classical, optimal and adaptive control. While hierarchical systems theory provides a useful conceptual framework, the quantitative analysis or synthesis of such systems is extremely difficult.

2.3 ASPECTS OF LEFT VENTRICULAR FUNCTION

We have stated that a clear-cut definition of a goal or goals is central to the systems approach. For a multi-level hierarchical organization like the cardiovascular system, such a definition is not easily made. The circulation serves many different purposes: temperature regulation, the maintenance of tissue metabolism, the transfer of waste products etc; and each of these factors indirectly or directly influences cardiovascular function. Ideally, a systems description should include these different interactions. In practise, however, it is necessary to concentrate analysis on specific isolated subsystems.

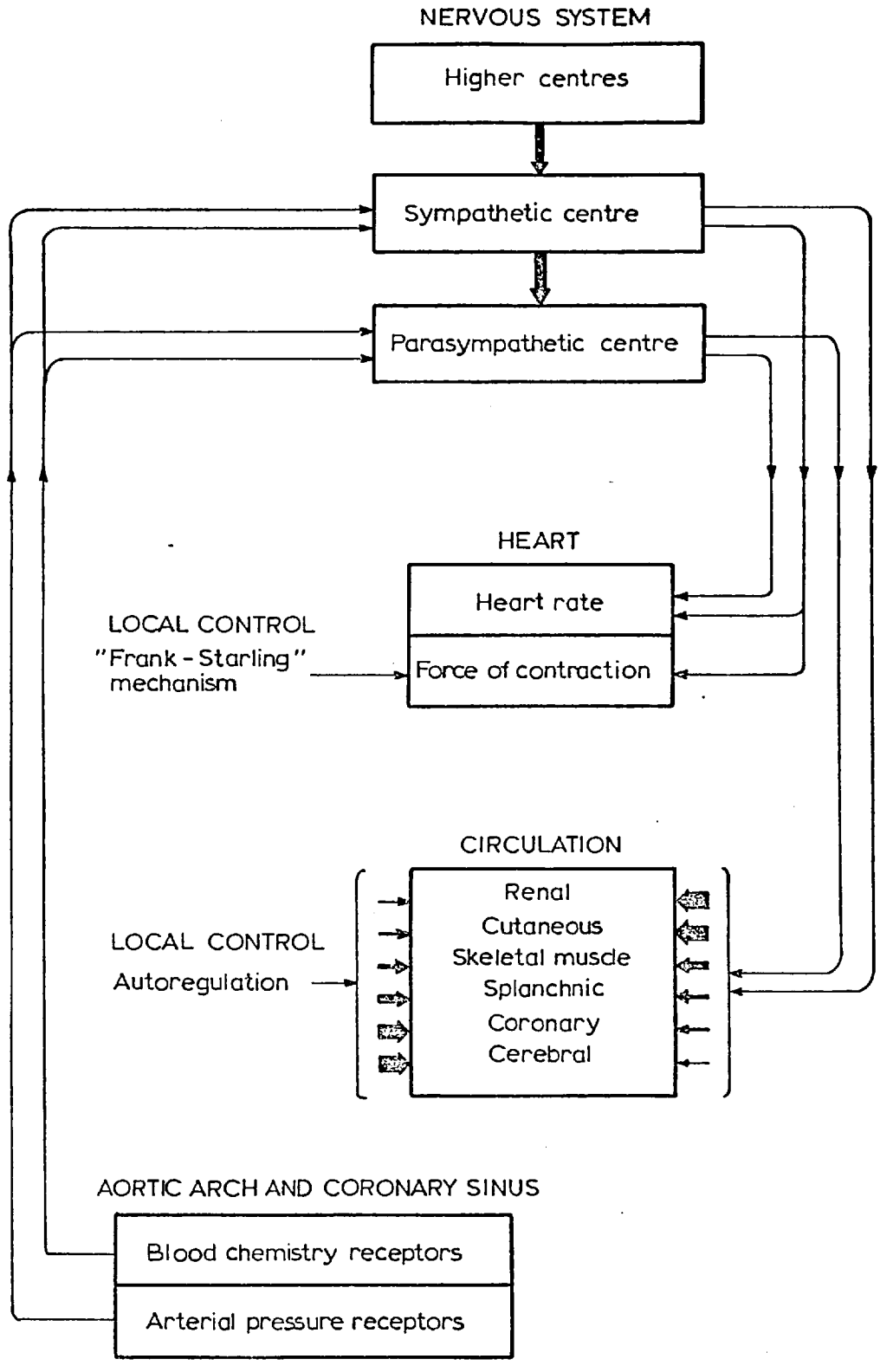

FIGURE 2.1: A simplified representation of the hierarchical control of the cardiovascular system.

This study is confined to static and quasi-static aspects of left ventricular function and at this level system goals are more readily defined. An attempt is made to analyse left ventricular performance using the methods of multivariate optimization theory; we recall that the essential steps in any such analysis are process identification and the choice of performance indices. System constraints and fundamental system variables are identified. From the discussion in the previous chapter it is clear that total myocardial energy utilisation and the balance of myocardial oxygen supply and demand are important indices of left ventricular performance and these are also considered in some depth.

THE HEART AS A PUMP

According to Burton (1972) there are four important phases in the cardiac cycle: isovolumic contraction, ejection, relaxation and filling. These mechanical events are represented in Fig. 2.2. With the onset of contraction, ventricular pressure rises until it excedes arterial pressure. The valves then open and blood is ejected forcefully into the aorta. Initially, ventricular pressure leads arterial pressure and this pressure gradient causes a rapid acceleration of flow. Peak flow occurs early in systole. The pressure gradient is reversed in the later stages of systole, but due to its momentum, blood continues to flow into the arterial system. With the change in the direction of flow, the valves shut and relaxation occurs followed by diastolic filling.

The aorta and the main arteries are distensible and during systole most of the blood ejected by the left ventricle is temporarily stored in the proximal circulation. Throughout the cardiac cycle, though, there is a continuous run-off

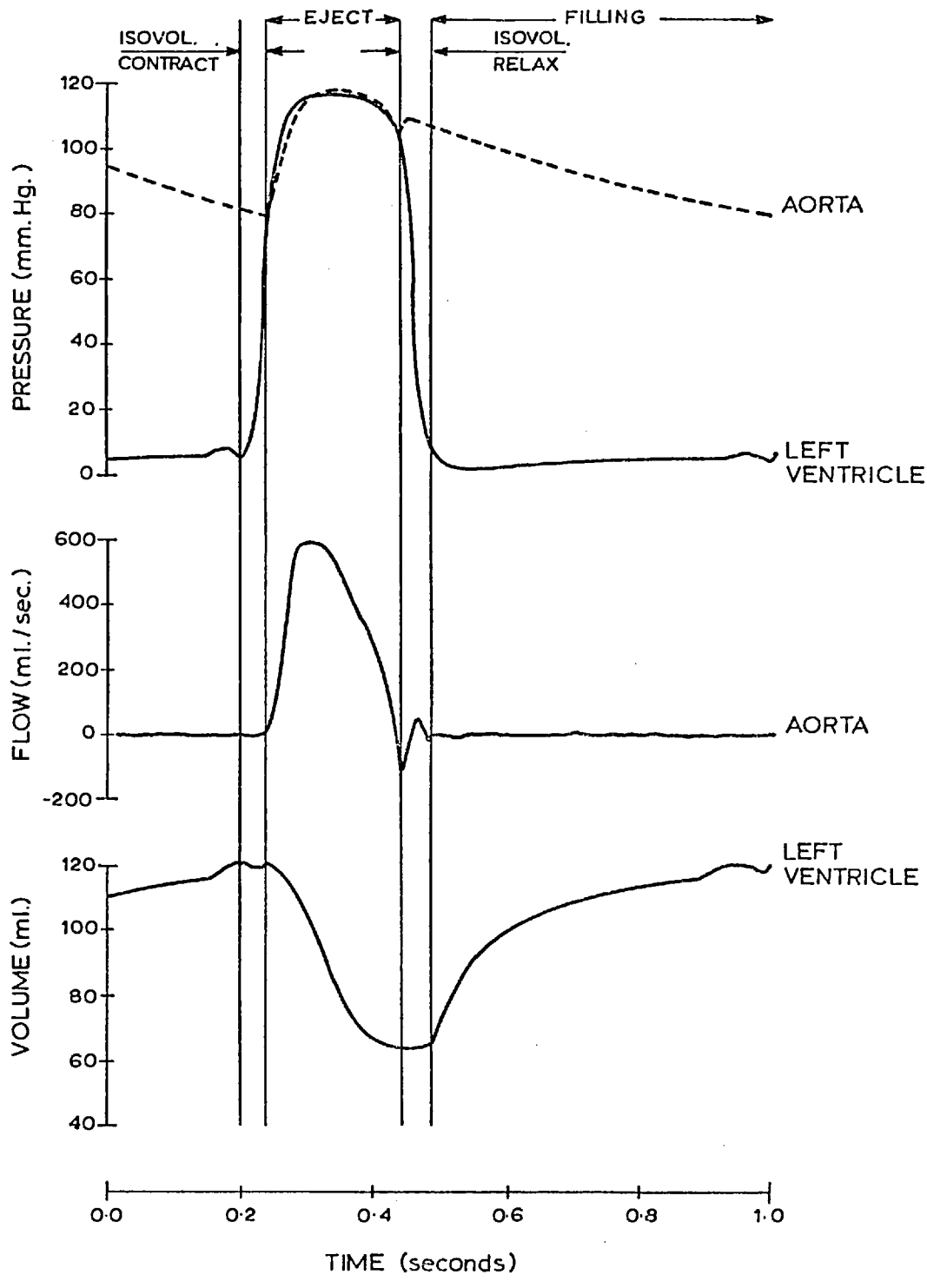

FIGURE. 2.2: Mechanical events of the cardiac cycle.

to the periphery and the variation of aortic pressure in diastole reflects this. The distensibility of the central arterial system, therefore, tends to smooth the pulsatile input flow. This decoupling of the left ventricle from the peripheral vascular load is sometimes called the Windkessel effect and it is crucial to the efficiency of cardiac pumping.

Cardiac output is given by the expression

$$CO = (V_D - V_S)\,HR = SV.HR \qquad 2.3.1$$

where V_D is end-diastolic volume, V_S is end-systolic volume, HR is heart rate and SV is stroke volume.

In any functional state, whether normal or pathological, there exists a minimum requirement for blood flow to the peripheral circulation. The generation of flow is therefore a fundamental constraint on the system.

It is also necessary to maintain an adequate hydraulic driving pressure, both to distribute blood flow to different peripheral vascular beds and to force this flow through the complex network of the micro-circulation. To maintain cerebral perfusion and to support the functional integrity of such rapidly metabolizing tissues as the heart or kidney, a mean pressure of at least 50mm Hg is required. The maintenance of arterial pressure is therefore considered to be a system restraint.

We have characterized the primary functional goal of the heart as the generation of flow. To complete the stage of process identification we must consider the parameters which determine left ventricular output.

THE CONTROL OF LEFT VENTRICULAR FUNCTION

One important determinant of left ventricular function is the direct relationship between ventricular end-diastolic volume or pressure and the force and speed of contraction. This is the Frank-Starling mechanism; if all other factors are held constant, increased volume loading will produce a greater stroke output. Left ventricular function is not, however, determined by this mechanism alone.

The duration of the isovolumic phase depends both on the rate of contraction and the arterial pressure at the onset of contraction. Throughout ejection, ventricular pressure, volume and flow are related in a way which reflects the instantaneous geometry of the ventricle and the dynamic properties of cardiac muscle. Further, during ejection the heart "sees" the hydraulic load presented by the circulation and this imposes an additional constraint on the relationship between pressure and flow.

Changes in the contractile state or inotropic level of the heart alter the force and speed of isovolumic contraction and the instantaneous pressure, volume, flow relationships during ejection. If all other factors are held constant, an increase in the inotropic level of the heart will increase stroke output, while a decrease will produce the opposite effect. Normally, a variation in contractile state is the result of sympathetic nerve activity and the associated release of noradrenaline. However, the frequency of contraction and a number of biochemical, humoral and pharmacological stimuli also influence inotropic level.

It is possible therefore to characterise cardiac function by the instantaneous values of pressure volume and flow throughout contraction. This trajectory is

uniquely determined by : (1) ventricular end-diastolic volume (2) arterial pressure at the onset of contraction (3) hydraulic input impedance (4) contractile state.

It is necessary to understand the influence of ventricular geometry on cardiac function. The left ventricle is a thick walled shell and thus the forces supported or developed by muscle fibres are related not just to ventricular pressure, but also to the spatial co-ordinates of the myocardium. To determine these forces we require a complex transformation based on an exact knowledge of ventricular geometry and myocardial structure. At a very simple level, however, it can be shown that ventricular transmural stresses are directly related to ventricular pressure and volume. Similarly, muscle fibre length can be associated with ventricular volume. If this analogy is extended it is possible to obtain some feeling for the way in which muscle properties determine cardiac function. Clearly, the Frank-Starling mechanism corresponds to the isometric "length-tension" behavior of isolated cardiac muscle.

In this study, we have adopted a quasi-static approach. If ventricular output is fixed and steady conditions are assumed, the arterial pressure at the onset of contraction cannot be treated as an independent parameter. Therefore the fundamental system variables are :

- end-diastolic volume
- hydraulic input impedance
- contractile state
- heart rate

MYOCARDIAL OXYGEN CONSUMPTION

The heart uses energy released by the degradation of substrates trapped in the phosphate bond of ATP. Under normal conditions this process is entirely oxidative and therefore myocardial oxygen consumption ($M\dot{V}O_2$) is a direct measure of total cardiac energy utilisation.

Cardiac energetics and myocardial oxygen utilisation have been the subject of intensive study and it is generally accepted that $M\dot{V}O_2$ is dependent on three main factors : transmural stress development, contractile state and heart rate. A very large proportion of total $M\dot{V}O_2$ is utilised by the left ventricle and, in general, most published data relates to the left ventricle alone. Much of what follows has been drawn from review articles by Sonnenblick et al (1968), Skelton and Sonnenblick (1974).

Hill (1911) showed that the energy requirements of skeletal muscle were a linear function of developed tensile force. A similar relationship is clearly reflected in the long established relationship between per beat myocardial oxygen consumption and peak systolic pressure. Using a canine isolated heart preparation Sarnoff et al (1958) found that $M\dot{V}O_2$ was well correlated with the product of heart rate and the integral of aortic pressure over the systolic interval. They defined this as the "tension-time index". However, we have stated that the forces developed by the left ventricle are not simply a function of pressure. If it is assumed that the left ventricle may be represented by a thin ellipsoid shell, the Laplace law gives an approximate relationship between ventricular pressure, volume and transmural stress. Although such assumptions are gross, indices based on simple estimates of peak developed wall stress correlate very well with

$M\dot{V}O_2$ - McDonald et al (1966). The importance of the time for which developed stress is maintained, however, is still uncertain.

In general, an increase in the contractile state of the heart leads to an increase in peak developed stress and a higher heart rate. This interaction makes it difficult to determine what component of the associated variation of $M\dot{V}O_2$ is due to the change in inotropic level alone. Careful analysis by Sonnenblick et al (1965), Graham et al (1968) has shown that a positive change in the inotropic level of the heart is associated with a significant increase in $M\dot{V}O_2$. At present the mechanism responsible for this increase in energy utilisation is not understood.

$M\dot{V}O_2$ is the product of per beat myocardial oxygen consumption and the number of contractions per minute. Any increase in heart rate must therefore tend to increase total myocardial oxygen consumption. Further, changes in the frequency of contraction also alter the contractile state of the heart, but Boerth et al (1969) have shown that the additional energy cost associated with the positive inotropic effect of increased heart rate is quite small.

Several other less important determinants of $M\dot{V}O_2$ should also be considered. Even in arrest a finite amount of energy is required to maintain the integrity of the tissues and this is known as basal or resting metabolism. Further energy is required to initiate contraction even when no pressure is generated. The magnitude of basal metabolism is accurately known, quite small and not effected by external factors. Analysis of activation energy is incomplete, but it is generally assumed to be negligable. The energy cost of external work has been the subject of much inconclusive study. It is now widely accepted that most

energy is utilised in the development of stress and that only a small additional component depends on the external work done by the heart.

CORONARY BLOOD FLOW

Coronary blood flow is determined by aortic pressure and the impedance of the coronary vascular bed. For the left ventricle the transmural stresses developed in contraction radically alter the impedance presented to coronary flow and this accounts for the phasic variation of left coronary flow seen in Fig. 2. 3. The systolic contribution to total coronary flow is quite small. Further, the distribution of left ventricular stress is nonlinear and for this reason the regional distribution of coronary flow during systole is not uniform. Moir (1972) states that flow to the subendocardium ceases entirely in systole. For the normal heart this effect is compensated partly by increased vasodilation in diastole and partly by the higher capillary density in the subendocardial region. During diastole, coronary vascular impedance is controlled by autoregulation mechanisms alone.

The concept of coronary reserve relates to the capacity of the coronary circulation to increase blood flow in response to increased myocardial metabolism. Normally, the reserve capacity for coronary vasodilation is very large indeed. For the second case illustrated in Fig. 2. 3, though, an arterial obstruction has reduced the effective coronary perfusion pressure, leading to submaximal vasodilation even in the resting state. The circulation is unable to produce further dilation and systolic blood supply is minimal; coronary flow

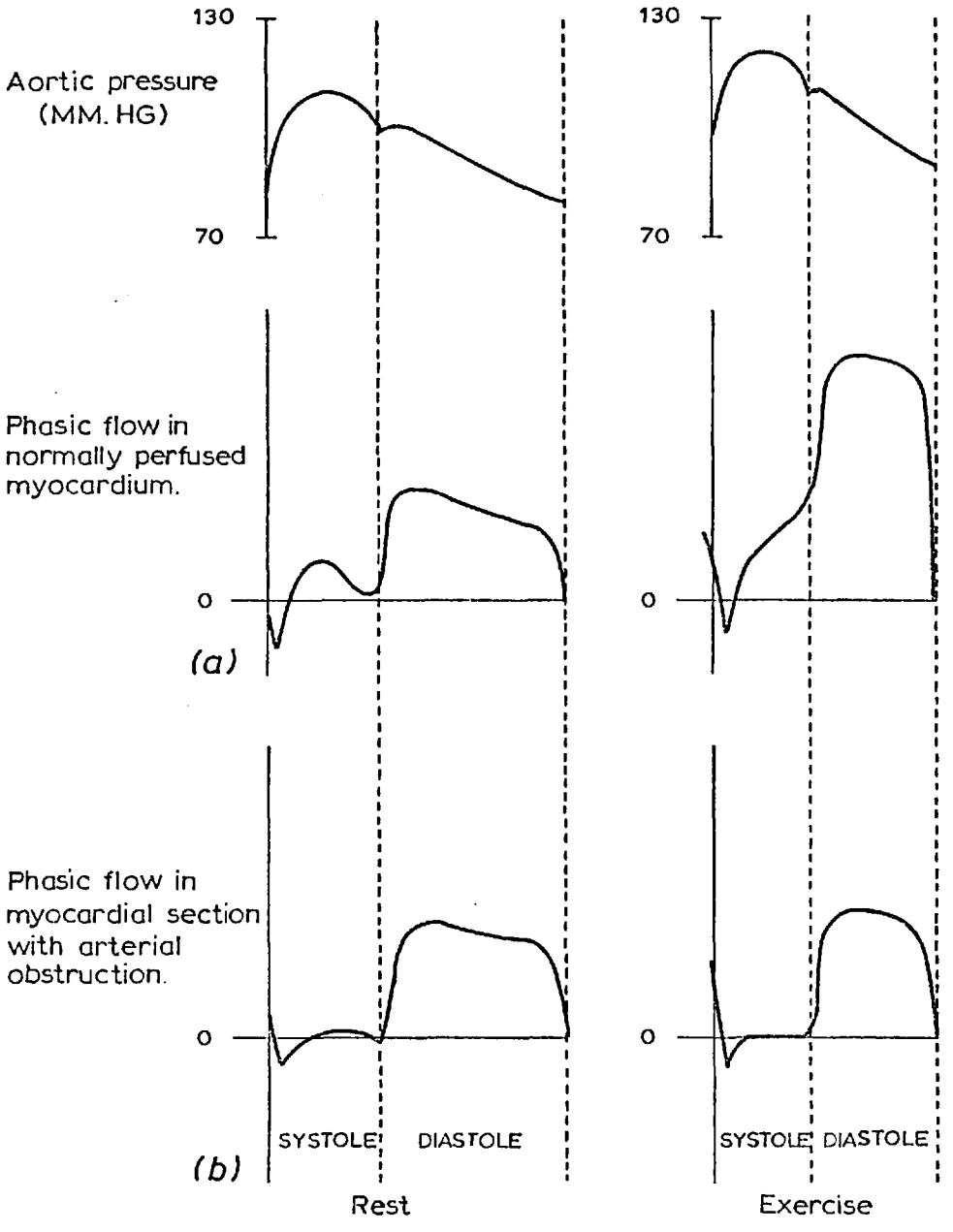

FIGURE 2.3: Representation of coronary flow under different haemodynamic conditions. *After Folkow and Neill (1971)*
(a) Normally perfused left ventricular myocardium
(b) Perfusion of myocardial section with arterial obstruction.

is therefore determined by diastolic pressure and the duration of diastole. Borst (1972) suggested that the integral of the aortic pressure waveform over the diastolic interval could be used as an index of the relative variation of maximal coronary flow (coronary reserve) under different haemodynamic conditions. Clearly, this index is particularly relevant to the ischaemic heart.

2.4 A SIMPLE OPTIMAL MODEL

In this section we consider some possible conditions for the optimization of left ventricular function and investigate the underlying factors which give rise to those conditions. The aims and approach used are very similar to those presented by Borst (1972) in a study of optimal left ventricular performance in angina pectoris. The reader is referred to this source. Common material is introduced here only when it is necessary to the sense of the outline or where there is a difference of emphasis.

APPROACH

A simple cardiovascular model is set up based on the assumptions:

- the left ventricle is a flow generator
- aortic input impedance is represented by a modified windkessel
- contractile state does not vary
- the left ventricle is a spherical shell

The generation of flow is characterised as the primary system constraint. From 2.3.1 it can be seen that there are an infinite number of combinations of heart rate and stroke volume which will satisfy a given flow constraint. In the previous section it was stated that left ventricular function is determined by four fundamental system parameters. We assume here that contractile state is fixed and this reduces to three the number of variables which must be considered. Further, due to the constraint on left ventricular output, only two of these variables can be truly independent and we choose heart rate and peripheral resistance as unconstrained parameters. Restraints are imposed on heart rate HR, stroke volume SV and mean arterial pressure MAP; these reflect normal physiological limitations on the system.

$$40 \leqslant HR \leqslant 180 \text{ (beats/min)}, \quad SV \leqslant 200 \text{ ml}, \quad 50 \text{ mm Hg} \leqslant MAP$$

Two indices of left ventricular performance or cost are considered: myocardial oxygen consumption ($M\dot{V}O_2$) and the balance of myocardial oxygen supply and demand. Maximal coronary flow and $M\dot{V}O_2$ are evaluated using established haemodynamic and derived indices. This work was intended as an orienting study and the approach is therefore intentionally simple.

HAEMODYNAMIC MODEL

The left ventricle is treated as a flow generator and an algorithm is set up to produce a flow waveform based on the characteristic physiological shape. For a given heart rate, the waveform is scaled to occupy the systolic interval

and the flow constraint is satisfied by adjusting the magnitude of peak flow. The characteristic triangular shape is retained under both these transformations.

According to Beneken (1965) the duration of ventricular systole T_{vs} is given by

$$T_{VS} = 0{\cdot}16 + 0{\cdot}20T \qquad 2.4.1$$

where T is the interbeat interval (seconds).

The duration of the phases of isovolumic contraction and relaxation are assumed to be $0.1.T_{vs}$ respectively and thus the systolic interval T_s is

$$T_S = 0{\cdot}8\,T_{VS} \qquad 2.4.2$$

This approximation is valid over the range $40 \leqslant HR \leqslant 180$ (beats/min)

The hydraulic load presented to the left ventricle is simulated by a modified windkessel; an electrical analogue for this model is given below.

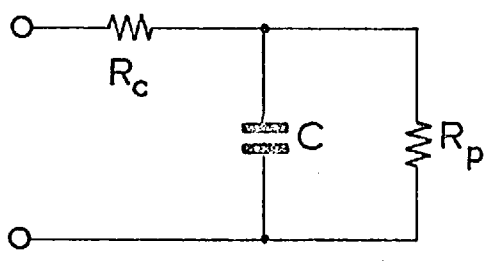

R_c = characteristic resistance

R_p = peripheral resistance

$C = 1/K$

K = elastic compliance

FIGURE 2.4: The modified windkessel

The elements R_c and C correspond to the characteristic resistance and the distensibility of the central arterial system, while R_p represents the peripheral vascular resistance. Despite its simplicity this model approximates the aortic

input impedance with reasonable accuracy; Elzinga and Westerhof (1973).

For the modified windkessel the relationship between pressure and flow at the input is given by

$$\frac{dP}{dt} + \alpha P = \beta F + R_c \frac{dF}{dt} \qquad 2.4.3$$

$$\text{where } \alpha = \frac{K}{R_p} \text{ and } \beta = \frac{K}{R_p}(R_p + R_c)$$

A fourth order Runge-Kutta method was used to obtain steady state solutions for 2.4.3. In Fig. 2.5 we present a typical input flow waveform and the pressure wave form which this generates. The parameters R_c and K were evaluated emperically using the approach given by Borst (1972).

EVALUATION OF PERFORMANCE INDICES

Detailed theoretical analyses of myocardial oxygen consumption are scarce. Burton (1957) presented the following expression for the energy cost of cardiac contraction.

$$E = a\int \tau dt + b\int PdV, \quad a > b \qquad 2.4.4$$

where τ is developed transmural tension, P is intra-ventricular pressure and V is intra-ventricular volume.

According to 2.4.4 then, myocardial energy utilisation is determined partly by the external work performed, but to a much greater extent by the magnitude of developed tension and the time for which this tension is maintained. The use

of developed force is more appropriate than tension here and to a reasonable approximation the force supported by a spherical shell is given by $F \hat{=} \pi P r^2$ where r is the internal radius. If some simple manipulations are performed on 2.4.4 we arrive at a composite expression for myocardial oxygen consumption ($M\dot{V}O_2$)

$$M\dot{V}O_2 = (a' \int_0^{T_{VS}} P_{LV} V^{2/3} dt + b' \int_0^{T} P_{LV} \dot{Q} dt) HR + c \qquad 2.4.5$$

where c is the basal metabolism; T is the interbeat interval, T_{VS} is the duration of ventricular systole P_{LV} is left ventricular pressure, V is left ventricular volume, $\dot{Q}$ is the aortic flow and HR is heart rate.

This expression appears to be reasonably plausible. It has been stated, however, that the relative energy costs of external work and the time for which developed force is maintained are still uncertain. For this reason we also evaluate several clinical (emperical) indices for $M\dot{V}O_2$; McDonald et al (1966), Sonnenblick et al (1968) etc. The "tension-time index"; Sarnoff et al (1958), is redefined here as the "pressure-time index".

We consider:

Force Time Index FTI $(\int_0^{T_{VS}} P_{LV} V^{2/3} dt) HR$ 2.4.6

Peak Developed Force PDF $(P_{LV} V^{2/3})_{MAX.} HR$ 2.4.7

Pressure Time Index PTI $\left(\int_0^{T_S} P_a \, dt'\right) HR$ 2.4.8

To estimate the variation of maximal coronary flow, we use the index proposed by Borst (1972)

Maximal Coronary Flow CBF $\left(\int_{T_S}^{T} P_a \, dt'\right) HR$ 2.4.9

In 2.4.8 and 2.4.9 the integral is evaluated over the systolic interval; T_S is the systolic interval and P_a is aortic pressure.

While expressions 2.4.8 and 2.4.9 can be evaluated from the simple haemodynamic model, 2.4.5, 2.4.6 and 2.4.7 can only be determined if the model is extended to include left ventricular pressure and ventricular volume. During systole, we assume that left ventricular and aortic pressures are identical, while the rate of change of left ventricular pressure in the phases of isovolumic contraction and relaxation is considered to be constant. A typical derived left ventricular pressure waveform is presented in Fig. 2.5.

The instantaneous volume can be obtained from

$$V = V_D - \int_0^t \dot{Q} \, dt \qquad 2.4.10$$

where V_D is the left ventricular end-diastolic volume.

It is still necessary, however, to find some method of evaluating V_D.

We assume that

$$V_D = dSV + V_o \qquad 2.4.11$$

the constants d and V_o are chosen to give realistic values for the ejection fraction and end-systolic volume.

RESULTS

The haemodynamic conditions simulated in this study correspond to rest and moderate exercise states for the adult human. For the results presented the compliance of the arterial system was assumed to be linear and unless otherwise stated myocardial oxygen consumption ($M\dot{V}O_2$) was evaluated using the composite expression 2.4.5. The proportionality constants a' and b' were determined from a typical value of $M\dot{V}O_2$ for a specified reference state; a complete list of parameter values is given in Table 2.1. This model was implemented on the IBM 1800 computer in the Engineering in Medicine Laboratory and the CDC 6400 and Cyber computers in the Imperial College Computing Centre.

In Fig. 2.7a we present $M\dot{V}O_2$ as a function of heart rate (HR) for three different simulated exercise states; in each case the value of the peripheral resistance R_P is adjusted to give a mean arterial pressure (MAP) of 100 m Hg. Consider first the result for a left ventricular output of 5.0 1/min. We note that there is a shallow minimum at the value HR= 60 beats/min and this reflects a trade-off between the different factors which determine $M\dot{V}O_2$. From Fig. 2.6 it can be seen that, for a fixed level of LV output and MAP, both peak systolic and mean systolic pressures increase as HR is decreased; this variation becomes more pronounced for higher values of LV output. Similarly, the magnitudes of end-diastolic volume, systolic interval and external work all become greater as HR is decreased. However, the reduction in the frequency of contraction tends to offset this increase in per beat energy cost.

We note also from Fig. 2.7a that as LV output is increased the location of the minimum $M\dot{V}O_2$ shifts to a higher value of HR. This is not simply the result of changes in volume loading. For the simulated exercise results, R_P was reduced as LV output was increased. In Fig. 2.7b R_p is reduced at a fixed level of output and it can be seen that, for this case also, the location for the minimum of $M\dot{V}O_2$ shifts to a higher value of HR. We conclude therefore that the shift in the $M\dot{V}O_2$ minima, for simulated exercise, is largely due to changes in the nature of the hydraulic input impedance.

It is also interesting to note from Fig 2.7a and Fig. 2.7b that doubling LV output at fixed levels of HR and MAP increases $M\dot{V}O_2$ by only about 25%, while an increase in MAP at fixed values of HR and LV output leads to an almost directly proportional increase in $M\dot{V}O_2$. This is the classical result; Sarnoff et al (1958).

Myocardial oxygen supply and demand functions are given in Fig. 2.7c. Clearly, the balance of myocardial oxygen supply is greatest for a lower HR than that for which $M\dot{V}O_2$ is minimized. This reflects the dominant influence of the diastolic interval as a determinant of maximal coronary flow; Borst (1972).

The simulated exercise results are most interesting since they suggest that the normal exercise response; an increased heart rate and a slightly increased stroke volume, is consistent with the optimization of cardiac energy costs. In the case where the balance of myocardial oxygen supply and demand is treated as the performance index, though, it appears that the normal exercise response is non-optimal. While there is some experimental support for the second finding

it is generally accepted, that for a fixed level of cardiac output and MAP, $M\dot{V}O_2$ decreases monotonically with heart rate. The apparent conflict here with the results of the present study must be resolved before we go any further.

We have stated that the $M\dot{V}O_2$ minima obtained from the model reflect the interaction of increased volume loading at low heart rates with the hydraulic load presented to the left ventricle. However, all controlled experimental analyses of $M\dot{V}O_2$ have been done at values of HR > 120 beats/min or have utilised a nonphysiological peripheral circulation. There is therefore no experimental data with which the results of the simulation can be directly compared. This does not, of course, prove the validity of these results and we must look critically at the assumptions on which the model is based.

From the analysis of left ventricular function presented in the previous section, it is clear that the instantaneous values of left ventricular pressure flow and volume are related in a complex fashion. The assumption that the left ventricle is a flow generator and the arbitrary way in which end-diastolic volume is estimated, therefore, represent quite gross simplifications. Further, the central arterial system is not linearly distensible. As pressure is increased beyond a given range arteries become progressively more rigid. We assessed the relative influence of these simplifications by varying the parameters d and V_o in expression 2.4.11 and by including a nonlinear compliance term. The results, for low heart rates particularly, were found to be altered in both cases. However, the errors introduced here are probably less significant than the uncertainties involved in estimating $M\dot{V}O_2$.

The left ventricle resembles an ellipsoid of revolution and the elastic properties of the myocardium are nonhomogenous, anisotropic and nonlinear. Our estimates of the transmural force developed by the left ventricle are obviously crude. Also, it can be seen from Fig. 2.7d that there is a considerable variation in the values of $M\dot{V}O_2$ predicted using different indices. For the index FTI, which includes the interval for which developed force is maintained, the predicted values for $M\dot{V}O_2$ at a fixed level of LV output and MAP exhibit a minimum with respect to HR. PDF, however, is based on the maximum value of developed force only and the values of $M\dot{V}O_2$ estimated in this case decrease almost linearly with HR.

We are forced to conclude therefore that while conditions for possible optimization have been shown to exist, no absolute significance can be attached to the detail of the results at this stage. Further, there is little point in increasing the sophistication of the present model unless it is based on a more detailed and accurate analysis of myocardial metabolism than is at present available.

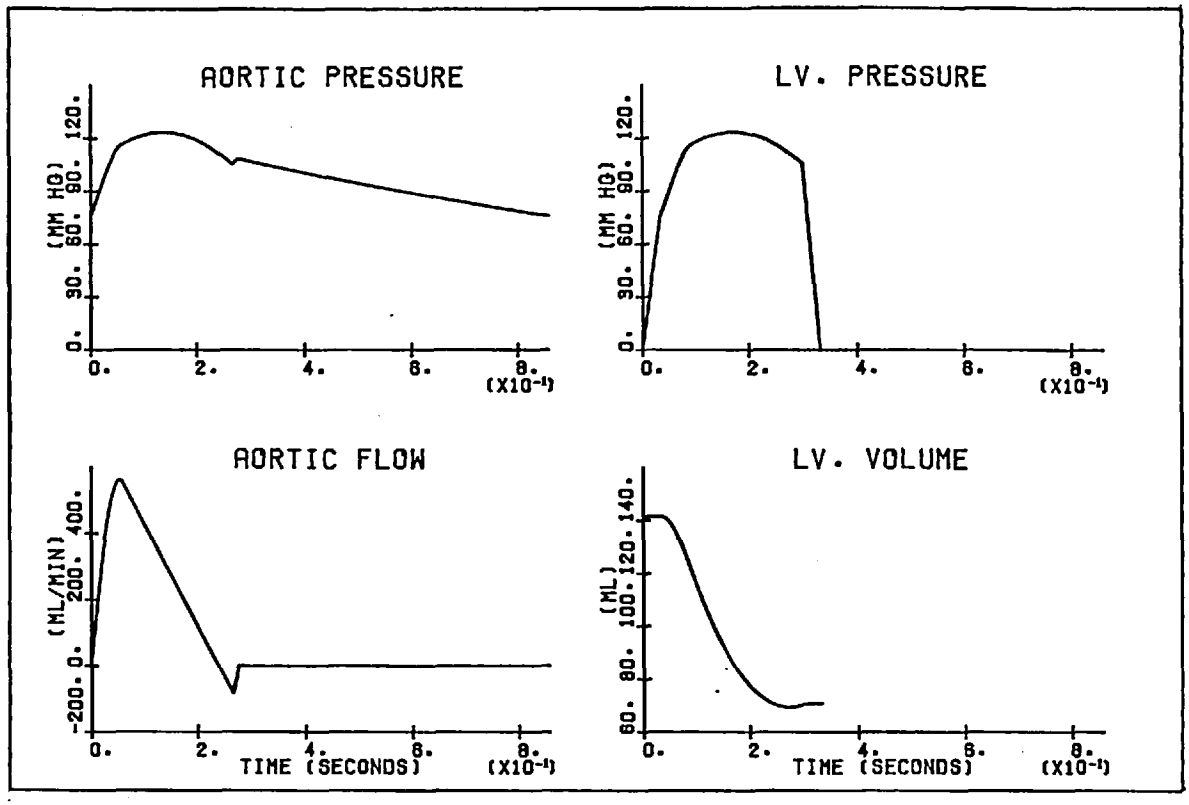

FIGURE 2.5: SIMULATED FLOW, PRESSURE AND VOLUME WAVEFORMS; CO 5.0 L/MIN, MAP 100 MM HG HR 70 BEATS/MIN

PARAMETER VALUES — TABLE 2.1

MODIFIED WINDKESSEL:	R_c	0.05 MM HG/ML/SEC,	K	0.7 MM HG/ML	
END-DIASTOLIC VOLUME:	D	1.1,	V_0	60 ML	
REFERENCE STATE:	CO	5.0 L/MIN,	MAP	100 MM HG,	HR 100 BEATS/MIN,
	MVO_2	8.5 ML O_2/MIN/100 G LV.			
METABOLISM:	A/B'	10.0,	c	1.5 ML O_2/MIN/100 G LV.	

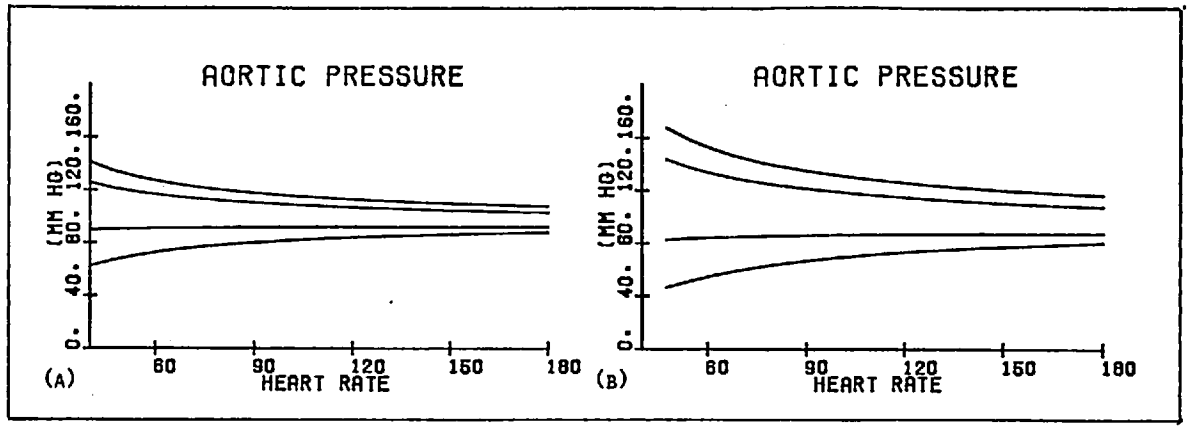

FIGURE 2.6: VARIATION OF AORTIC PRESSURE WITH HEART RATE; PEAK SYSTOLIC, MEAN SYSTOLIC, MEAN DIASTOLIC AND END-DIASTOLIC PRESSURES, RESPECTIVELY
(A) CO 5.0 L/MIN, MAP 100 MM HG (B) CO 10 L/MIN, MAP 100 MM HG

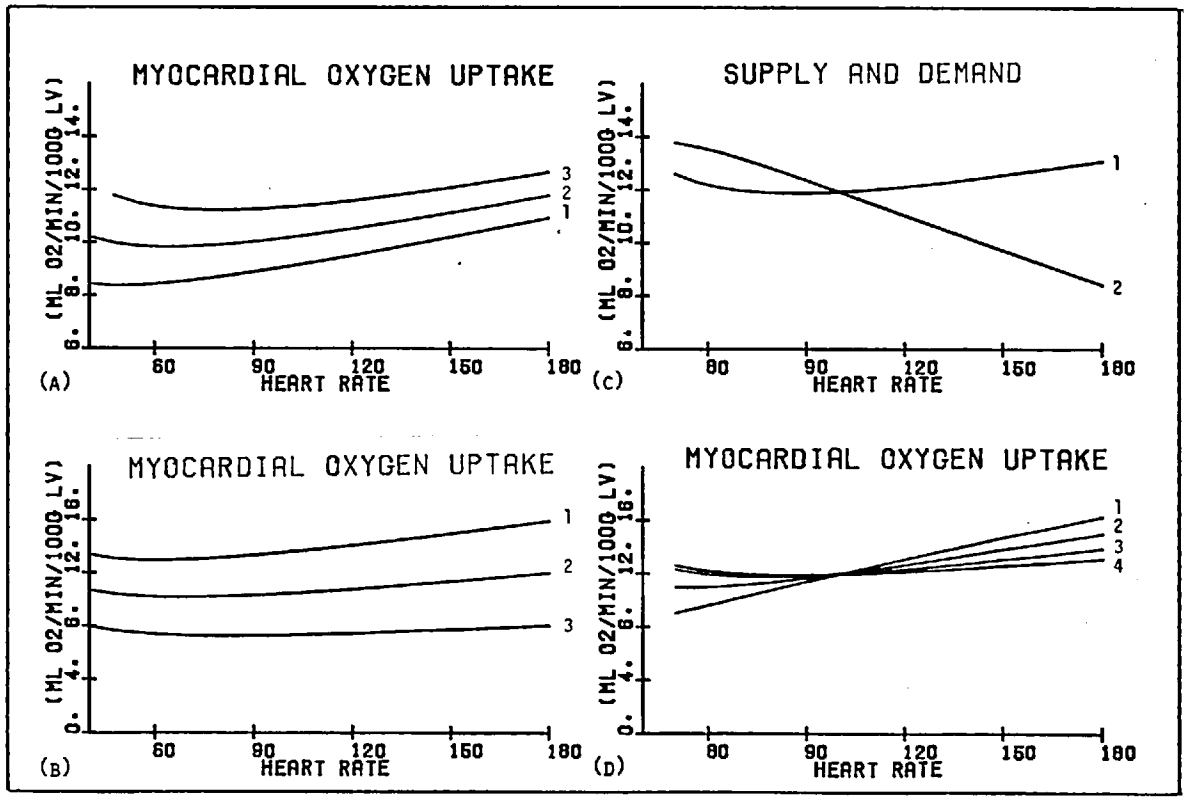

FIGURE 2.7: VARIATION OF MYOCARDIAL OXYGEN SUPPLY AND DEMAND WITH HEART RATE
(A) MAP 100 MM HG; 1. CO 5.0 L/MIN 2. CO 7.5 L/MIN 3. CO 10.0 L/MIN
(B) CO 7.5 L/MIN; 1. MAP 140 MM HG 2. MAP 100 MM HG 3. MAP 60 MM HG
(C) CO 10.0 L/MIN; 1. $M\dot{V}O_2$ 2. CBF
(D) CO 10.0 L/MIN; 1. PTI 2. PDF 3. FTI 4. $M\dot{V}O_2$

2.5 DISCUSSION

The aim of this study is to consider the feasibility of applying multi-variate optimization theory to specific aspects of cardiac function. In this chapter we have attempted to set up a general systems framework on which such an approach might be based.

The left ventricle is characterized as a multi-variate pump the output of which is determined by four fundamental system parameters: end-diastolic volume, hydraulic input impedance, contractile state and heart rate. We identify the generation of flow as the most important functional goal of the heart. Thus the flow requirements of the peripheral circulation are treated as the primary system constraint and the maintenance of arterial pressure is seen as important restraint on the system. Such an approach is common to other systems analyses of cardiac function - Sagawa (1967), Herndon and Sagawa (1969), Topham and Warner (1967). Cardiac energy utilisation and the balance of myocardial oxygen supply and demand are proposed as possible indices of performance or "cost".

Despite its simplicity, the model of left ventricular function based on this analysis serves several useful purposes. It clarifies the way in which the various determinants of myocardial "cost" interact and points to the existence of possible optimal conditions. The possibility that for a given cardiac output there may be a heart rate for which myocardial energy utilisation is minimized is of particular interest and should be considered in greater depth. However, analysis of the shortcomings of the model reveals problems in some areas of

more general interest.

To reliably apply the systems approach which has been proposed we require quantitative descriptions of both myocardial oxygen utilisation and coronary supply as functions of the fundamental parameters listed. Ideally, these descriptions should be obtained for a wide range of normal and pathological states. At present, however, such information is not directly available from the literature and experimental data relating to low heart rates and a normal peripheral circulation is particularly scarce.

For the left ventricle myocardial oxygen utilisation and coronary supply are closely related to the stresses developed throughout the cardiac cycle. The approximations of total ventricular transmural force used in the model were extremely simple and it is possible to obtain more accurate estimates of the force developed by muscle fibre in the ventricular wall. We have stated that the regional balance of oxygen supply and demand is a crucial index of left ventricular performance in myocardial ischaemia. Clearly, it is important to establish whether the oxygen supply and demand balance at points within the myocardium is accurately reflected by the balance of oxygen supply and demand for the ventricle as a whole. A realistic analysis of the left ventricular stress distribution could provide one approach to this problem.

In the work which now follows we try to answer some of the questions which have been raised here.

3. NOTES ON EXPERIMENTAL DESIGN

3. NOTES ON EXPERIMENTAL DESIGN

The aim of the experiments described in the chapters which follow was to establish whether the concepts of optimal cardiac function, already introduced, have any realistic practical basis. We wish to obtain rigorous multi-variate descriptions of those indices of left ventricular performance which relate to myocardial energy utilisation and the balance of myocardial oxygen supply and demand. Results for the lower range of heart rates, in the presence of a normal peripheral circulation, are of particular interest.

We begin with a brief critique of previous experimental work. Myocardial oxygen utilisation and more recently the balance of myocardial oxygen supply and demand have been the subject of intensive experimental study; in the preceding chapter we considered some empirical indices of myocardial oxygen consumption ($M\dot{V}O_2$) based on this analysis. It was shown, however, that detailed predictions on the balance of myocardial oxygen supply and demand cannot be made on the basis of simple indices alone. Neither is it possible to obtain much further information on this subject from the published results of the experimental studies. This is mainly due to the experimental and statistical approaches which have been adopted.

Much of the experimental work which has led to the resolution of the fundamental determinants of $M\dot{V}O_2$ has been based on the isovolumic left ventricular preparation or has utilised a nonphysiological peripheral circulation;

Sarnoff et al (1958), Graham et al (1968), etc. These results cannot, therefore, be directly related to the normal state. In those experiments which do relate more directly to the normal state; Rodbard et al (1964), McDonald et al (1966), etc., the limited number and restricted range of the measurements made in each experiment, the pooling of results from several experiments and the use of simple linear multi-variate statistics, preclude further more detailed analysis.

Before a more rigorous multi-variate experimental approach can be developed there are a number of practical constraints which must be taken into account. It has been stated that left ventricular function is determined by four basic factors: end-diastolic volume, hydraulic input impedance, contractile state and heart rate. To date, though, there exists no single quantitative index for contractile state and while aortic input impedance can be determined accurately, the way in which this information should be included in the analysis is not immediately obvious.

The proposed approach is based on the bi-variate analysis of experimental data with respect to heart rate (HR) and mean arterial pressure (MAP). Left ventricular output and contractile state are both fixed at a constant level and specific indices of left ventricular performance are then evaluated for different combinations of the independent variables HR and MAP; end-diastolic volume can be treated as a dependent variable here.

For a fixed level of left ventricular output the hydraulic load presented to the left ventricle is mainly determined by the peripheral vascular resistance

and the heart rate. In this case, however, the magnitude of the peripheral resistance and mean arterial pressure are linearly related. Thus, if experimental observations are spread uniformly throughout the range of the independent variables HR and MAP, it should be possible to characterise the variation of different indices of left ventricular function for a wide range of loading conditions. Clearly, contractile state (or inotropic level) cannot be included in this analysis as an independent variable in the same sense as HR or MAP. For a given experiment, however, we can compare the variation of specific indices of left ventricular performance, with respect to HR and MAP, for two or more different levels of contractile state. This may provide some insight into the effects of changing inotropic level.

Obviously, the success of this approach depends on the stability with which the experimental preparation can be maintained. It is essential that contractile state should not change in an uncontrolled fashion or, at least, that there should be criteria for discarding experimental results if a spontaneous change in inotropic level does occur.

The use of nonlinear multi-variate analysis is sensible only if the function under consideration has been adequately sampled with respect to its independent variables. Both the range and the number of observations are important here and the results of different experiments should not be pooled. In reality the number of separate observations which can be obtained in a single experiment is limited and the experimental protocol must be carefully planned.

In summary, the success of the proposed experimental approach depends on:

- the ability to control left ventricular output, peripheral resistance, contractile state and heart rate over the normal physiological range
- the stability with which the preparation can be maintained
- the speed and accuracy with which measurements can be made

Essentially, the series of experiments which we now describe may be regarded as a feasibility study of a specific multi-variate systems approach.

4. METHODS

4.1 EXPERIMENTAL METHOD

Preparation

Protocol

4.2 INSTRUMENTATION

4.3 DATA PROCESSING

Analogue to Digital Conversion

Preliminary Digital Processing

Derivative Indices of Contractile State

Aortic Input Impedance

Hydraulic Power Transfer

Multi-Variate Analysis

4. METHODS

4.1 EXPERIMENTAL METHOD

All experiments were performed and directed by Dr. J. H. Chamberlain at Guy's Hospital, London.

PREPARATION

Adult dogs weighing between 20 and 35 kg were studied. Anaesthesia was induced with intravenously administered thiopentane (25 mg/kg) and the animals were respired with a mixture of 0.01% halothane, 40% oxygen and 60% nitrous oxide, using intermittent positive pressure ventilation. A right thoracotomy was performed to give easy access to the spine and a modified right heart bypass was used - see Fig. 4.1. The pulmonary artery was cannulated together with the superior and inferior vena cavae. The azygos vein was divided and a flexible cannula passed through it into the right ventricle. Systemic venous return and right heart drainage were directed into a reservoir under siphon action and venous blood was then pumped through a heat exchanger ($37 \pm 0.5^{\circ}$ C) into the pulmonary artery using a calibrated variable speed roller pump. Snugging the cannulae in the superior and inferior vena cavae and the pulmonary artery completely isolated the right heart. The drainage into the right ventricle was therefore total coronary flow minus left ventricular thebesian drainage. The bypass was initially primed with Dextran 70 in 5% dextrose and,

thereafter, circulating volume was maintained by slowly adding blood from donor animals to the reservoir.

Cannulae were inserted through the femoral arteries and advanced into the descending aorta. The resultant arterial blood flow was passed through a second roller pump into the reservoir and it was therefore possible to control aortic pressure by varying the speed of this pump.

Complete sympathetic block was induced using spinal anaesthesia; 10 - 20 cc of 1% Marcaine were injected into the interspinus through the thoracotomy and this produced a rapid and profound depression of mean arterial pressure and heart rate. Arterial pressure was restored by the intravenous infusion of noradrenaline, the rate of infusion being determined by a small calibrated roller pump.

Heart rate was controlled by atrial pacing and low heart rates were obtained using a method very similar to that described by Levy et al (1972). The vagus nerves were divided in the neck, bilaterally sectioned and the distal end of the right vagus was laid across a pair of shielder silver electrodes. Short repetitive bursts of square wave stimulation were applied with a stimulus duration of 1 - 2 mS; the repetition rate of the stimulation bursts was determined by the required heart rate. In two experiments mecamilamine hydrochloride was used instead of spinal anaesthetic to induce sympathetic block. Since this is a ganglion blocker the use of vagal stimulation to obtain lower heart rates was precluded in these cases.

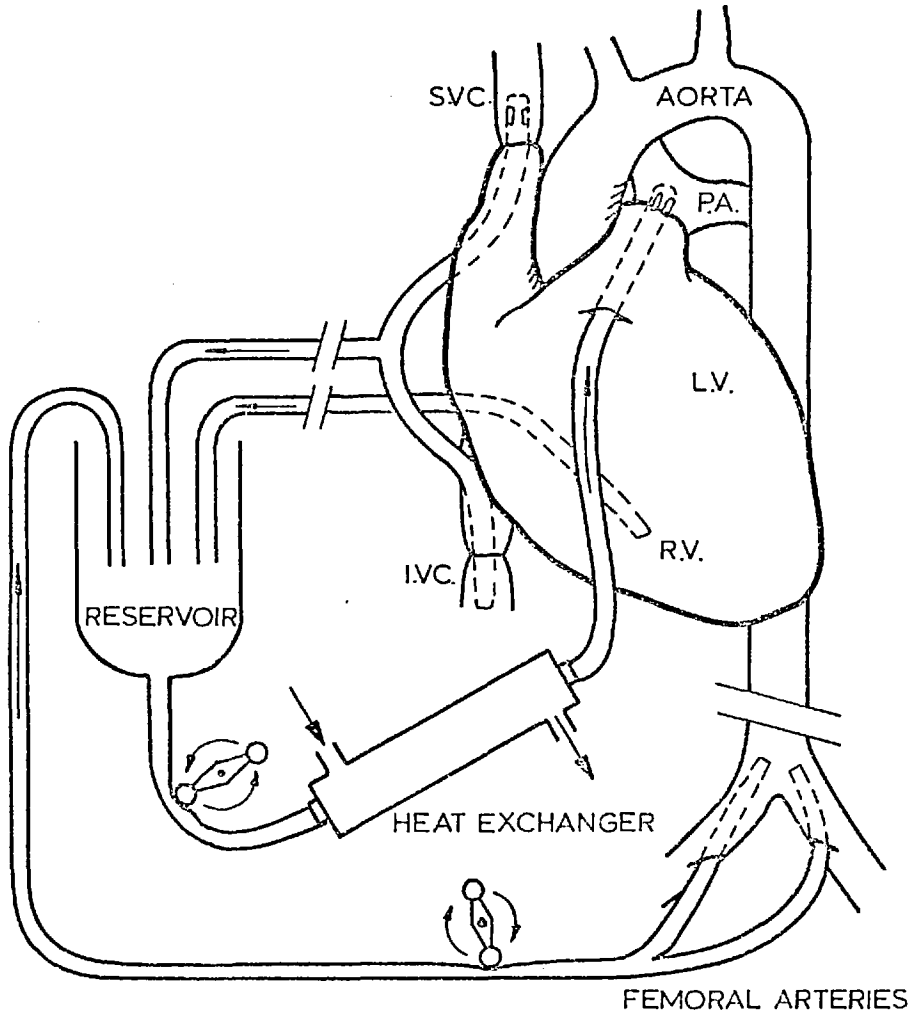

FIGURE 4·1: Right heart bypass preparation
L.V.- left ventricle, R.V.-right ventricle, S.V.C. and I.V.C.-superior and inferior vena cavae, P.A.- pulmonary artery.

PROTOCOL

Left ventricular output was set at a level normalised with respect to body weight. This provided a basis for comparing the results of different experiments; typical flow values were 100 ml/min/Kg and 150 ml/min/Kg. The rate of noradrenaline infusion was also fixed at a constant level and the pump setting noted.

The experiments were based on the measurement of coronary venous flow and arterial and coronary venous oxygen contents for a predetermined set of interventions; different combinations of heart rate (HR) and mean arterial pressure (MAP). For each intervention several minutes were allowed for the preparation to stabilize and then rapid measurements of coronary venous flow were made. When at least 3 consecutive results were obtained with a repeatibility better than 2%, samples of arterial and coronary venous blood were removed in numbered glass syringes and stored in ice for analysis at the end of the experiment. The measurement of coronary flow was continued throughout the sampling interval. In general, this complete process took between 5 and 10 minutes.

HR and MAP were varied according to a predetermined scheme. The procedure here was to set the desired level of MAP using the femoral shunt and then to pace the heart at specified values of HR. This process was repeated for different magnitudes of MAP. A typical set of experimental interventions is represented in Fig. 4.3 and in some experiments an attempt was made to obtain two complete sets of such HR-MAP combinations, each corresponding to a different level of contractile state or left ventricular output.

It has been stated that the success of this approach depends on the stability with which the preparation can be maintained. For this reason blood gases and electrolyte balance were checked at regular intervals throughout the experiment and where necessary blood chemistry was corrected. Further, at various stages within each experiment the pacer was switched off and measurements were made at the intrinsic heart rate. It was found that the intrinsic heart rate was a sensitive indicator of shifts in the inotropic level.

At the conclusion of each experiment the weight of the heart and the left ventricle were determined.

4.2 INSTRUMENTATION

A simple technique was developed for the rapid and accurate measurement of coronary venous flow. This was based on the method of timed collection; the time for blood to fill the known volume between two spaced electrodes in a measurement U-tube. Typically, the collection time was between 20 and 30 seconds, sufficient to average flow over several respiratory cycles. Collection time was determined using a digital counter-timer and an electronic circuit was constructed to control the counter-timer and to generate a marker pulse during the timing interval. A complete description of the methods used is given in Appendix A.

Arterial and coronary venous oxygen contents were obtained using a Lexington Instruments electrolytic cell analyser. This method is faster, less prone to

operator error and according to Fusako et al (1973) as accurate as the standard manometric technique of Van Slyke and Neill (1924). Duplicate determinations of oxygen content were made for each sample and pairs which differed by more than 0.2 ml 0_2/100 ml blood were rejected. A Radiometer Copenhagen blood gas analyser and calibrated electrode system were used to determine $p0_2$, pCO_2, pH and the electrolyte balance. In addition to these measurements a number of other physiological variables were monitored throughout each experiment - see Fig. 4.2.

Aortic flow was monitored with an S.E. Laboratories SEM 275 sine wave flow meter; comprehensive reviews of this flow measurement technique have been given by Bergel and Gessner (1966), Mills (1972). We checked the frequency response of the flow meter using the method presented by Goodman (1966). All flow probes had been previously calibrated under conditions of steady blood flow and for calibration purposes the output of the flow meter could be switched to two preset voltage levels corresponding to maximum and zero magnitization current, respectively. It should be noted that the latter is not the same as the meter output when there is no flow. The flow baseline depends, to some extent, on the type and positioning of the probe and must therefore be determined from the flow signal each time the meter is used.

The flow probes were placed on the ascending aorta distal to the coronary arteries and probe size was carefully chosen to minimize constriction of the aorta. Electromagnetic flow meters are extremely prone to electrical interference and it was necessary to isolate the vagal stimulating electrodes both physically and electrically. We were, however, unable to prevent artifacts in the flow signal

due to atrial pacing.

Aortic and left ventricular pressures were monitored using Millar Instruments PG-350 catheter-tipped solid state pressure transducers and TCB 100 control units. According to the manufacturers specifications the frequency response, linearity and drift for this system are excellent and independent tests confirm this. It was possible to switch the output of the control unit to any one of 10 preset voltage levels corresponding to the calibration range - 100 mm Hg - 100 mm Hg.

Initially, the left ventricular pressure transducer was inserted through an incision in the apical dimple. This procedure led to bruising in the apical region and in later experiments the catheter was passed into the common carotid artery and advanced through the aorta into the left ventricle. The aortic pressure probe was inserted into the internal mammary artery and then passed into the ascending aorta. During systole the left ventricular and aortic pressure signals should follow each other very closely. We found that spurious results were obtained if the transducers were too close to the left ventricular or aortic walls and it was necessary to position the pressure probes very carefully indeed. Further, to determine the hydraulic input impedance accurately the aortic pressure probe should be located just behind the flow probe. In the absence of X-ray facilities we positioned the aortic pressure transducer by first advancing the catheter into the left ventricle and then withdrawing it a short distance.

Blood temperature was monitored using a thermistor probe inserted into the right ventricle. In order to use this transducer it was necessary to construct a simple bridge amplifier and a complete description of this device is given in Appendix A. For calibration purposes it was possible to switch the output of

this amplifier to two preset voltage levels corresponding to $30^{o}C$ and $40^{o}C$, respectively.

ECG, heart rate (HR), mean arterial pressure (MAP) and the derivative of left ventricular pressure $\frac{dP}{dt}_{LV}$ were also monitored. The last three were obtained using on-line signal processing. A simulataneous oscilloscope display of any four variables was available. ECG, aortic flow, left ventricular pressure, aortic pressure, coronary flow timing marker and blood temperature were recorded using a P.I. instrumentation tape recorder; F.M. mode was used and the recording speed was 3.75 inches/second. Aortic flow, left ventricular pressure, aortic pressure, timing marker, blood temperature, HR, MAP and $\frac{dP}{dt}_{LV}$ were recorded using a Devices chart recorder at a low paper speed. A complete analogue record of each experiment was made on magnetic tape and chart paper. Channel calibration levels were recorded at the beginning of each new magnetic tape.

4.3 DATA PROCESSING

The steps involved in processing the experimental data are represented in Fig. 4.2.

The six channels of analogue data stored on magnetic tape were digitized using the IBM 1800 in the Engineering in Medicine Laboratory and for each

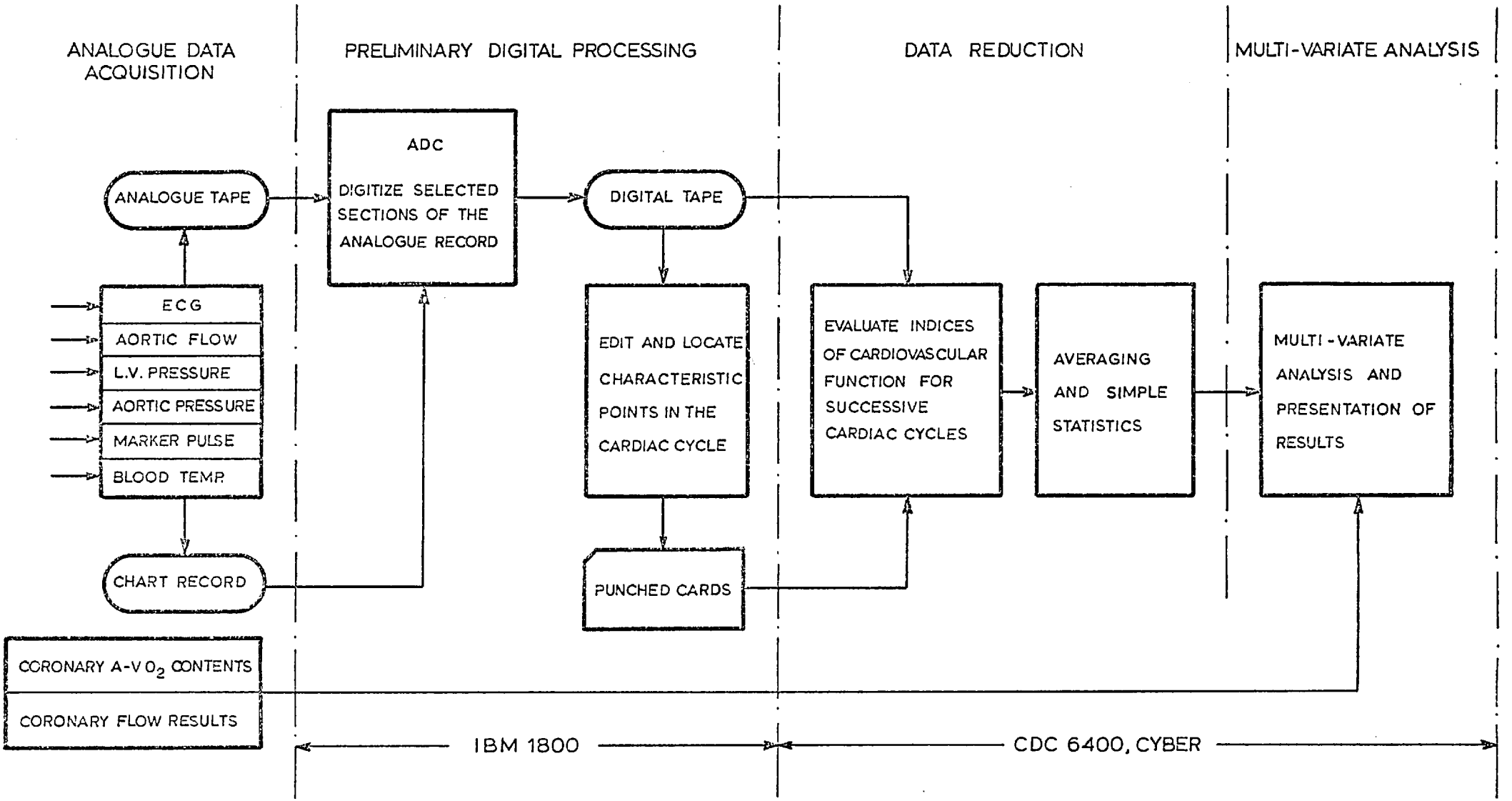

FIGURE.4.2: Data processing procedure

intervention a predetermined section of the experimental record was written as a separate file on digital magnetic tape. To analyse this data it was first necessary to locate several characteristic points within each cardiac cycle. Clearly, it was essential that these points should be located accurately and consistently. The digital record was edited and preprocessed using the IBM 1800 and for each heart beat the onset of ventricular contraction, the onset of ejection and the finish of ejection were detected automatically. The selected locations for each of these points were visually checked and where necessary corrected; this information was encoded and punched on data cards. Both the digital tape and the data cards were then transferred to the CDC 6400 and Cyber computers in the Imperial College Computer Centre.

The data obtained in preprocessing the digital tape was now used to control the reduction sequence. For each intervention a predetermined section of the experimental record was analysed. Sets of indices of left ventricular function were evaluated from the left ventricular pressure, aortic flow and aortic pressure waveforms for successive cardiac cycles. The mean values for each of these indices were then calculated and simple confidence levels allocated.

We considered :

- the interbeat interval, the systolic interval and the interval from the onset of contraction to peak left ventricular pressure
- aortic stroke flow
- left ventricular end-diastolic pressure, peak left ventricular pressure, mean aortic pressure, end-diastolic, end-systolic, mean systolic and peak aortic pressures

- standard derivative indices of contractile state
- aortic input impedance and the efficiency of hydraulic power transfer

The average value of the blood temperature was also determined.
These indices were evaluated over at least 15 respiratory cycles; typically 60 - 200 consecutive heart beats.

In this way the stored data for each of the interventions in a given experimental record was reduced to set of indices of left ventricular function. Before these results could be analysed further, however, it was necessary to characterise each intervention with respect to the fundamental system variables. In particular it was essential to establish whether any spontaneous change in contractile state had occurred during the experiment and to discard any results affected from the analysis. Three criteria were used here: the variation of standard derivative indices of contractile state, the stability of the intrinsic heart rate and the nature of the "left ventricular function " plot; the effectiveness of these criteria is fully discussed in the next chapter.

The results were sorted into sets for which left ventricular output and contractile state were fixed and each intervention was therefore characterised by the independent variables heart rate (HR) and mean arterial pressure (MAP) - see Fig. 4.3. Experimental results were now subjected to nonlinear bi-variate analysis to determine their dependence on HR and MAP. This was done by fitting a general polynomial surface to the experimental data points using the least squared error criterion; the significance of the best fit surface was assessed using some of the standard tests of multi-variate regression statistics. Myocardial oxygen consumption ($M\dot{V}O_2$), coronary blood flow, maximal coronary

flow and the efficiency of hydraulic energy transfer were considered here, together with a number of the other indices of left ventricular function already listed. For some experiments this process was repeated for results corresponding to a further level of left ventricular output or contractile state.

Details of the computer programs used here are given in appendix B and in Appendix C we review the statistical basis for multi-variate regression analysis. However, it is necessary to consider some of the more important steps in the data processing scheme in further depth and this will be done in the pages which follow.

ANALOGUE TO DIGITAL CONVERSION

Six channels of analogue data were simultaneously digitized. These were: (1) ECG (2) left ventricular pressure (3) aortic flow (4) aortic pressure (5) coronary flow timing marker (6) blood temperature. The analogue tape was played back at 10 times the recording speed and analogue to digital conversion was externally synchronized at 12 KHz giving a sampling rate for each channel of 200 Hz. Channels 1-4 were low pass filtered using active Butterworth filters, while for channels 5-6 the low pass output filters for the tape recorder were used. The high frequency cut-off for each channel was set as close as possible to the real time Nuyquist frequency (the highest frequency present in the signal).

For the ECG it is generally assumed that frequency components up to 40 Hz are sufficient to reproduce the QRS complex. There is some doubt, however, as to the number of harmonics required to faithfully reproduce the aortic flow waveform; Mills (1972). We set the high frequency cut-off at 40 Hz here and found this more than adequate over the complete range of canine heart rates. For the left ventricular pressure and aortic pressure waveforms the high frequency cut-off chosen was 30 Hz. Gabe (1972) has shown that this upper limit is sufficient to accurately reproduce the rate of change of left ventricular pressure for the full range of normal heart rates.

According to the Nuyquist criterion a continuous signal can be completely reconstituted from its sampled version if the sampling rate is twice the Nuyquist frequency. In practise, however, it is convenient to sample at a rate which is sufficiently high to allow accurate signal processing without reconstitution. The use of unreconstituted sampled data obviously introduces uncertainties which are a function of the inter-sample timing and these errors are most pronounced in the evaluation of left ventricular end-diastolic pressure (LVEDP) and derivative indices such as the maximum rate of change of left ventricular pressure $\left.\frac{dP}{dt}_{LV}\right|_{MAX.}$ A trade-off exists here between the increased accuracy associated with high sampling rates and the generation of an excessive number of samples. For a sampling rate of 200 Hz the errors introduced by the use of unreconstituted sampled data were typically:

$$LVEDP \leqslant 0.5 \text{ mm Hg}, \quad \left.\frac{dP}{dt}_{LV}\right|_{Max} \leqslant 3\%$$

For each intervention a predetermined length of the experimental record was digitized; the sections for which coronary venous flow and coronary arterio-venous oxygen difference results were obtained. These sections were identified from the chart record and then the coronary flow timing markers were used to find the corresponding analogue tape positions. The channel calibration levels were also digitized. Each discrete section of the experimental record was stored on digital tape as a separate file and prefixed by a header.

PRELIMINARY DIGITAL PROCESSING

For each experiment the data stored on magnetic tape was edited and preprocessed prior to reduction; details of the programs used here are given in Appendix B. The digital record was visually checked, tape positions were found for the channel calibration levels and the aortic flow baseline was identified. Most important, though, the locations for the onset of ventricular contraction, the onset of ejection and the finish of ejection were obtained for successive cardiac cycles. We consider now some of the criteria used to detect these characteristic points.

It can be seen from Fig. 4.4 that ventricular contraction is associated with a sudden discontinuity in the rate of change of left ventricular pressure and this feature was used to locate the onset of contraction. First, left ventricular end-diastolic pressure was selected by eye for several cardiac cycles and the first derivative of pressure was evaluated for these points.

The left ventricular pressure record was then scanned and the existence of contraction was detected by the positive crossing of a preset threshold. From these points a running difference was passed back through the record until a discontinuity was located; the criterion here was to compare the central difference for successive samples with the previously evaluated reference.

This approach was found to be both efficient and accurate. From Fig. 4.4. it can be seen that during the phase of isovolumic contraction the rate of change of left ventricular pressure is clearly defined with respect to the background noise. Therefore, in 'looking' back from the threshold we greatly reduce the probability of noise introducing errors in the detection of left ventricular end-diastolic pressure. Further, using this technique it is possible to discriminate between the onset of atrial and ventricular contraction.

The onset and finish of ejection are reflected in both the aortic flow and aortic pressure waveforms and can be detected from either. It was simpler to use the aortic flow waveform here since, unlike aortic pressure, this signal has a stable baseline. At high heart rates, however, the flow record was often contaminated by the pacing artifact and in these cases it was necessary to use the pressure waveform. The onset of ejection was located in exactly the same way as the onset of ventricular contraction. The end of ejection was detected from the reversal of pressure or flow associated with valve closure using a very similar technique.

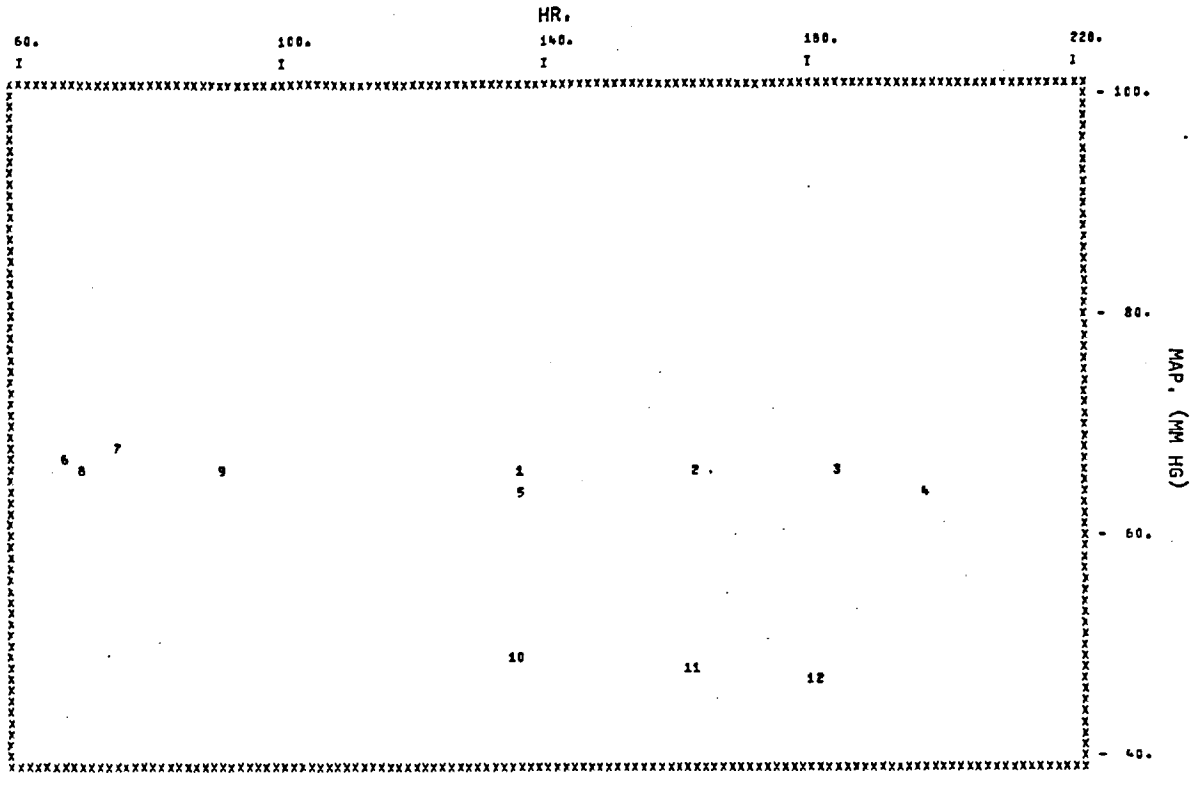

FIGURE 4.3: REPRESENTATION OF A TYPICAL SET OF EXPERIMENTAL INTERVENTIONS; HR AND MAP ARE SPECIFIED FOR EACH INTERVENTION

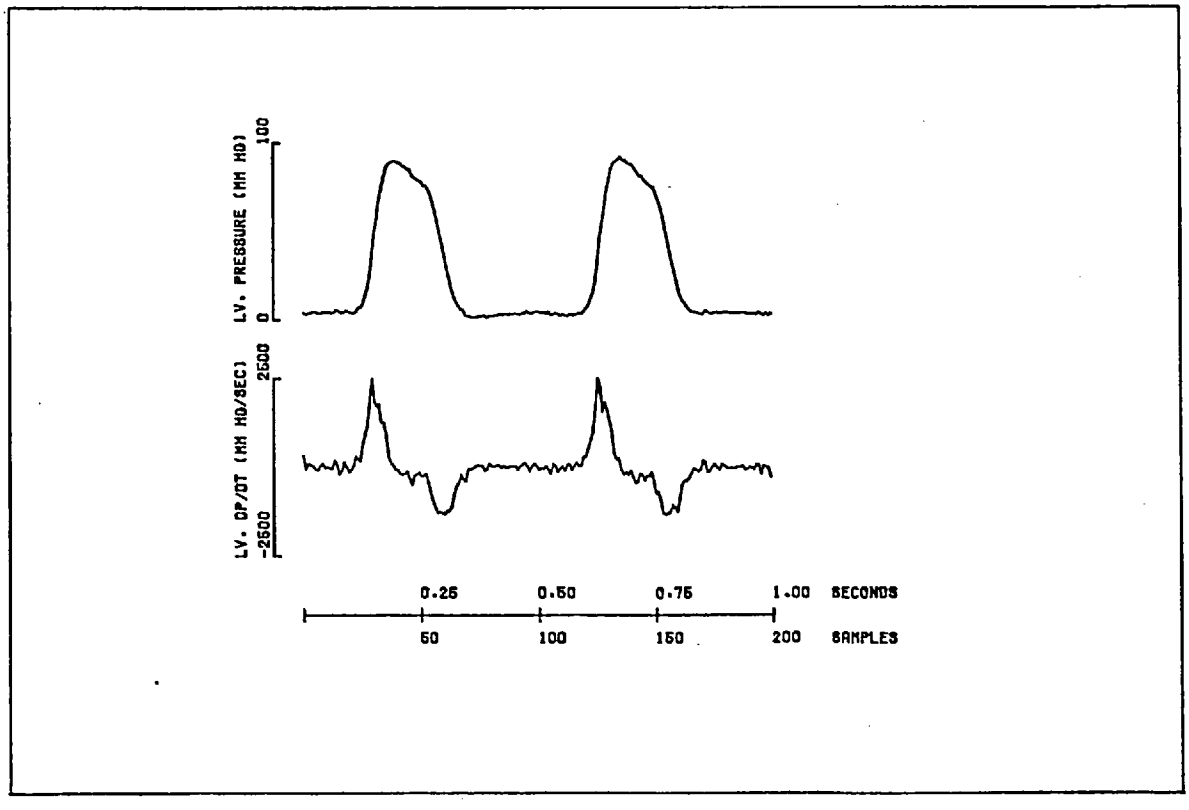

FIGURE 4.4: TYPICAL EXPERIMENTAL RECORD FOR LV. PRESSURE; THE RATE OF CHANGE OF LV. PRESSURE WAS OBTAINED BY DIGITAL SIGNAL PROCESSING

DERIVATIVE INDICES OF CONTRACTILE STATE

A change in contractile state is generally defined as an alteration of the functional state of the myocardium which is not related to changes in ventricular end-diastolic volume - preload, or hydraulic input impedance - afterload. It has long been recognised that an increase in inotropic level leads to a positive change in the rate of development of contractile force and this is reflected in both the aortic flow and left ventricular pressure waveforms. Unfortunately, most indices of contractile state which are based on derivative measurements are influenced to some extent by load changes and for this reason no universally accepted index of contractile state exists. We therefore evaluated several standard derivative indices of contractile state. If nothing else, this provided an excellent opportunity for investigating the relative changes in these parameters under widely varying load conditions. We now give a brief description of the indices of contractile state evaluated.

$\left.\frac{dP}{dt}\,LV\right|_{Max}$; the maximum rate of change of left ventricular pressure. This index certainly reflects changes in contractile state, but it is strongly load dependent.

$\left.\frac{d\ln P}{dt}\,LV\right|_{Max}$; the maximum normalised rate of change of left ventricular pressure. Grossman et al (1971) proposed the use of this parameter, which they found to be largely independent of afterload variations. They state, however, that it is partially dependent on preload variations.

$\left.\frac{dP}{dt}_{LV}\right|_{Max} / P^0_{LV}$; P^0_{LV} is the left ventricular pressure for the maximum rate of change of pressure. According to Cheung et al (1974) this parameter is load independent.

$\left.\frac{d\dot{Q}}{dt}\right|_{Max}$; maximum aortic acceleration. Noble et al (1966) state that this index is relatively load independent.

AORTIC INPUT IMPEDANCE

The concept of hydraulic impedance has proved to be extremely useful in studies of the relationships between pulsatile pressure and flow in the cardiovascular system; Gessner (1972). We evaluated the aortic input impedance here since this provides a convenient representation of the hydraulic load presented to the left ventricle. Additionally, a general basis for the analysis of left ventricular external work follows directly from this approach.

Fourier analysis is based on the fact that a typical periodic waveform can be represented as the sum of discrete sinusoidal and cosinusoidal components. In phasor notation each frequency component is specified by the magnitude and phase of a single cosine term.

$$f(t) = \sum_{n=0}^{\infty} C_n \cos\left(\frac{2\pi nt}{T} + \phi_n\right) \qquad 4.3.1$$

where

$$C_o = \frac{1}{2} A_o$$

$$C_n = \sqrt{(A_n^2 + B_n^2)} \qquad 4.3.2$$

$$\phi_n = \tan^{-1}\left(-\frac{B_n}{A_n}\right)$$

T is the period and $f(t) = f(t+T)$

A_O, A_n, B_n are the Fourier coefficients for the DC. term, the n th. cosine component and the n th. sine component, respectively.

For sampled data it is necessary to use a discrete form of the Fourier transform to obtain these coefficients. Let the continuous signal f(t) be represented in the interval $t_o \leqslant t \leqslant t_o + T$, by N equally spaced samples f (k), K = 0, 1, 2, .. , N - 1. In this case the Fourier coefficients can be obtained from the expressions :

$$A_n = \frac{2}{N}\sum_{k=0}^{N-1} f(k) \cos \frac{2\pi nk}{N}$$

$$B_n = \frac{2}{N}\sum_{k=0}^{N-1} f(k) \sin \frac{2\pi nk}{N} \qquad 4.3.3$$

$$k = 0, 1, 2, ---, N-1$$

Providing the sampling theorem has been satisfied, the original sampled waveform is completely reproduced by

$$f(k) = \sum_{n=0}^{n=M} C_n \cos \left(\frac{2\pi}{N} nk + \Phi_n\right) \qquad 4.3.4$$

$$k = 0, 1, 2, ---, N-1$$

$$M = \begin{cases} N/2 - 1, & N \text{ even} \\ (N-1)/2, & N \text{ odd} \end{cases}$$

where C_n and Φ_n are evaluated from 4.3.2 and 4.3.3.

The sampled representation of the aortic pressure and flow signals is therefore given by :

$$P_a(k) = \sum_{n=0}^{n=M} P_n \cos \left(\frac{2\pi}{N} nk + \varphi_n\right) \qquad 4.3.5$$

$$\dot{Q}(k) = \sum_{n=0}^{n=M} \dot{Q}_n \cos \left(\frac{2\pi}{N} nk + \Psi_n\right)$$

$$k = 0, 1, 2, ---, N-1$$

By analogy with network theory, the magnitude $|Z_n|$ and phase ξ_n of the hydraulic impedance spectrum Z_n are specified by :

$$|Z_n| = \frac{P_n}{\dot{Q}_n} \qquad 4.3.6$$

$$\xi_n = \varphi_n - \psi_n$$

The concept of hydraulic impedance, which has been developed here, should not strictly be applied to nonlinear systems. If the nonlinear variations introduced are small over the range of the signals considered, though, the system can be treated as linear and Fourier analysis applied. According to Gessner (1972) it is valid to use this quasi-linear approximation for vascular impedance. Outside the normal range of pressures, however, the mechanical properties of the central arterial system become progressively more nonlinear and care should be taken when comparing impedances estimated under different loading conditions.

Before going any further we must consider the nature of the experimental pressure and flow signals in greater detail. Due to respiratory variation the aortic pressure waveform is not, in general, absolutely periodic and thus the fundamental condition of Fourier analysis is not satisfied. Under steady state conditions, however, consecutive cardiac cycles are very similar and a single cycle may be considered to represent a complete series of beats. For each aortic pressure cycle : $P_a(t)$ $t_0 \leq t \leq t_0 + T$, T is the interbeat interval;

we removed the baseline drift using

$$P_a^*(t) = P_a(t) - \frac{P_a(t_o+T) - P_a(t_o)}{T}(t-t_o) \qquad 4.3.7$$

and Fourier analysis was then applied to the corrected signal $P_a^*(t)$

For the aortic flow waveform the use of the electromagnetic flow meter introduces some additional problems. Most electromagnetic flow meters have a non-ideal frequency response and in some cases it is necessary to correct the frequency components of the aortic flow signal before using expression 4.3.6 to determine the impedance spectrum. The frequency response of the flow meter used here was obtained by Goodman's (1966) method. For the aortic pressure waveform frequency components above the sixth harmonic are small and subject to noise. The impedance spectrum was therefore determined up to the sixth harmonic only (24 Hz at a heart rate of 240 beats/min). Over this frequency range we found that the amplitude response of the flow meter was essentially flat, but that phase varied linearly with frequency. This corresponds to a fixed time delay and was therefore simply corrected.

In general, the aortic flow baseline was identified from the mean value of flow during diastole. However, where incorrect probe placement led to signal drift in diastole, we assumed that zero flow was given by the samples immediately prior to ejection.

It has been stated that the electromagnetic flow meter is extremely prone to electrical interference and in Fig. 4.5 we present a typical aortic flow waveform contaminated by pacing artifacts. Except at high heart rates

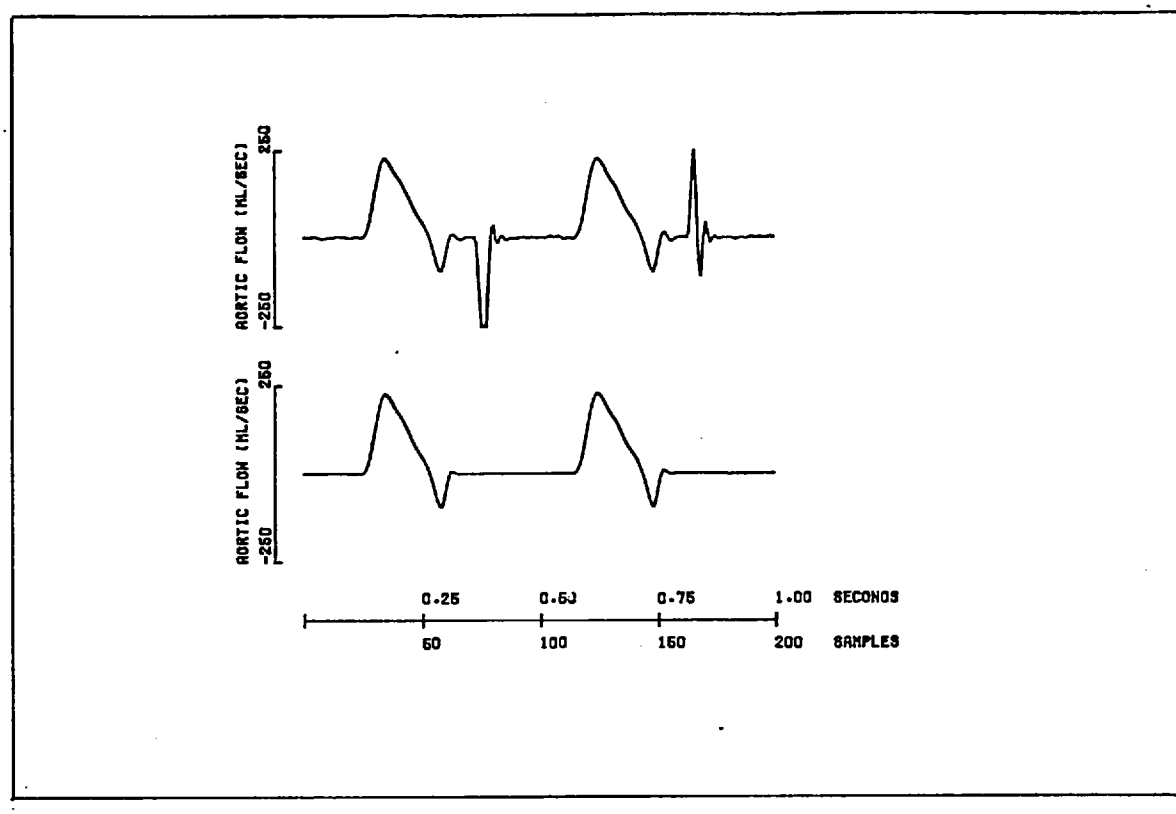

FIGURE 4.5: REMOVAL OF PACING ARTIFACTS FROM THE AORTIC FLOW RECORD

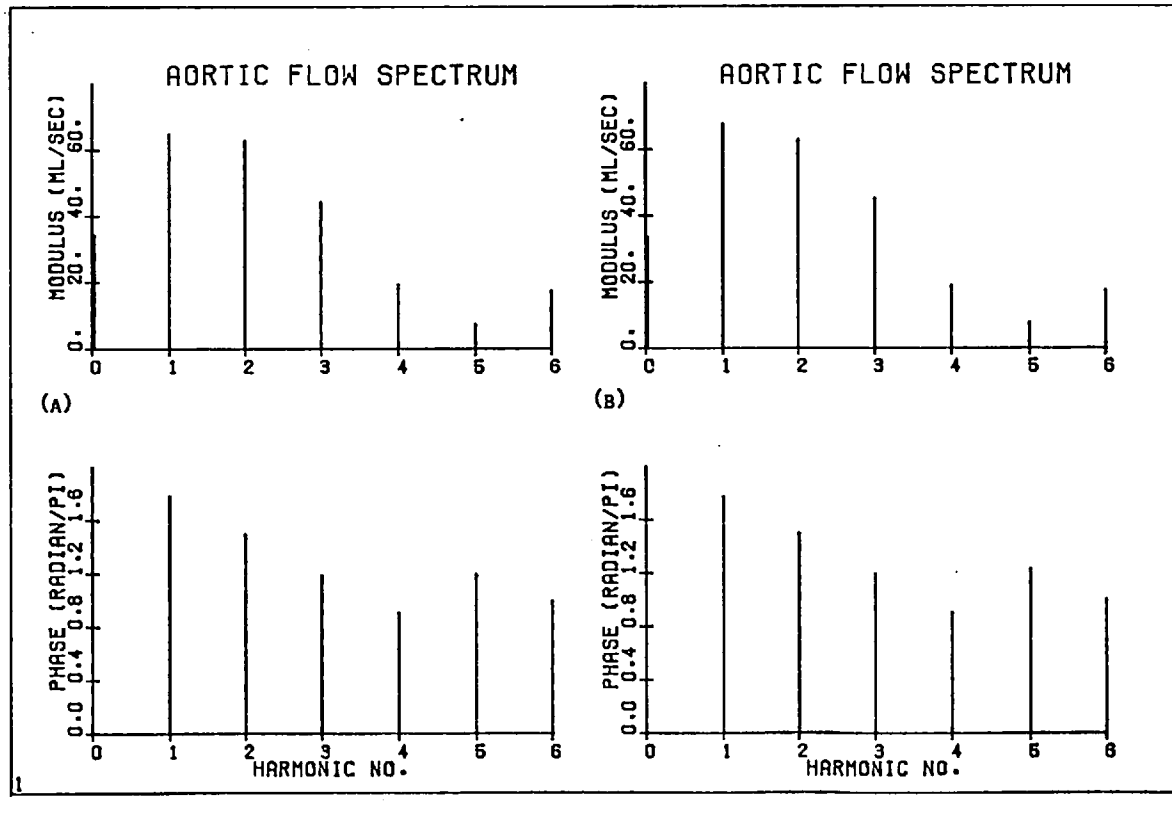

FIGURE 4.6: EFFECT OF REMOVING PACING ARTIFACTS FROM THE AORTIC FLOW RECORD; FREQUENCY SPECTRA FOR A FLOW RECORD WITHOUT ARTIFACTS
(A) CORRECTION ALGORITHM NOT APPLIED (B) CORRECTION ALGORITHM APPLIED

these artifacts generally occurred during the diastolic interval and the flow signal was quite simply corrected. At the finish of ejection a cosine taper was applied to return the signal to the baseline, where it was assumed to remain for the rest of diastole. The effect of this correction is shown in Fig. 4.5 and it is important to assess what errors this produces in the true aortic flow spectrum. A cycle of the unpaced flow waveform was subjected to Fourier analysis. The correction algorithm was then applied to this waveform and the frequency spectrum again determined. We present the results in Fig. 4.6 and it can be seen that the aortic flow spectrum is only slightly modified by the correction process. No attempt was made to correct those flow signals in which the ejection phase was distorted by the pacing artifact.

HYDRAULIC POWER TRANSFER

The production of pulsatile flow in an elastic system requires the input of both potential and kinetic energy. To maintain fluid flow at a given pressure, energy must be delivered to the system at an adequate rate; this is defined as the flow work rate and is given by the product of pressure and flow. The total energy requirement is determined by the sum of the flow work rate and the kinetic energy of the fluid moving into the system. We consider only the flow work rate here since, for the left ventricle, the kinetic energy term is difficult to evaluate and quite small.

The instantaneous flow work rate is

$$\dot{W}(t) = P_a(t)\,\dot{Q}(t) \qquad 4.3.8$$

Averaging this over a cardiac cycle we obtain

$$\overline{\dot{W}} = \frac{1}{T}\int_{t_o}^{t_o+T} P_a(t)\,\dot{Q}(t)\,dt \qquad 4.3.9$$

If we represent the continuous signals $P_a(t)$, $Q(t)$ by their Fourier series representations 4.3.1, it can be shown after some simple manipulation that

$$\overline{\dot{W}} = \overline{\dot{W}_r} + \overline{\dot{W}_i} \qquad 4.3.10$$

where

$$\overline{\dot{W}_r} = P_o\,\dot{Q}_o + \tfrac{1}{2}\sum_{n=1}^{\infty} P_n\,\dot{Q}_n \cos\xi_n \qquad 4.3.11$$

and

$$\overline{\dot{W}_i} = \tfrac{1}{2}\sum_{n=1}^{\infty} P_n\,\dot{Q}_n \sin\xi_n \qquad 4.3.12$$

$\overline{\dot{W}_i}$ is an imaginary term representing energy stored in elasticity and inertia, which can be recovered by the system. $\overline{\dot{W}_r}$ represents the total input power requirements. This can be decomposed into a DC term which gives the power transferred to the system and harmonic components which give the pulsatile losses. Therefore, the efficiency of hydraulic power transfer is

$$\%\ \text{Efficiency} = \frac{100\,P_o\,\dot{Q}_o}{P_o\,\dot{Q}_o + \tfrac{1}{2}\sum_{n=1}^{\infty} P_n\,\dot{Q}_n} \qquad 4.3.13$$

The aortic pressure and flow probes were placed distal to the coronary arteries and thus the hydraulic power transfer determined at this site underestimates the total power generated by the left ventricle. However, the efficiency of hydraulic power transfer should be very similar in both cases.

MULTIVARIATE ANALYSIS

Consider the typical set of experimental interventions represented in Fig. 4.3. Left ventricular output and contractile state were fixed and thus each intervention is characterised by the values of the independent variables heart rate (HR) and mean arterial pressure (MAP). It was difficult to control MAP precisely with the preparation used in these experiments and the interventions were, in general, unevenly spaced with respect to the independent variables. Further, the experimental observations contained, in differing degrees, uncertainties which were due to measurement error and to the inherent variability of the preparation. Clearly, there were problems here both in the presentation of the experimental results and in establishing the underlying relationships reflected by these results.

A number of methods for the presentation of unevenly sampled "spatial" data have been given in the literature. Mostly, these techniques depend on finding a set of weighted interpolation functions which exactly fit the experimental data points. Such an approach was not applicable in this case and we used the methods of multi-variate regression analysis instead.

A general function or regression surface

$$Z' = f(HR, MAP) \qquad 4.3.14$$

was fitted to the experimental observations using the least squared error criterion. Z' the dependent variable represents a specific index of left ventricular function. Implicit in this approach is the assumption that the errors of observation are random and associated with the dependent variable only. Thus, if there are sufficient observations to balance out these errors, the best fit surface should reflect the underlying relationship between the experimental observations. The approach is quite general and its accuracy depends entirely on choosing the correct type of functional relationship. Typically, a general bi-variate polynomial was used as the regression function. The contribution of the higher order terms was assessed by evaluating the standard error of estimate and the index of correlation as successive polynomial co-efficients were introduced. Both these indices were corrected for the bias caused by the limited sample size and unless there was a definite reduction in the adjusted standard error of estimate and an increase in the adjusted index of correlation the higher order function was not considered to be significant. The adjusted standard error of estimate was also used to assess the absolute reliability of the experimental regression surfaces for indices such as myocardial oxygen consumption ($M\dot{V}O_2$), in which the measurement error was significant.

The methods described here were used extensively both in the presentation and in the interpretation of the experimental data. This approach should only be applied to slowly varying functions and for accuracy the observations should be spread uniformly throughout the range of the independent variables. A brief review of the relevant statistical theory is given in Appendix C.

5. EXPERIMENTAL RESULTS

5.1 INTRODUCTION

5.2 ASPECTS OF LEFT VENTRICULAR FUNCTION

Ventricular Pumping Capacity

Contractile State

Aortic Input Impedance

5.3 ASPECTS OF LEFT VENTRICULAR PERFORMANCE

Hydraulic Power Transfer

Myocardial Oxygen Consumption

Myocardial Oxygen Supply and Demand

5.4 DISCUSSION

5. EXPERIMENTAL RESULTS

5.1 INTRODUCTION

The results discussed here are based on data from six successful experiments. These were drawn from a series of experiments performed over the period 22nd January - 28th July, 1974. We would have wished for a larger pool of results, but the experiments proved to be complex. Surgical and experimental techniques took some time to develop and, initially, the rate of success was low.

All experiments were performed using the methods described in the previous chapter. Left ventricular output and the rate of noradrenaline infusion were fixed; measurements were made for predetermined combinations of the independent variables heart rate (HR) and mean arterial pressure (MAP). The left ventricular performance surfaces presented here are based on at least 10 such measurements and in all 79 separate determinations of myocardial oxygen consumption ($M\dot{V}O_2$) were made. In four experiments left ventricular output and noradrenaline infusion rate were fixed throughout; low heart rates HR < 120 beats/min were obtained in two experiments only. In one further case the rate of noradrenaline infusion was increased during the experiment and thus it was possible to obtain left ventricular function surfaces for two discrete levels of contractile state. Similarly, two different levels of left ventricular output were also compared.

The results of these experiments were encouragingly consistent. Although specific results only are presented here, they are, in general, typical of our other experimental findings.

5.2 ASPECTS OF LEFT VENTRICULAR FUNCTION

VENTRICULAR PUMPING CAPACITY

It has been stated that if all other factors are held constant an increase in left ventricular end-diastolic volume will lead to an increase in stroke output. This is the Frank-Starling mechanism.

Sarnoff et al (1960), Herndon and Sagawa (1967), Sagawa (1969) have made comprehensive studies of the capacity of the heart to increase stroke power and stroke volume. In Fig. 5.1 we reproduce the classic "left ventricular function " curve given by Sarnoff et al (1960) and in Fig. 5.2a we present a similar relationship from our experimental results. It should be noted that in the latter case left ventricular output was fixed; stroke volume (SV) and left ventricular end-diastolic pressure (LVEDP) were determined at different levels of heart rate (HR) and mean arterial pressure (MAP). In the other studies, however, end-diastolic volume and stroke output were increased by raising atrial filling pressure at a constant HR. Despite this difference in approach the experimental left ventricular function curve presented in Fig. 5.2a coincides very closely with previous results.

From Figs. 5.1 and 5.2a it can be seen that an increase in end-diastolic

volume, reflected here by the magnitude of LVEDP, leads to an increase in stroke power. For a low output the variation of stroke power with LVEDP is almost linear. However, for higher levels of stroke output the capacity of the left ventricle to increase stroke power from an enlarged end-diastolic volume becomes progressively more limited until a very large increase in LVEDP is required to produce a marginal change in output. The dependence of left ventricular function on both pressure and volume loading is implicit in this presentation; if MAP is fixed, an increase in LVEDP leads to proportional increases in stroke power and SV, but the SV corresponding to a given LVEDP will be reduced if the level of MAP is raised or vice verse.

Consider the flow constraint presented in Fig. 5.2b; this gives the SV, HR combinations which satisfy a required level of left ventricular output. As HR is reduced, SV is increased and at low heart rates the incremental change in stroke volume becomes very large indeed. If MAP is fixed it can be seen from Fig. 5.2a that at some point the left ventricle will be unable to meet the flow constraint. As this limit is approached the change in end-diastolic pressure required to generate the necessary increase in SV becomes more pronounced, the ventricle dilates and left ventricular function becomes progressively less efficient. Clearly, if MAP is raised or the required level of left ventricular output is increased, this limiting case will be reached at higher values of HR.

CONTRACTILE STATE

Changes in contractile state alter left ventricular function and this is reflected by variations in coronary blood flow and myocardial oxygen utilisation.

It is essential, therefore, to establish that the inotropic level of the heart did not shift spontaneously during the experiment or, if this did happen, to discriminate between sets of results relating to different levels of contractile state. Three different criteria were considered here: the variation of the derivative indices of contractile state reviewed in the previous chapter, the nature of the "left ventricular function" relationship and the level of the intrinsic heart rate.

First, we consider the load dependence of the derivative indices of contractile state for an experiment in which, by all other indications, the level of contractile state remained constant. The intrinsic HR did not change and the left ventricular function curve (Fig. 5.3c) is continuous and well defined.

In Fig. 5.3a the experimental values of

$$\left.\frac{dP}{dt}\,LV\right]_{Max},\quad \left.\frac{d\ln P}{dt}\,LV\right]_{Max},\quad \left.\frac{dP}{dt}\,LV\right]_{Max}\Big/P^{o}_{LV},\quad \left.\frac{d\dot{Q}}{dt}\right]_{Max}$$

for a fixed level of MAP are superimposed on the same plot, as functions of HR. It should be recalled that left ventricular output was constant and thus as HR was reduced SV and end-diastolic volume increased. Therefore, the variation of HR is associated with changes in preload; the effects of HR on inotropic level are not considered here. For the results presented in Fig. 5.3b afterload was varied by changing MAP at a fixed level of HR. It can be seen that both the normalised indices

$\left.\frac{d\ln P}{dt}\,LV\right]_{Max}$ and $\left.\frac{dP}{dt}\,LV\right]_{Max}\Big/P^{o}_{LV}$ are independent of afterload changes, but that only the latter is not influenced by preload variations. This was a particularly stable preparation and, despite the possible range of

fluctuation indicated by the standard deviation of each index, the results are extremely consistent.

In Fig. 5.4 we reproduce the same plots for a different experiment and essentially both sets of results are in agreement. The preparation in the second case, though, was somewhat less stable. For the lowest value of HR in Fig. 5.4a, all indices are significantly larger than might have been predicted and this suggests the occurrence of a positive shift in inotropic level. However, no corresponding change was observed in either the left ventricular function curve or the intrinsic HR.

We now compare the variation of $\frac{dP}{dt}_{LV}\Big]_{Max} / P^{o}_{LV}$ and the change in the left ventricular function curve for an experiment in which contractile state was altered, in a controlled fashion, by increasing the rate of noradrenaline infusion. The results are given in Fig. 5.5. From Fig. 5.5b it can be seen that a change in contractile state results in a discrete shift of the left ventricular function curve and this is a well established result. For the derivative index of contractile state also, there is a slight change in the values estimated. immediately before and after the variation in the noradrenaline infusion rate (Fig. 5.5a). Over the complete set of interventions, however, this change is masked to some extent by apparently random fluctuations. Finally, we note that an increase in inotropic level is associated with a higher intrinsic HR.

For this type of experiment at least, it appears that the most reliable method for establishing whether a spontaneous change in contractile state has taken place is provided by plotting the left ventricular function curve. A constant intrinsic HR was also found to be an excellent indication of a stable contractile

state. Both these criteria were used to group results for multi-variate regression analysis.

We will discuss the effects of changes in contractile state on coronary blood flow, myocardial oxygen utilisation and the balance of myocardial oxygen supply and demand in the next section.

AORTIC INPUT IMPEDANCE

Experimental studies of the aortic input impedance for dogs have been made by O'Rourke and Taylor (1967), O'Rourke (1970) and the features of the different impedance spectra obtained are very similar. The impedance modulus at zero frequency gives the resistance to steady flow. For the low frequency range; 0 - 2Hz, the impedance moduli fall very rapidly indeed, but for higher frequencies they remain relatively constant with a magnitude much less than the DC. resistance. At zero frequency the phase angle is 0^{o}. It drops to between -50^{o} and -60^{o} in the low frequency range and gradually returns to 0^{o} as frequency is further increased.

In Fig. 5.6 we present the aortic input impedance results for two separate experiments and these are in close agreement with the findings of other workers. There is an apparent discrepancy, though, in the phase response of Fig. 5.6b; this was due to the use of an uncorrected fluid filled catheter to monitor aortic pressure in the final experiment. If the modulus plots are inspected carefully it can be seen that for both cases there are two minima in the frequency ranges; 2 - 4Hz and 5 - 7Hz, respectively. According to O'Rourke and Taylor (1967),

this is caused by the existence of two discrete reflecting sites in the systemic circulation.

The significance of the impedance characteristics of the ascending aorta is immediately obvious if we consider the impedance spectrum in relation to the aortic flow spectra presented in Fig. 5.7. A large proportion of the energy in the aortic flow waveform is contained in the lower harmonics and the impedance presented to these components is very small indeed. For this reason O'Rourke and Taylor (1967) state that the power required to maintain oscillatory flow is not much greater than that which would be needed if the heart were a steady flow source. Thus the nature of the hydraulic load presented to the left ventricle is an important determinant of the efficiency of hydraulic power transfer and also, by inference, of the efficiency of myocardial energy utilisation. It is important, therefore, to consider the way in which the aortic input impedance changes under different physiological conditions. Unfortunately, our pool of experimental results is limited, but some predictions can be made from them.

We recall the modified windkessel model introduced in Chapter 2. It can be shown that the frequency response for this configuration is given by :

$$|Z| = \frac{U}{1+\omega^2 V^2}\left[1+\omega^2(V^2+W^2)+\omega^4 V^2 W^2\right]^{\frac{1}{2}}$$

$$\xi = \tan^{-1}\left[\frac{\omega(V-W)}{1+\omega^2 VW}\right] \qquad 5.2.1$$

where ω is the angular frequency and

$$U = R_c + R_p$$

$$V = \frac{R_p R_c}{R_c + R_p}$$

$$W = \frac{R_p}{K}$$

R_c is the characteristic resistance, R_p is the peripheral resistance K is the elastic compliance.

we note that :

$$|Z|_{\omega=0} = R_c + R_p$$

$$|Z|_{\omega=\infty} = R_c \qquad 5.2.2$$

R_p and R_c were evaluated directly from the experimental impedance results presented in Fig. 5.6a and a suitable value was chosen for K. The frequency response for this windkessel representation is given in Fig. 5.8 and it can be seen that the agreement between the simple haemodynamic model and the experimental results is quite reasonable.

Consider now the effect of varying the peripheral resistance R_p with R_c and K fixed. Obviously, the DC. resistance will be altered here, but from Fig. 5.8a it can be seen that the frequency response is scarcely influenced by changes in the peripheral resistance. However, when the value of the elastic

compliance is increased, with R_p and R_c constant, the modulus curve is shifted to the right and vice verse (Fig. 5.8b).

These predictions can be related to corresponding experimental results from the literature. For the normal range of mean arterial pressures O'Rourke and Taylor (1967) have shown that changes in the peripheral resistance alter the impedance spectrum at low frequencies only. As pressure loading is increased beyond these levels, though, the arterial system becomes progressively more rigid. From our previous analysis it can be argued that the impedance moduli must be shifted to the right under these circumstances and the experimental results of O'Rourke (1970) confirm this prediction. Thus, the modified windkessel provides an excellent representation of the aortic input impedance. Under hypertensive conditions, however, the nonlinear distensibility of the central arterial system must be taken into consideration.

5.3 ASPECTS OF LEFT VENTRICULAR PERFORMANCE

HYDRAULIC POWER TRANSFER

The heart is a pulsatile pump and some losses are associated with the conversion of the oscillatory power developed by the left ventricle into the steady power delivered to the peripheral circulation. In Figs. 5.11 and 5.12 we present two three dimensional plots, derived from our experimental results, for the efficiency of this hydraulic power transfer. For each surface left ventricular output was constant. Thus for a given level of MAP steady power was constant and the observed reduction in efficiency with HR corresponds

to an increase in total developed power. Efficiency also decreased if MAP was lowered at a fixed HR. This reflects the fact that the reduction in total developed power with MAP was proportionately less than the decrease in steady power. Clearly, though, the efficiency of hydraulic power transfer cannot be linearly related to MAP as these plots suggest and this discrepancy was introduced by inadequate experimental sampling with respect to MAP.

Very similar comments apply to the observed variation of peak left ventricular pressure (Figs. 5.9d and 5.10d). Peak left ventricular pressure increased with decreasing HR and the reduction in peak pressure with MAP was proportionately less than the decrease in MAP.

The variation in the efficiency of hydraulic power transfer with HR and MAP is determined by the nature of the aortic flow waveform and by the characteristics of the hydraulic load presented to the left ventricle. This becomes clearer if we modify 4.3.11, the expression for the total flow work rate (total developed power).

It can be shown that

$$\bar{\dot{W}}_r = \dot{Q}_0^2 |Z_0| + \frac{1}{2}\sum_{n=1}^{\infty} \dot{Q}_n^2 |Z_n| \cos \xi_n \qquad 5.3.1$$

Q_n is the nth harmonic of the aortic flow waveform; Z_n and ξ_n are the corresponding terms for the impedance modulus and phase angle, respectively. The first term on the right gives the steady power, while the second term gives the contribution of the pulsatile components.

The analysis which follows is very close to that given by O'Rourke and Taylor (1967). In Fig. 5.7 we have superimposed the moduli for the first six

harmonics of four different aortic flow waveforms; left ventricular output and MAP were constant in each case. It can be seen that as HR is decreased and SV increases, the energy in the aortic flow waveform spreads progressively to the higher components and this leads to an increase in the pulsatile power developed by the left ventricle. The nature of the aortic input impedance contributes very little to this increase in pulsatile losses with HR. In the range HR < 120 beats/min the impedance moduli corresponding to the first harmonic of the flow increase (Fig. 5.6), but due to the variation of the phase angle the magnitude of the in-phase impedance $|Z_n| \cos \xi_n$ actually decreases slightly. Thus, although the nature of the hydraulic load leads to an increased aortic pulse pressure at low heart rates, the associated phase shift between the pressure and flow waveforms tends to offset any contribution to the pulsatile power.

For the normal resting state hydraulic power transfer efficiency is around 90% and the relative variation of total developed power with HR is quite small. The reduction in efficiency with MAP is entirely determined by the characteristics of the aortic input impedance. We recall that the left ventricle is effectively decoupled from the peripheral vascular load and decreasing the peripheral resistance R_p alters the input impedance spectrum in the low frequency range only. Therefore, although steady power is reduced with MAP, it follows from 5.3.1 that the contribution of the pulsatile components will be unchanged. Further, the variation of this pulsatile contribution with HR is also unchanged and thus the relative dependence of total developed power on HR will be directly increased.

A similar analysis can be applied to the experimental results for both aortic pulse pressure and peak left ventricular pressure. Thus, the variation of total developed power and peak left ventricular pressure with HR is determined by the nature of the aortic flow waveform and by the characteristics of the aortic input impedance. In exercise, or at a reduced level of MAP, the relative magnitude of this variation with HR becomes increasingly more pronounced.

MYOCARDIAL OXYGEN CONSUMPTION

In Figs. 5.13 and 5.14 we present two three dimensional plots of myocardial oxygen consumption ($M\dot{V}O_2$) as a function of HR and MAP. Left ventricular output was set at approximately the same normalised level in both cases and the experimental results for myocardial oxygen utilisation were subjected to nonlinear bi-variate regression analysis.

The two plots have some obvious common features; $M\dot{V}O_2$ is linearly related to MAP and there is a strong linear correlation between $M\dot{V}O_2$ and HR in the range HR > 120 beats/min. These results are in close agreement both with our findings in other experiments and with published experimental data relating to similar conditions.

For the range HR < 120 beats/min the results are most interesting. In both cases the relationship between $M\dot{V}O_2$ and HR is nonlinear. There is a shallow minimum at HR = 80 beats/min in Fig. 5.13 while for Fig. 5.14 the variation of $M\dot{V}O_2$ with HR suggests the possible existence of a minimum in the range HR < 60 beats/min. To some extent the location and perhaps even the existence of

these minima are imposed by the simple functions with which we have characterized the experimental data. However, for low heart rates, the nonlinear dependence of $M\dot{V}O_2$ on HR is pronounced and appears to be statistically significant.

This result certainly could not have been predicted from the behavior at high heart rates. It is, however, consistent with the observed variation of several factors which determine $M\dot{V}O_2$. We were unable to measure left ventricular volume directly, but the experimental values for LVEDP, presented in Figs, 5.9c and 5.10c, reflect the variation of left ventricular end-diastolic volume with HR. The change in LVEDP was relatively small for the range $120 < HR < 200$ beats/min, but LVEDP increased rapidly for heart rates below this range. Similarly, the variation of peak left ventricular pressure and total developed power with HR was most pronounced for $60 < HR < 120$ beats/min.

From Figs. 5.13 and 5.14 it can also be seen that the decrease in $M\dot{V}O_2$ with MAP is proportionately less than the reduction in MAP. If we define the efficiency of myocardial energy utilisation as the ratio of steady output power to $M\dot{V}O_2$ then, for these results at least, myocardial efficiency decreases with MAP. Again, this finding is correlated with the observed variation of peak left ventricular pressure and total developed power.

We must consider the apparent discrepancies between the myocardial oxygen consumption surfaces. The most obvious difference is in the variation of $M\dot{V}O_2$ with HR; in Fig. 5.13 the minimum is located at HR = 80 beats/min, while in Fig. 5.14 the minimum occurs at HR < 60 beats/min. From Figs. 5.9 and 5.10 it can be seen that the relative variation of both peak left ventricular

pressure and LVEDP was more pronounced in the first case than in the second.

The difference in the experimental conditions is most apparent if we consider the left ventricular function curves (Figs. 5.3c and 5.4c). In the first case the limits of ventricular pumping capacity were obviously approached at low heart rates, but this did not occur in the second case. We recall that left ventricular output was normalised with respect to the bodyweight of the experimental animal. However, the bodyweight was very much greater for the first experiment than for the second and this may have been the source of the apparent difference in volume loading.

It has been stated that the ability of the left ventricle to increase SV from an enlarged end-diastolic volume becomes progressively more limited. As the limits of left ventricular pumping capacity are approached very large increases in end-diastolic volume are required to produce a marginal increment in SV and, under these circumstances, developed transmural stress and per beat oxygen consumption will increase rapidly as HR is reduced. Thus, the observed nonlinear variation of $M\dot{V}O_2$ with HR can be related both to the increase in peak left ventricular pressure as HR is decreased and to the physical constraints on left ventricular function.

On the basis of the criteria already discussed, contractile state appeared to be constant for the experimental interventions on which these surfaces are based. For the first of these (Fig. 5.13) the preparation was extremely stable throughout the experiment, but in the second (Fig. 5.14) a spontaneous change in inotropic level occurred and it was necessary to discard some of the results. It should also be noted that in the second case no measurements were

obtained in the range $60 < HR < 80$ beats/min and thus less significance can be attached to the surface extrapolated in this region.

Finally, we consider the effect on $M\dot{V}O_2$ of changes in contractile state. The experimental results for myocardial oxygen utilisation at a reference level of noradrenaline infusion were characterized in the usual way. In Fig. 5.21a a function based on this analysis is compared with experimental $M\dot{V}O_2$ results for a higher level of noradrenaline infusion; left ventricular output and MAP were the same in both cases. It can be seen that a positive change in inotropic level results in a distinct increase in $M\dot{V}O_2$ for all values of HR. Unfortunately, no results were obtained here for the lower range of heart rates.

MYOCARDIAL OXYGEN SUPPLY AND DEMAND

It has been stated that the effective coronary perfusion pressure (the perfusion pressure during diastole) is an important determinant of maximal coronary blood supply. Thus, the index CBF given in 2.4.9 approximates the haemodynamic constraints on possible coronary supply.

In Figs. 5.15 and 5.16 we present two three dimensional "coronary supply" surfaces based on the experimental values of CBF. We have transformed these surfaces into units of myocardial oxygen consumption by arbitrarily choosing a fixed value for the coronary vascular resistance during diastole and assuming that coronary arteriovenous oxygen extraction is maximal.

It can be shown that

$$\text{coronary supply} = k\bar{P}_D \frac{T_D}{T} \qquad 5.3.2$$

k is a proportionality constant, $\bar{P}_D$ is the mean value of aortic pressure during diastole, T_D is the diastolic interval and T is the interbeat interval. This expression gives some insight into the observed variation of coronary supply with HR and MAP. For a given level of MAP, $\bar{P}_D$ was only slightly altered as HR decreased (Figs. 5.9b and 5.10b) and thus the variation in coronary supply with HR was determined by the relative variation of T_D and T. Further, reducing MAP at a fixed HR resulted in proportional decrease in $\bar{P}_D$ and therefore in coronary supply.

The relationship between myocardial oxygen supply and demand becomes clearer if we superimpose the experimental myocardial oxygen consumption and coronary supply surfaces on the same plot. Consider the intersection of the supply and demand surfaces in Figs.5.19 and 5.20. Below this line the effective coronary perfusion pressure is not sufficient to satisfy myocardial oxygen demand even under conditions of maximal coronary vasodilation. Reducing MAP further, or increasing HR, clearly worsens the imbalance of supply and demand. From these results it appears that the balance of myocardial oxygen supply and demand will be maximized at the lowest possible HR and the highest possible MAP.

Myocardial oxygen consumption is given by

$$M\dot{V}O_2 = CF(AO_2 - VO_2) \qquad 5.3.3$$

where CF is coronary flow, AO_2 is the arterial oxygen content and VO_2 is the coronary venous oxygen content. In general, AO_2 remains relatively constant and coronary flow is controlled by autoregulation such that coronary arteriovenous oxygen extraction (A-V O_2) is submaximal. Obviously, if oxygen extraction was complete coronary flow would be exactly correlated with $M\dot{V}O_2$. However, coronary flow is also influenced by haemodynamic and mechanical factors; thus any limitation of coronary supply should be reflected by an increase in A-V O_2.

We will consider the experimental variation of A-V O_2 in the light of the predictions made from the composite myocardial oxygen supply and demand surfaces. It was found that decreasing MAP at a given HR always resulted in an increase in A-V O_2 (Figs. 5.9f and 5.10f). Thus the experimental results are consistent with our prediction that the balance of myocardial oxygen supply and demand will be made worse by reducing MAP. However, for a fixed level of MAP, A-V O_2 was nonlinearly related to HR (Figs. 5.9e and 5.10e). The variation of oxygen extraction for the range $120 < HR < 200$ beats/min corresponds to the predicted improvement in the supply and demand balance with decreasing HR, but this correspondence is not maintained for low heart rates.

Possible coronary supply is dependent both on arterial pressure and the impedance of the coronary circulation under conditions of maximal vasodilation. For the coronary supply surfaces presented in Figs. 5.15 and 5.16 we have assumed that the coronary vascular resistance during diastole is constant. At low heart rates, though, ventricular enlargement will lead to constriction of the

coronary circulation. If HR is reduced, and the left ventricle further enlarged, the increase in coronary vascular resistance during diastole may limit coronary supply despite the improvement in effective perfusion pressure. The experimental variation of A-V O_2 with HR suggests that this is, in fact, the case. Apparently, therefore, the coronary supply surfaces presented here are not accurate for conditions of extreme volume loading.

These conclusions could have been reached from the coronary venous flow surfaces presented in Figs. 5.17 and 5.18. Clearly, the variation of coronary flow here was not determined entirely by autoregulation. In particular, it should be noted that coronary flow decreased monotonically with HR and thus the observed variation of $M\dot{V}O_2$ at low heart rates was due to increased oxygen extraction.

Finally, we consider the effect of an increase in contractile state on coronary flow. From Fig. 5.21b it can be seen that a positive change in inotropic level increased coronary venous flow for all heart rates; the corresponding results for $M\dot{V}O_2$ have already been discussed.

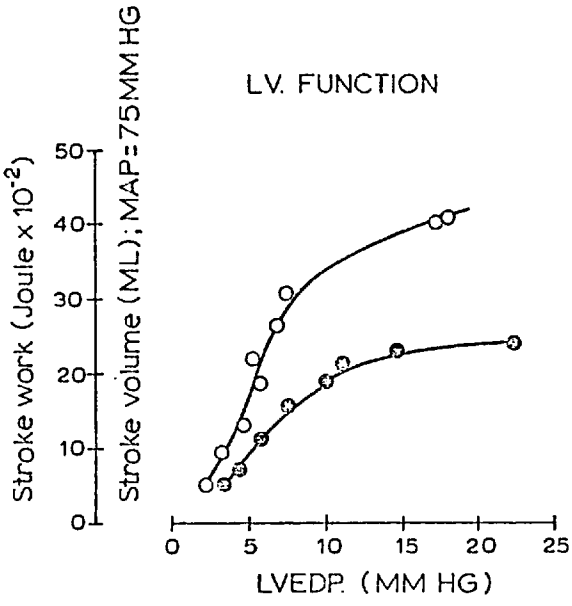

FIGURE 5.1: Relationship between L.V. stroke work and L.V. end-diastolic pressure; *After Sarnoff et al. (1960)* Both vagi cut. Heart rate constant at 171 beats/min.
o Increased inotropic level; stimulation of left stellate ganglion.
• Control

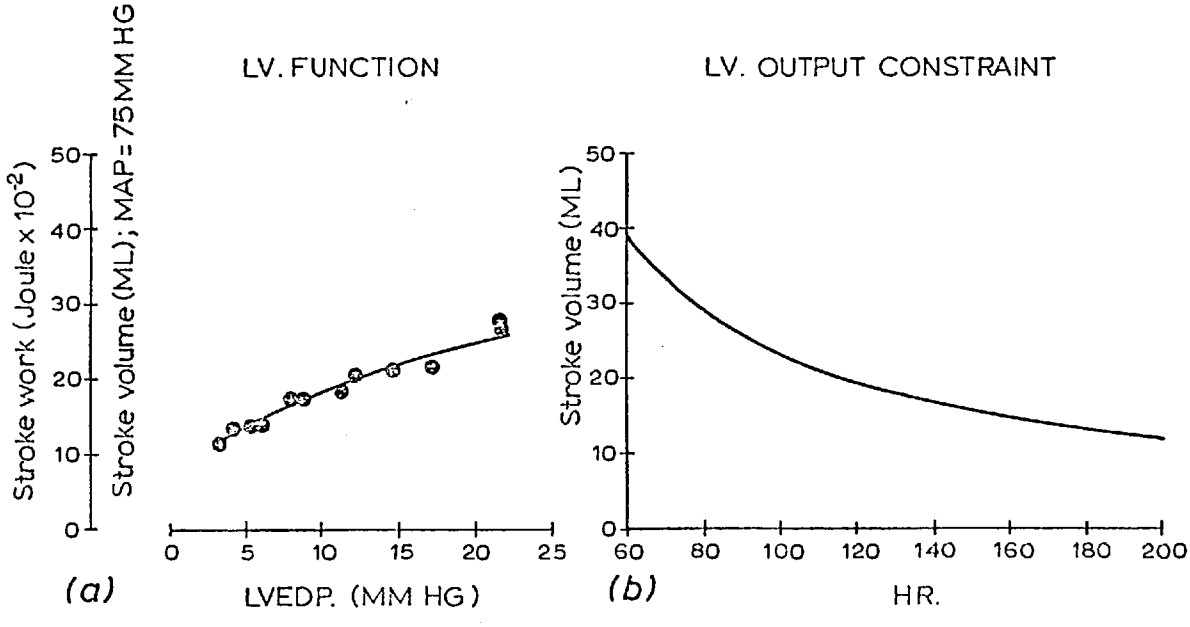

FIGURE 5.2: LV. pumping capacity in relation to the constraint on LV. output Exp. 1; Bodyweight 23 Kg, LV. output 2·3 L/min.

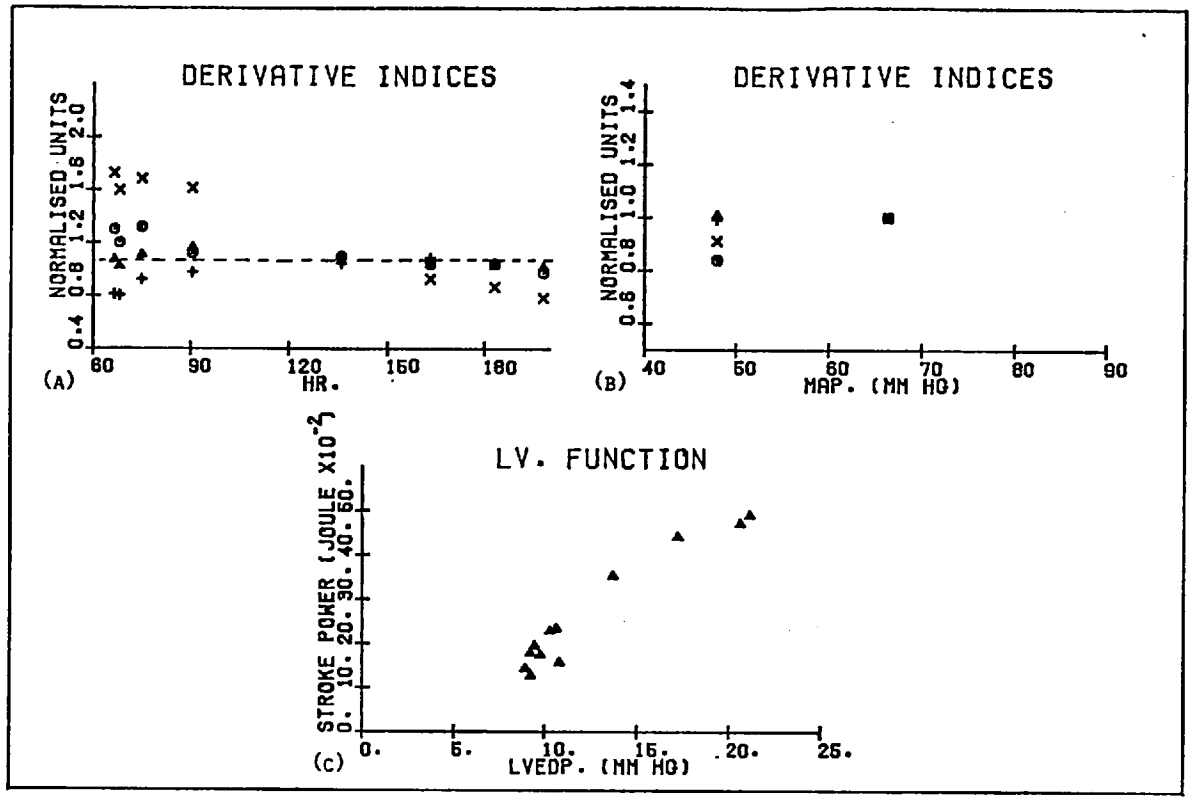

FIGURE 5.3: COMPARISON OF DIFFERENT INDICES OF CONTRACTILE STATE
EXP. 3; BODYWEIGHT 36 KG, LV. OUTPUT 3.6 L/MIN, INTRINSIC HR 136 BEATS/MIN
(A) VARIATION OF DERIVATIVE INDICES OF CONTRACTILE STATE WITH HEART RATE
(B) VARIATION OF DERIVATIVE INDICES OF CONTRACTILE STATE WITH MEAN ARTERIAL PRESSURE
$\odot - \frac{dP}{dt}_{LV}\Big)_{Max}$, $\times - \frac{d\dot{Q}}{dt}\Big)_{Max}$, $\blacktriangle - \frac{dP}{dt}_{LV}\Big)_{Max}/P^{O}_{LV}$, $+ - \frac{d\ln P}{dt}_{LV}\Big)_{Max}$
(C) LV. FUNCTION CURVE

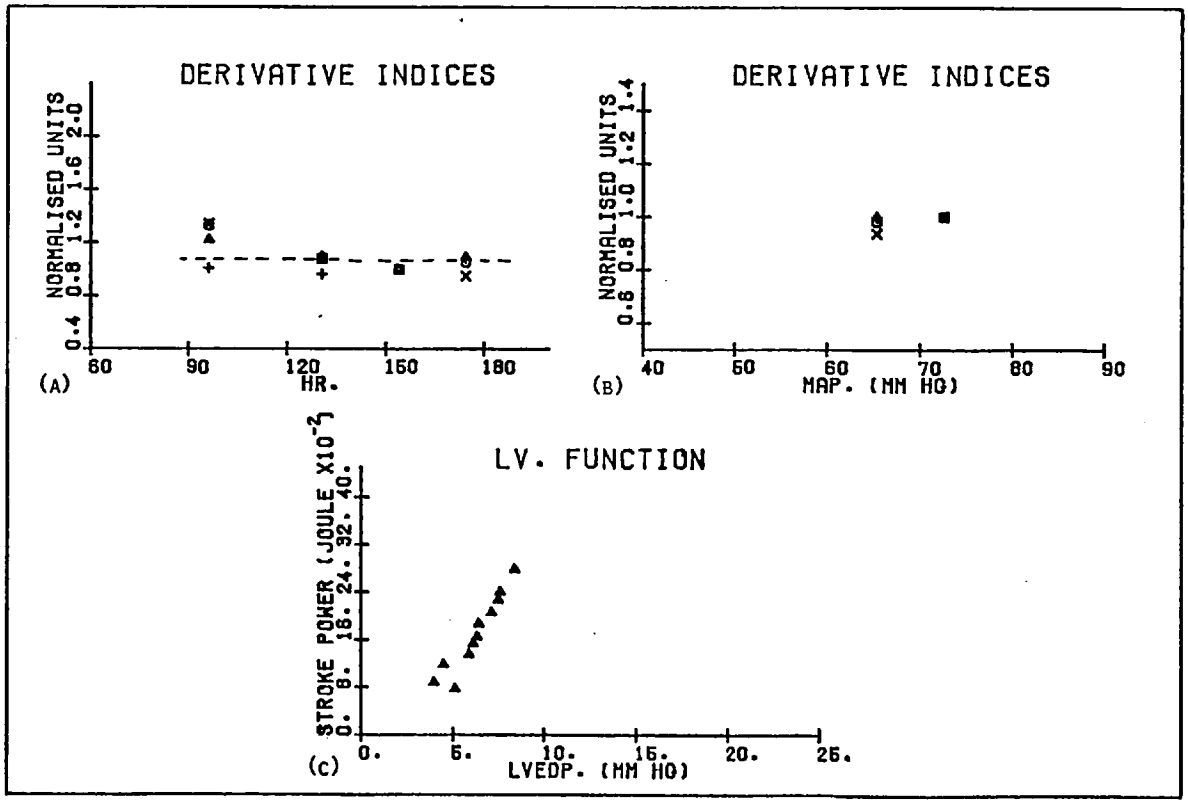

FIGURE 5.4: COMPARISON OF DIFFERENT INDICES OF CONTRACTILE STATE
EXP. 6; BODYWEIGHT 25 KG, LV. OUTPUT 2.5 L/MIN, INTRINSIC HR 130 BEATS/MIN

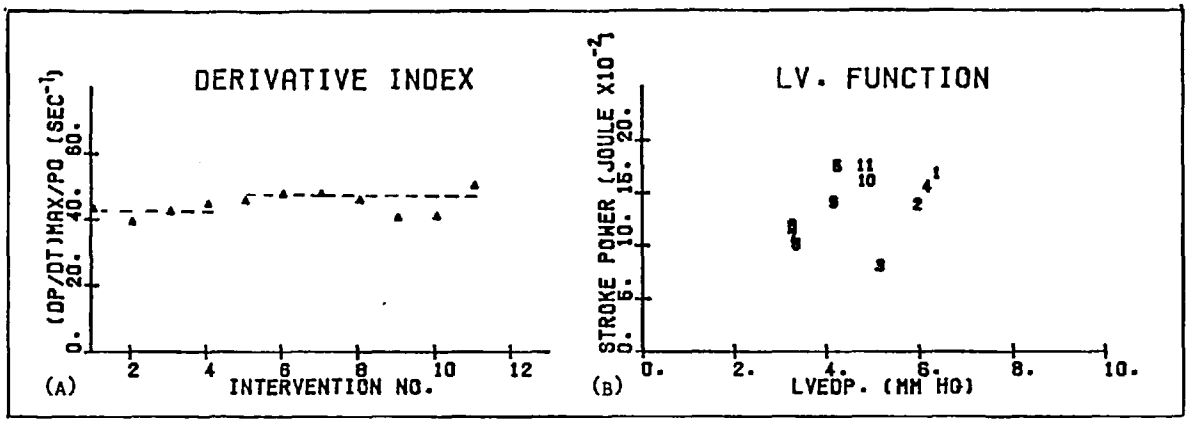

FIGURE 5.5: EFFECT OF CHANGING THE LEVEL OF CONTRACTILE STATE
EXP. 5; BODYWEIGHT 25 KG, LV. OUTPUT 2.5 L/MIN, INTRINSIC HR BEFORE AND AFTER CHANGE IN NORADRENALINE INFUSION RATE 121 BEATS/MIN AND 130 BEATS/MIN, RESPECTIVELY
(A) $\frac{dP}{dt}LV\Big)_{Max}/P^{0}_{LV}$ FOR SUCCESSIVE INTERVENTIONS (B) LV. FUNCTION CURVES

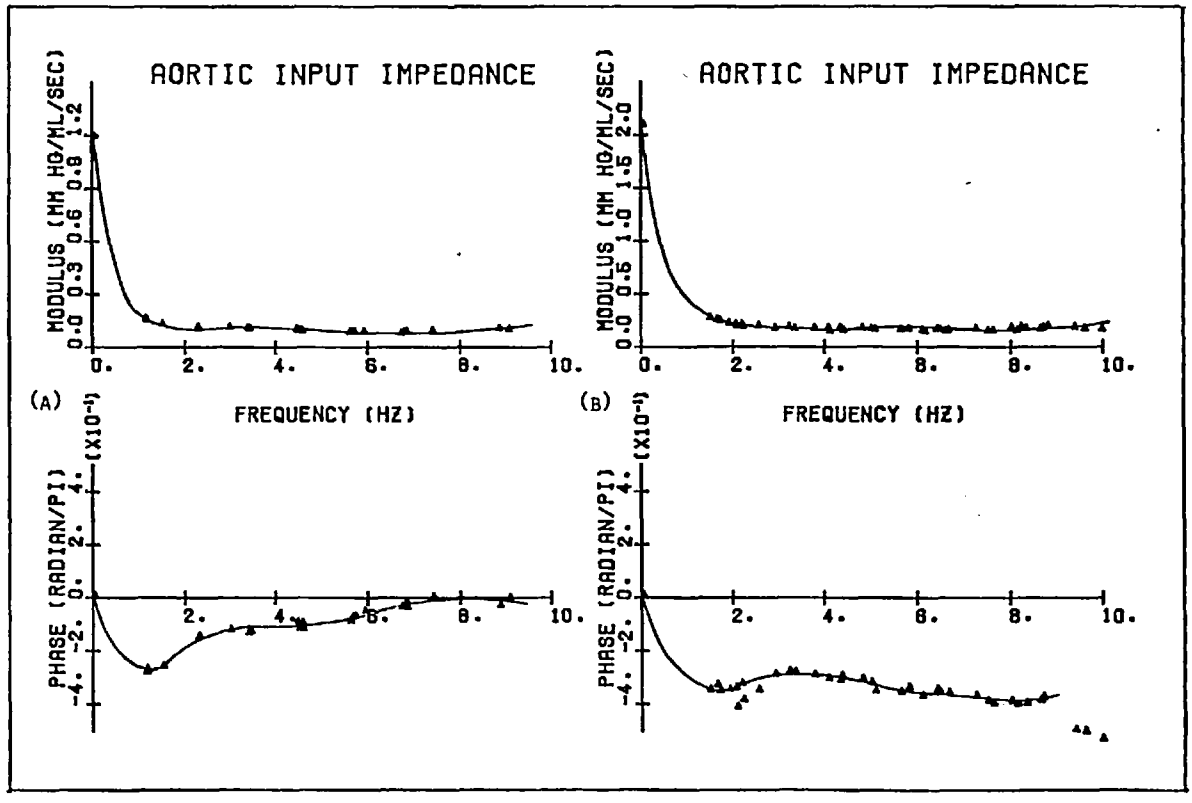

FIGURE 5.6: AORTIC INPUT IMPEDANCE SPECTRA; TYPICALLY THESE WERE AVERAGED OVER 20 CARDIAC CYCLES
(A) EXP. 3; MAP 65 MM HG (B) EXP. 6; MAP 65 MM HG

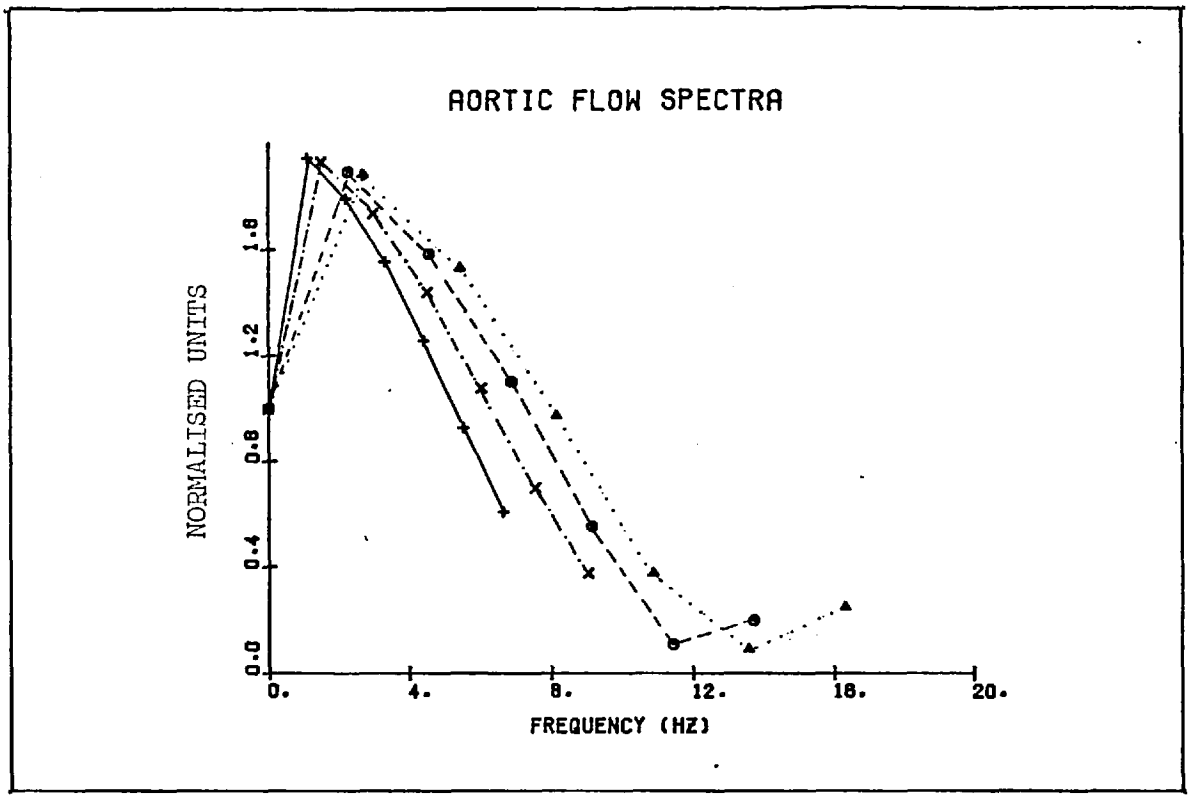

FIGURE 5.7: NORMALISED MODULI FOR THE FIRST SIX HARMONICS OF AORTIC FLOW AT DIFFERENT HEART RATES; EXP. 3.
+–+ HR 68 BEATS/MIN, x–x HR 89 BEATS/MIN, ⊙–⊙ HR 136 BEATS/MIN,
▲–▲ HR 164 BEATS/MIN

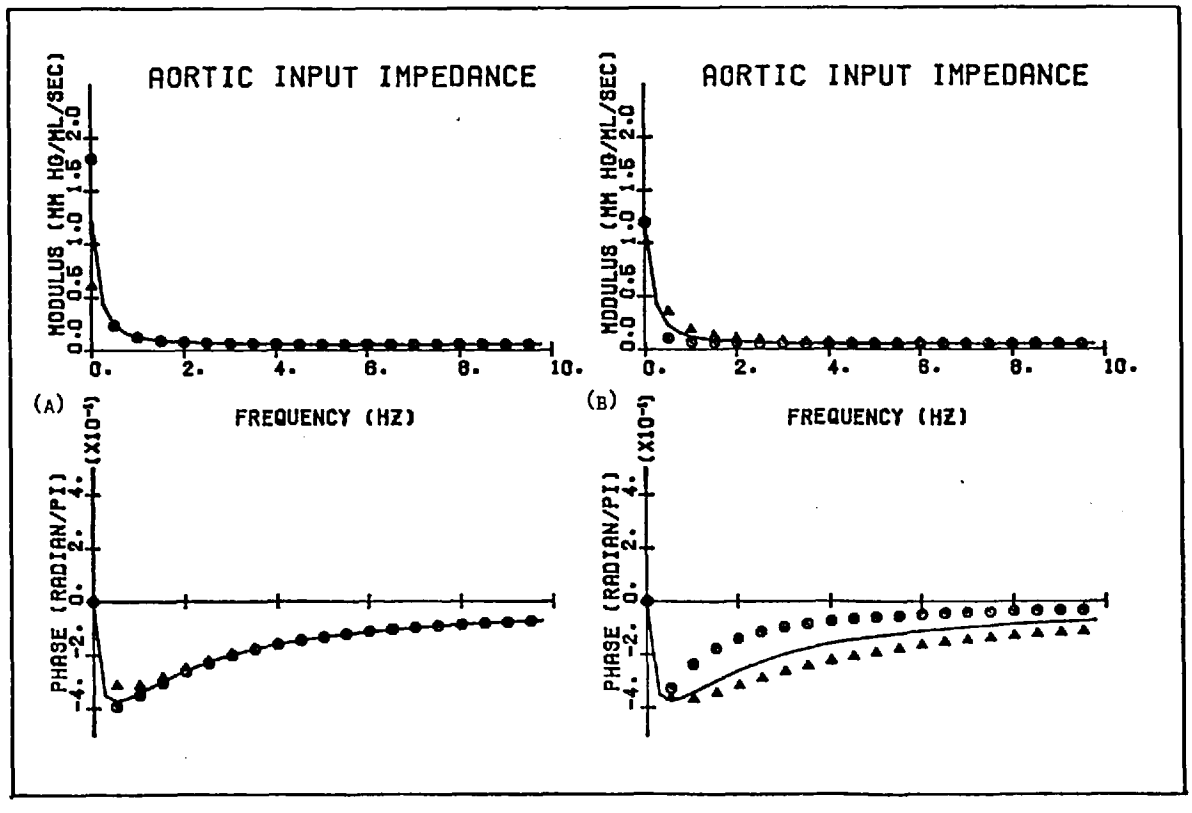

FIGURE 5.8: SIMULATION OF THE AORTIC INPUT IMPEDANCE SPECTRUM WITH A MODIFIED WINDKESSEL MODEL
REFERENCE CASE; R_p 1.15 MM HG/ML/SEC, R_c 0.05 MM HG/ML/SEC, K 0.7 MM HG/ML
(A) EFFECT OF VARYING PERIPHERAL RESISTANCE ▲ R_p 0.55 MM HG/ML/SEC,
⊙ R_p 1.75 MM HG/ML/SEC
(B) EFFECT OF VARYING ELASTIC COMPLIANCE ⊙ K 0.3 MM HG/ML,
▲ K 1.1 MM HG/ML

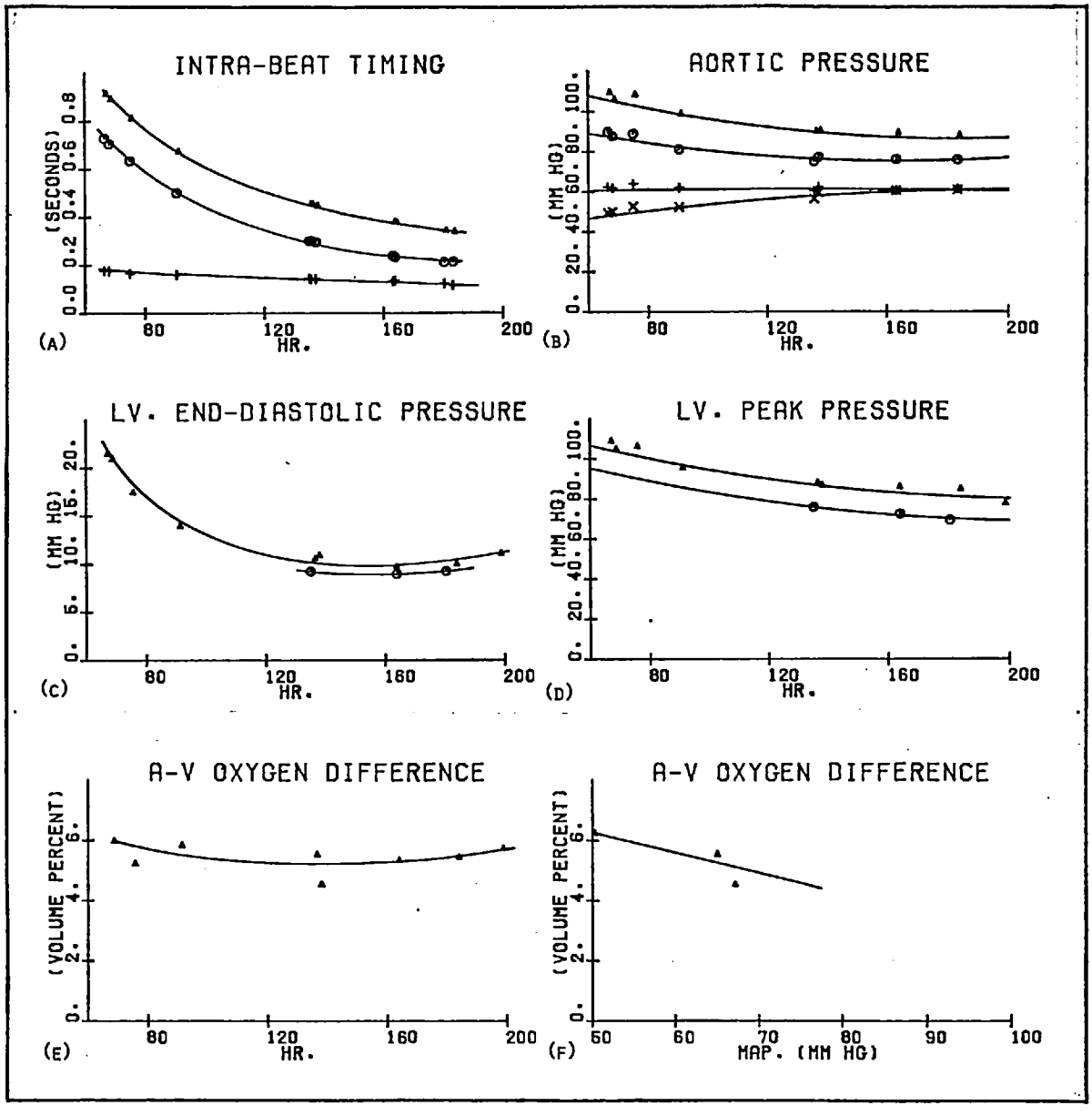

FIGURE 5.9: DETERMINANTS OF MYOCARDIAL OXYGEN CONSUMPTION AND POSSIBLE CORONARY SUPPLY; EXP. 3.

(A) VARIATION OF INTRA-BEAT TIMING WITH HEART RATE; ▲ INTERBEAT INTERVAL, ⊙ DIASTOLIC INTERVAL, + SYSTOLIC INTERVAL

(B) VARIATION OF AORTIC PRESSURE WITH HEART RATE; MAP 65 MM HG
▲ PEAK SYSTOLIC PRESSURE, ⊙ MEAN SYSTOLIC PRESSURE,
+ MEAN DIASTOLIC PRESSURE, X END-DIASTOLIC PRESSURE

(C) VARIATION OF LV. END-DIASTOLIC PRESSURE WITH HEART RATE
▲ MAP 65 MM HG, ● MAP 50 MM HG

(D) VARIATION OF PEAK LV. PRESSURE WITH HEART RATE
▲ MAP 65 MM HG, ⊙ MAP 50 MM HG

(E) VARIATION OF CORONARY A-V OXYGEN DIFFERENCE WITH HEART RATE; MAP 65 MM HG

(F) VARIATION OF CORONARY A-V OXYGEN DIFFERENCE WITH MEAN ARTERIAL PRESSURE; HR 136 BEATS/MIN

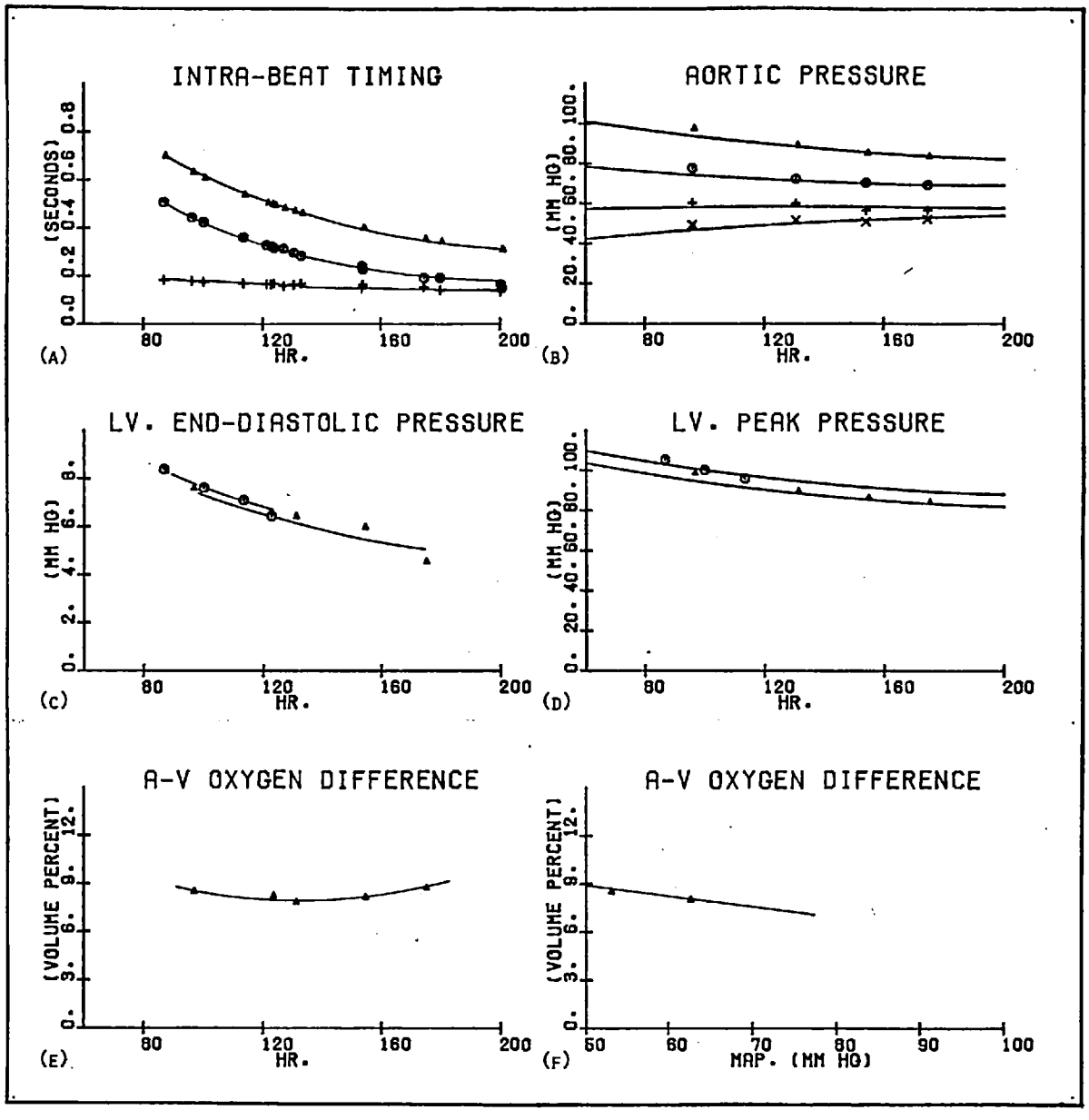

FIGURE 5.10: DETERMINANTS OF MYOCARDIAL OXYGEN CONSUMPTION AND POSSIBLE CORONARY SUPPLY; EXP. 6.

(A) VARIATION OF INTRA-BEAT TIMING WITH HEART RATE; ▲ INTERBEAT INTERVAL, ⊙ DIASTOLIC INTERVAL, + SYSTOLIC INTERVAL

(B) VARIATION OF AORTIC PRESSURE WITH HEART RATE; MAP 63 MM HG
▲ PEAK SYSTOLIC PRESSURE, ⊙ MEAN SYSTOLIC PRESSURE,
+ MEAN DIASTOLIC PRESSURE, × END-DIASTOLIC PRESSURE

(C) VARIATION OF LV. END-DIASTOLIC PRESSURE WITH HEART RATE
⊙ MAP 70 MM HG, ▲ MAP 63 MM HG

(D) VARIATION OF PEAK LV. PRESSURE WITH HEART RATE
⊙ MAP 70 MM HG, ▲ MAP 63 MM HG

(E) VARIATION OF CORONARY A-V OXYGEN DIFFERENCE WITH HEART RATE; MAP 63 MM HG

(F) VARIATION OF CORONARY A-V OXYGEN DIFFERENCE WITH MEAN ARTERIAL PRESSURE; HR 200 BEATS/MIN

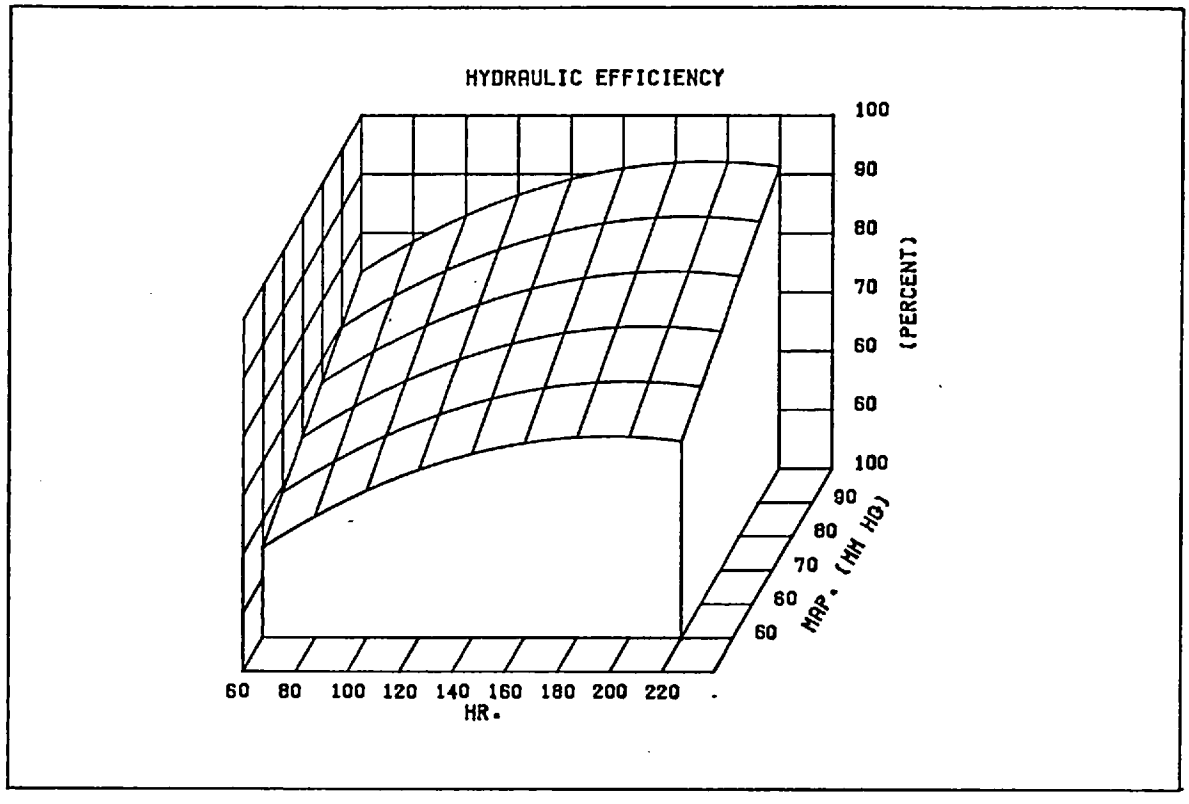

FIGURE 5.11: THREE DIMENSIONAL PLOT OF HYDRAULIC POWER TRANSFER EFFICIENCY; EXP. 3.

SUMMARY OF THE REGRESSION ANALYSIS TABLE 5.1

EFFICIENCY %	$16.4 + 0.415\ HR + 0.358\ MAP - 0.00108\ HR^2$								
HR BEATS/MIN	137.3	163.1	135.8	66.5	74.9	68.0	90.6	135.1	163.8
MAP MM HG	66.9	66.4	64.8	67.9	69.0	67.0	66.5	50.0	48.7
EFFICIENCY % (MEASURED)	77.8	78.8	76.2	63.4	64.7	65.2	68.8	70.5	72.9
EFFICIENCY % (CALCULATED)	77.0	79.1	76.1	63.6	66.2	63.7	69.0	70.7	72.9

ADJUSTED STANDARD ERROR OF ESTIMATE 1.055 ADJUSTED INDEX OF CORRELATION 0.984

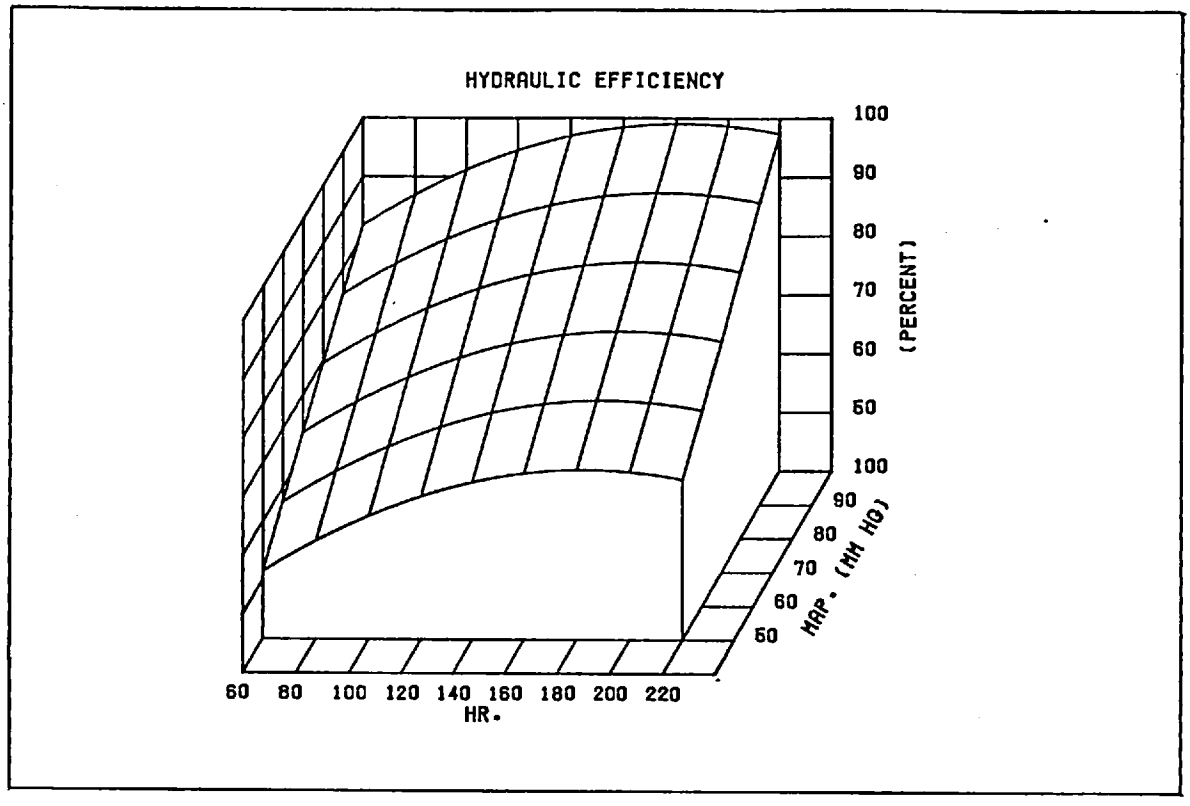

FIGURE 5.12: THREE DIMENSIONAL PLOT OF HYDRAULIC POWER TRANSFER EFFICIENCY; EXP. 6.

SUMMARY OF THE REGRESSION ANALYSIS TABLE 5.2

EFFICIENCY %	0.15 + 0.423 HR + 0.603 MAP - 0.00116 HR^2
HR BEATS/MIN	123.8 133.0 153.7 200.0 127.0 121.3 200.5 130.5 96.3 86.9 100.2 113.4 122.8
MAP MM HG	63.4 62.5 63.1 62.5 65.2 55.5 52.8 64.4 65.3 72.6 72.1 70.2 68.4
EFFICIENCY % (MEASURED)	71.6 73.0 74.3 76.0 74.6 68.6 70.0 76.2 69.8 71.2 74.3 76.0 76.8
EFFICIENCY % (CALCULATED)	73.0 73.6 75.8 75.6 74.5 67.9 70.3 74.4 69.5 72.0 74.4 75.6 75.8
ADJUSTED STANDARD ERROR OF ESTIMATE 1.076	ADJUSTED INDEX OF CORRELATION 0.992

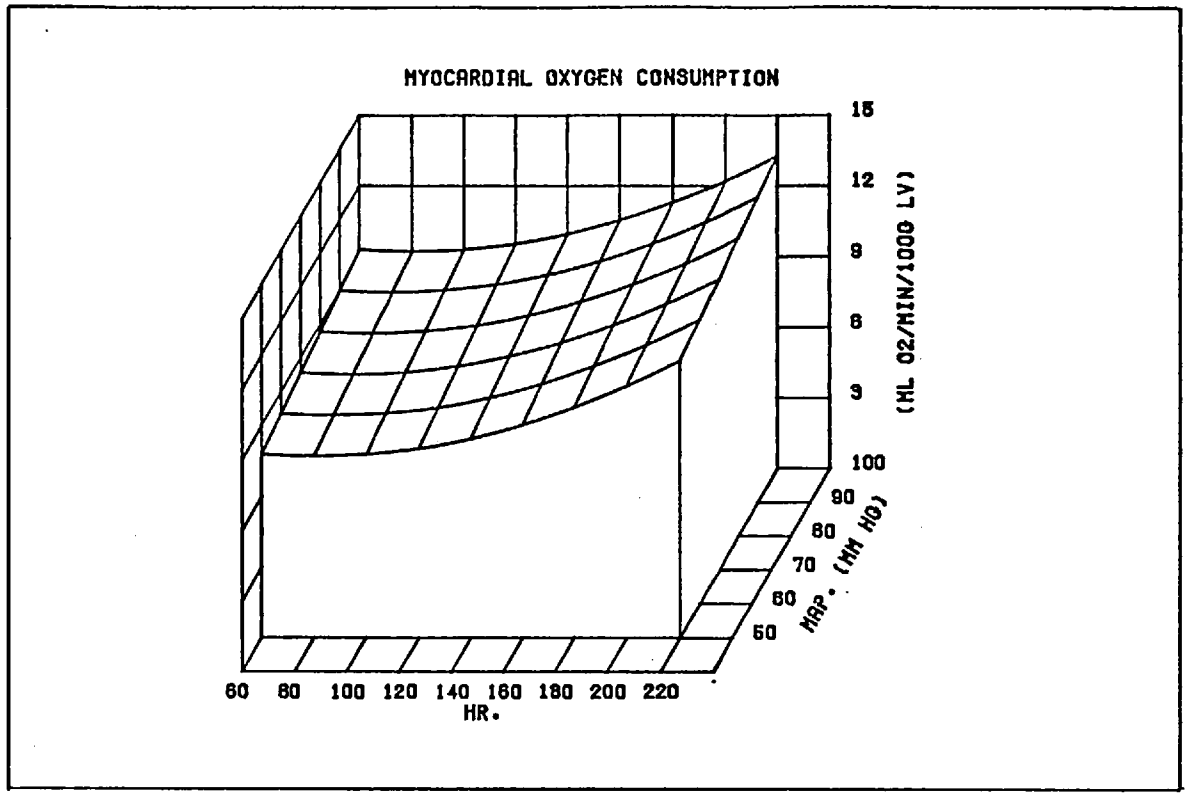

FIGURE 5.13: THREE DIMENSIONAL PLOT OF MYOCARDIAL OXYGEN CONSUMPTION; EXP. 3.

SUMMARY OF THE REGRESSION ANALYSIS TABLE 5.3

$\dot{M}VO_2$ ML O_2/MIN/100 G LV. $7.5 - 0.0325\ HR + 0.0299\ MAP + 0.000205\ HR^2$

HR BEATS/MIN	137.3	163.1	183.2	187.0	135.8	74.9	68.0	90.6	135.1	163.8	180.2
MAP MM HG	66.9	66.1	66.4	64.3	64.8	69.0	67.0	66.5	50.0	48.7	47.8
$\dot{M}VO_2$ ML O_2/MIN/100 G LV. (MEASURED)	7.84	9.83	10.27	11.04	9.82	7.85	8.16	8.97	8.38	8.20	10.44
$\dot{M}VO_2$ ML O_2/MIN/100 G LV. (CALCULATED)	8.91	9.64	10.42	11.04	8.81	8.28	8.28	8.23	8.35	9.14	9.74

ADJUSTED STANDARD ERROR OF ESTIMATE 0.788 ADJUSTED INDEX OF CORRELATION 0.731

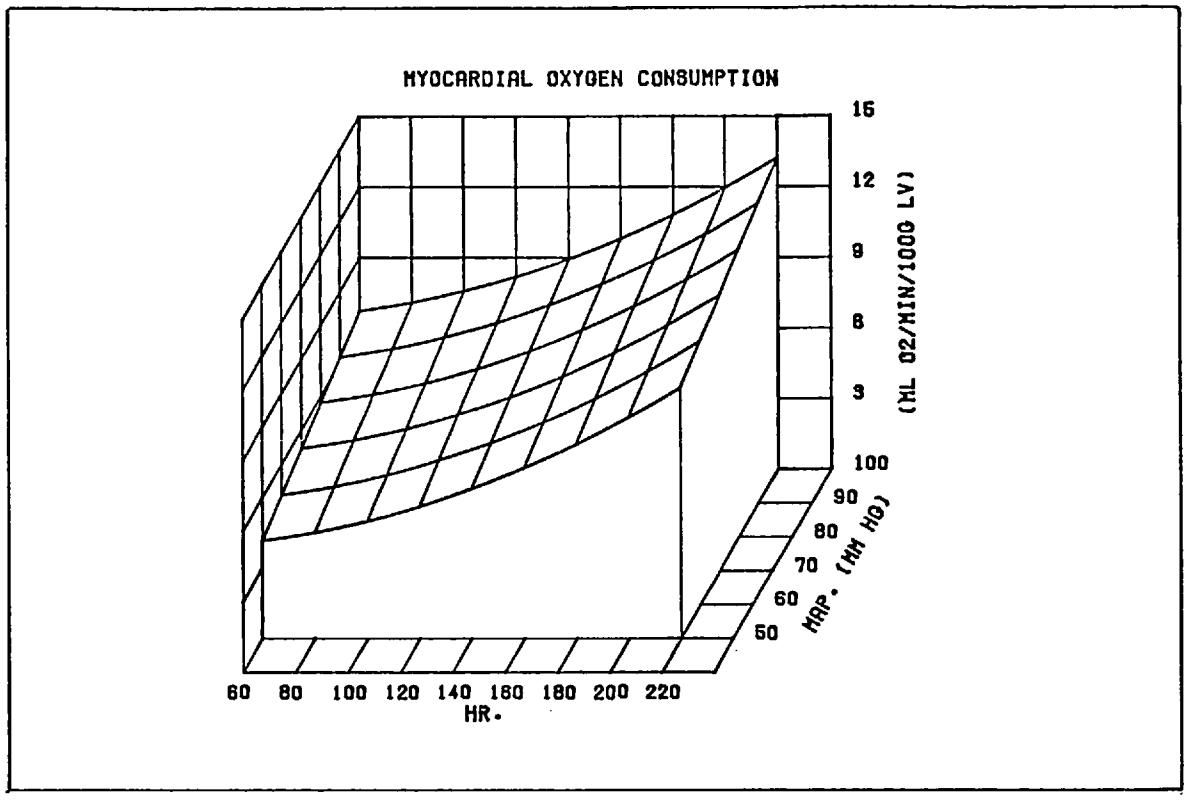

FIGURE 5.14: THREE DIMENSIONAL PLOT OF MYOCARDIAL OXYGEN CONSUMPTION; EXP. 6.

SUMMARY OF THE REGRESSION ANALYSIS TABLE 5.4

$\dot{M}VO_2$ ML O_2/MIN/100 G LV.	$1.37 - 0.0579\ HR + 0.0511\ MAP + 0.000166\ HR^2$									
HR BEATS/MIN	121.3	200.5	174.5	154.0	130.5	96.3	86.9	100.2	113.5	122.8
MAP MM HG	55.5	52.8	62.2	62.3	64.4	65.3	72.6	72.1	70.2	68.4
$\dot{M}VO_2$ ML O_2/MIN/100 G LV. (MEASURED)	5.72	9.46	8.72	7.90	6.60	6.21	6.75	5.88	6.50	6.49
$\dot{M}VO_2$ ML O_2/MIN/100 G LV. (CALCULATED)	5.95	9.58	8.59	7.60	6.73	5.69	5.83	6.14	6.44	6.66
ADJUSTED STANDARD ERROR OF ESTIMATE 0.308								ADJUSTED INDEX OF CORRELATION 0.972		

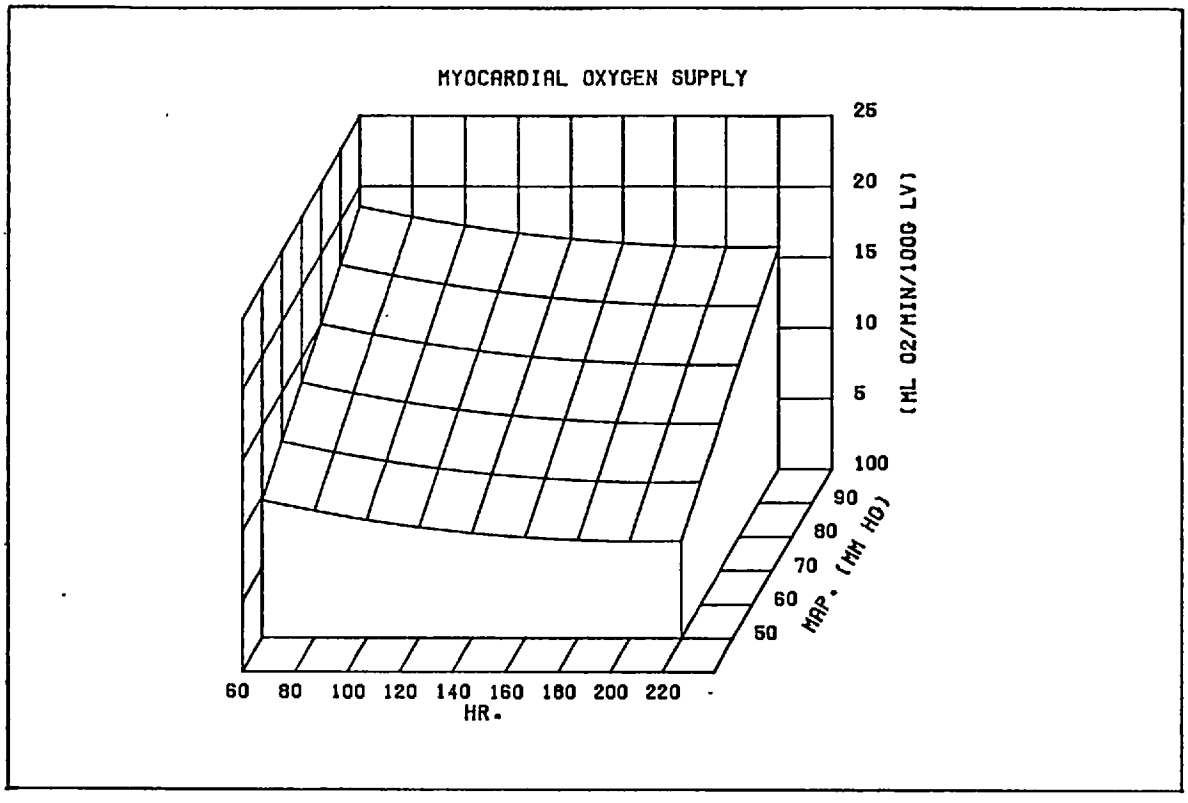

FIGURE 5.15: THREE DIMENSIONAL PLOT OF POSSIBLE CORONARY SUPPLY; EXP. 3.

SUMMARY OF THE REGRESSION ANALYSIS TABLE 5.5

SUPPLY ML O_2/MIN/100 G LV.	$3.8 - 0.056\ HR + 0.167\ MAP + 0.000137\ HR^2$										
HR BEATS/MIN	137.3	163.1	183.2	135.8	66.5	74.9	68.0	90.6	135.1	163.8	180.2
MAP MM HG	66.9	66.1	66.4	64.8	67.9	69.0	67.0	66.5	50.0	48.7	47.8
SUPPLY ML O_2/MIN/100 G LV. (MEASURED)	10.5	9.7	9.9	10.2	12.6	12.7	12.3	11.7	7.5	6.8	6.7
SUPPLY ML O_2/MIN/100 G LV. (CALCULATED)	10.5	10.0	9.8	10.1	12.7	12.5	12.4	11.6	7.5	6.9	6.6

ADJUSTED STANDARD ERROR OF ESTIMATE 0.130 ADJUSTED INDEX OF CORRELATION 0.998

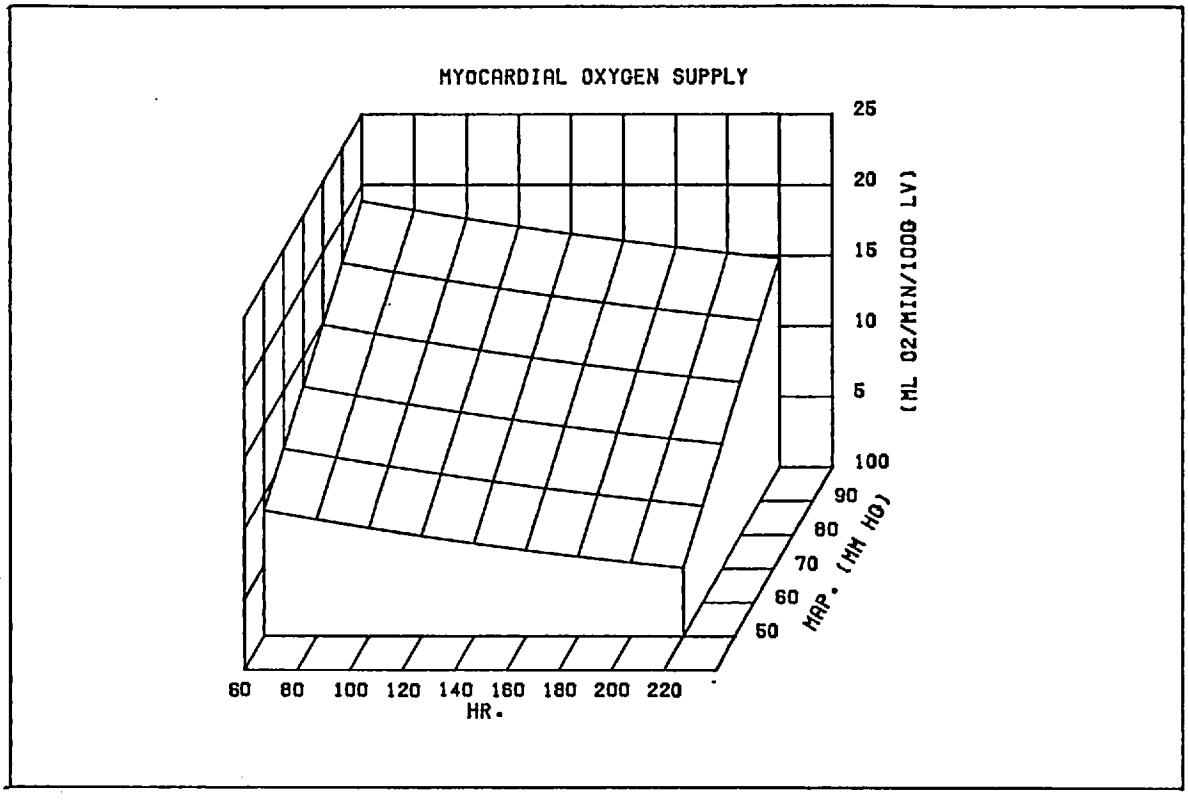

FIGURE 5.16: THREE DIMENSIONAL PLOT OF POSSIBLE CORONARY SUPPLY; EXP. 6.

SUMMARY OF THE REGRESSION ANALYSIS TABLE 5.6

SUPPLY ML O_2/MIN/100 G LV.	1.12 - 0.0387 HR + 0.199 MAP + 0.000048 HR^2									
HR BEATS/MIN	123.8	133.0	153.7	179.9	200.0	218.3	127.0	121.3	226.3	200.5
	174.5	154.0	130.5	96.3	86.9	100.2	113.5	122.8		
MAP MM HG	63.4	62.5	63.1	62.3	62.5	63.5	65.2	55.5	52.1	52.8
	62.2	62.3	64.4	65.3	72.6	72.1	70.2	68.4		
SUPPLY ML O_2/MIN/100 G LV. (MEASURED)	9.7	9.2	9.1	8.2	7.9	7.7	10.0	8.4	5.1	5.8
	7.9	8.3	9.7	10.8	12.5	12.0	11.3	10.6		
SUPPLY ML O_2/MIN/100 G LV. (CALCULATED)	9.7	9.3	8.9	8.1	7.7	7.6	10.0	8.2	5.2	5.8
	8.2	8.7	9.7	10.8	12.6	12.1	11.3	10.7		

ADJUSTED STANDARD ERROR OF ESTIMATE 0.189 ADJUSTED INDEX OF CORRELATION 0.995

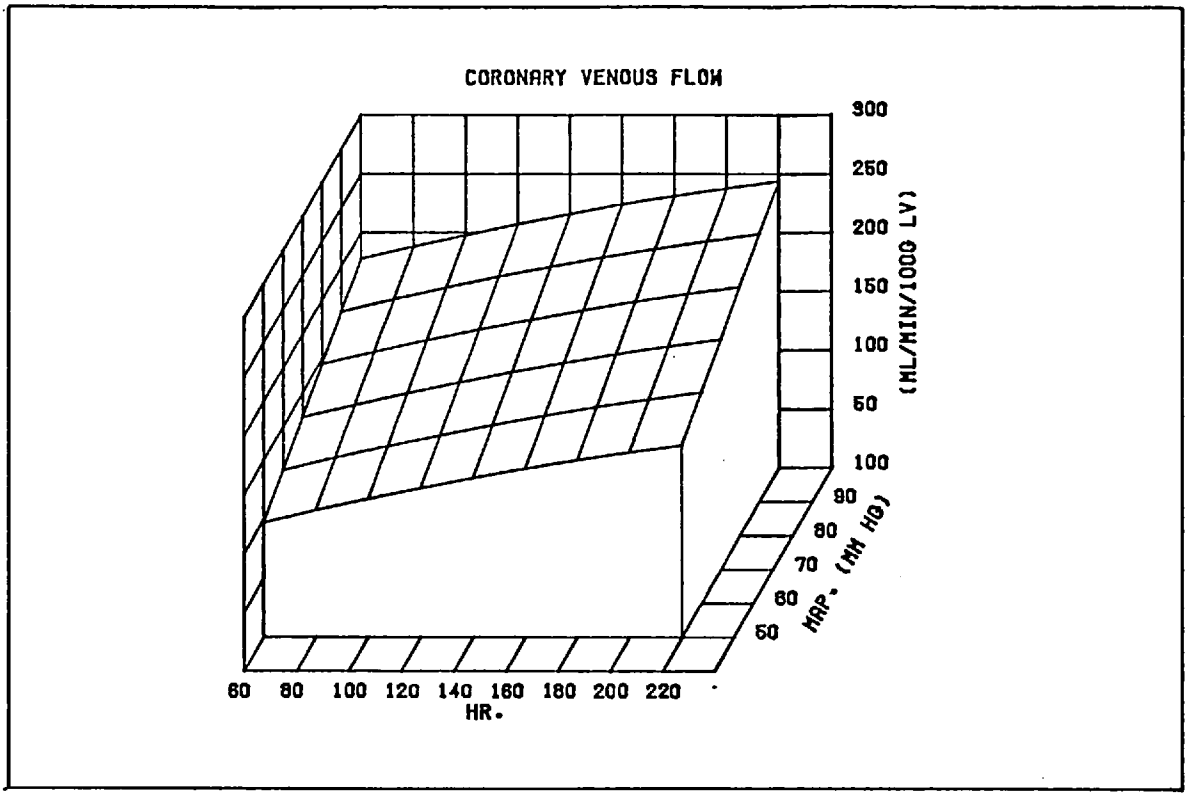

FIGURE 5.17: THREE DIMENSIONAL PLOT OF CORONARY VENOUS FLOW; EXP. 3.

SUMMARY OF THE REGRESSION ANALYSIS TABLE 5.7

CV FLOW ML/MIN/100 G LV.	$-18.5 + 0.638\ HR + 1.61\ MAP - 0.000805\ HR^2$								
HR BEATS/MIN	137.3	163.1	183.2	187.0	135.8	74.9	68.0	90.6	135.1
	163.8	180.2							
MAP MM HG	66.9	66.1	66.4	64.3	64.8	69.0	67.0	66.5	50.0
	48.7	47.8							
CV FLOW ML/MIN/100 G LV. (MEASURED)	160.2	170.2	174.6	177.7	163.8	138.5	125.8	141.8	124.0
	143.8	154.6							
CV FLOW ML/MIN/100 G LV. (CALCULATED)	161.5	170.4	178.1	179.8	157.5	135.7	128.8	139.7	133.4
	142.7	154.6							

ADJUSTED STANDARD ERROR OF ESTIMATE 5.67 ADJUSTED INDEX OF CORRELATION 0.954

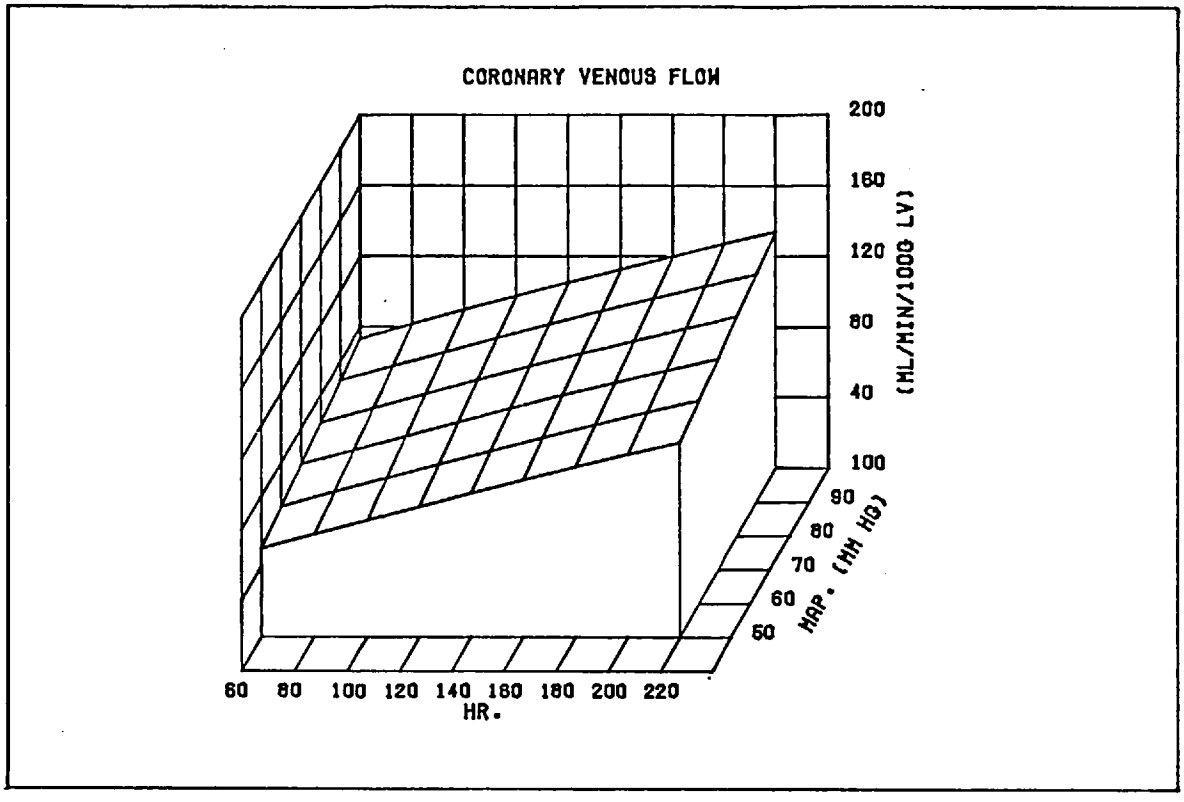

FIGURE 5.18: THREE DIMENSIONAL PLOT OF CORONARY VENOUS FLOW; EXP. 6.

SUMMARY OF THE REGRESSION ANALYSIS TABLE 5.8

CV FLOW ML/MIN/100 G LV.	$0.879 + 0.447\ HR + 0.465\ MAP - 0.000248\ HR^2$								
HR BEATS/MIN	121.3	226.3	200.5	174.5	154.0	130.5	96.3	86.9	100.2
	113.5	122.8							
MAP MM HG	55.5	52.1	52.8	62.2	62.3	64.4	65.3	72.6	72.1
	70.2	68.4							
CV FLOW ML/MIN/100 G LV. (MEASURED)	75.4	113.4	104.0	101.4	98.7	85.7	74.4	74.6	74.4
	77.4	80.7							
CV FLOW ML/MIN/100 G LV. (CALCULATED)	77.2	113.5	105.0	100.2	92.7	84.8	72.0	71.6	76.7
	81.0	83.8							

ADJUSTED STANDARD ERROR OF ESTIMATE 3.642 ADJUSTED INDEX OF CORRELATION 0.967

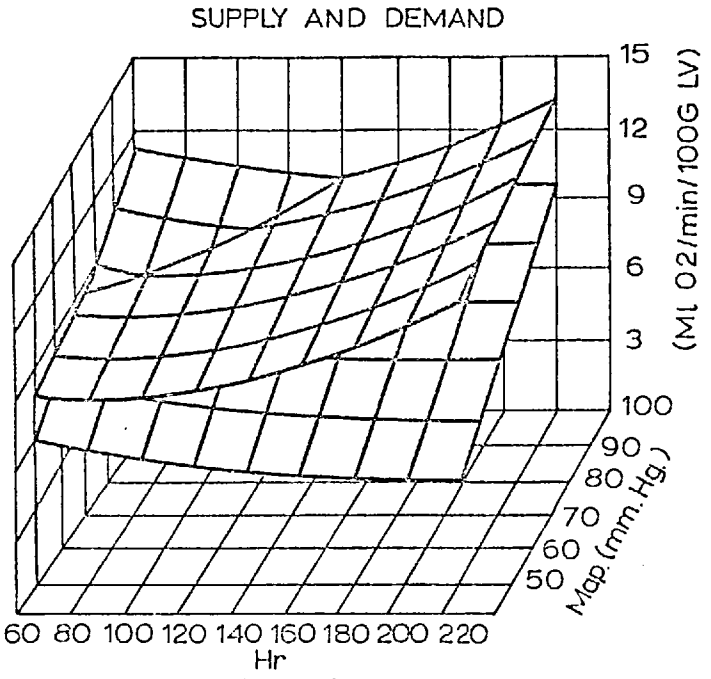

FIGURE 5.19: Composite three dimensional supply and demand plots; Exp. 3.

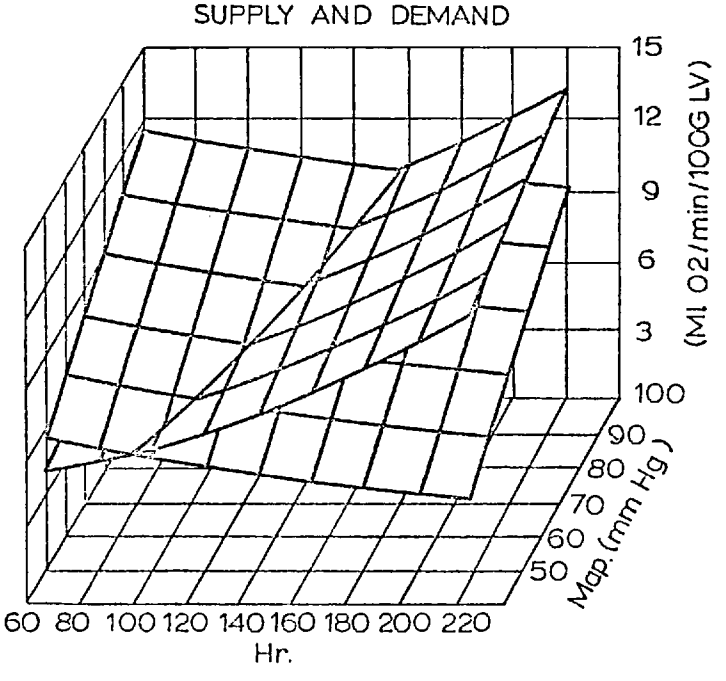

FIGURE 5.20: Composite three dimensional supply and demand plots; Exp. 6.

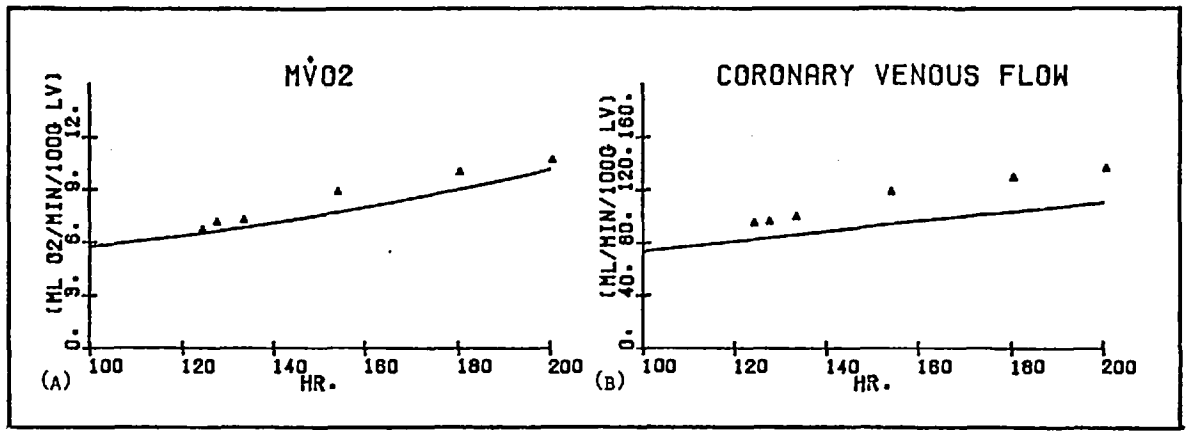

FIGURE 5.21: EFFECT OF CHANGING THE LEVEL OF CONTRACTILE STATE; EXP. 5.
(A) MYOCARDIAL OXYGEN CONSUMPTION BEFORE —— AND AFTER ▲ AND AFTER AN INCREASE IN NORADRENALINE INFUSION RATE
(B) CORONARY VENOUS FLOW BEFORE AND AFTER AN INCREASE IN NORADRENALINE INFUSION RATE

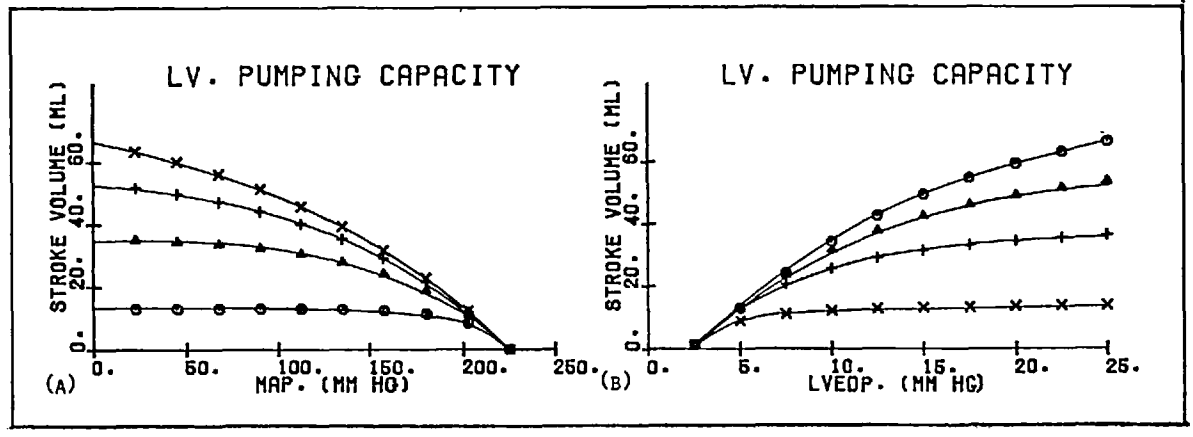

FIGURE 5.22: LV. PUMPING CAPACITY AS A FUNCTION OF LV. END-DIASTOLIC PRESSURE AND MEAN ARTERIAL PRESSURE; (AFTER SAGAWA, 1967)
(A) × LVEDP 20 MM HG, + LVEDP 15 MM HG, ▲ LVEDP 10 MM HG, ⊙ LVEDP 5 MM HG
(B) ⊙ MAP 50 MM HG, ▲ MAP 100 MM HG, + MAP 150 MM HG, × MAP 200 MM HG

5.4 DISCUSSION

The aim of this study is to establish whether the concept of optimal cardiac function has any realistic practical basis. To this extent, the series of experiments described in these chapters may be regarded as a feasibility study of a specific multi-variate systems approach. In particular we wished to obtain experimental performance surfaces for several indices of left ventricular "cost" and to investigate the underlying factors which determine these surfaces. This was seen as a possible basis for the analysis of specific aspects of normal and pathological left ventricular function.

The results will be discussed in the light of these aims. First, though, we consider the adequacy of the experimental method.

It has been stated that the success of the experimental approach used here depends on:

- the ability to control left ventricular output, peripheral resistance, contractile state and heart rate over the normal physiological range
- the stability with which the preparation can be maintained
- the speed and accuracy with which measurements can be made

The emphasis on stability and control suggests the use of either an isolated heart or heart-lung preparation. This would, however, have introduced a number of difficult problems in the simulation of a physiological peripheral circulation and the maintenance of normal metabolism. The modified right

heart bypass preparation used here provided a compromise between the requirements of stability and control and the need to maintain " normal physiology "; Section 4.1, Fig. 4.1. With this preparation it was possible to satisfy the most important of the requirements listed above. There were, however, a number of inherent problems.

Although the technique of vagal stimulation was used in several instances to produce steady low heart rates the method was difficult to apply and not always reliable. Also, the use of spinal anaesthetic led to a reduction in MAP which could not be entirely corrected by intravenous noradrenaline infusion. In general, therefore, the experimental preparations tended to be hypotensive and, using the femoral arteriovenous shunt, MAP could only be reduced further. Thus, it was possible to vary MAP over a limited range only. Finally, the determination of oxygen content was time consuming and, despite careful analysis and duplicate checking of the results, more subject to error than any other experimental measurement.

In all other respects the experimental and analytical techniques used proved satisfactory. We must, however, emphasize the importance of a rationally planned experimental protocol here. Bi-variate nonlinear regression analysis was used extensively both for the presentation and the interpretation of experimental data; the accuracy of this method depends entirely on adequate sampling with respect to the independent variables HR and MAP. Further, it was essential that these experimental samples should relate to the same level of contractile state. Two criteria were used: the nature of the left ventricular function curve and the variation of the intrinsic heart rate. On this

basis it was possible to detect a spontaneous shift in inotropic level and to discard any results effected from the analysis. However, this approach could not be used to correct for slow drifts in the functional state of the preparation. Where possible, the HR, MAP values for successive interventions were ordered so that time dependent errors would be evenly spread throughout the range of the independent variables and thus averaged out in the regression analysis. Clearly, therefore, it is necessary to consider the number, the range and the order of the interventions when planning the protocol for an experiment of this type.

The most striking of the experimental results is the apparent existence of a heart rate for which $M\dot{V}O_2$ is minimized. This has not previously been demonstrated. We found also that the effective coronary perfusion pressure was closely correlated with MAP, but that the relative variation of $M\dot{V}O_2$ with MAP was proportionately less than the change in MAP. Thus, although $M\dot{V}O_2$ is reduced by lowering MAP, the balance of myocardial oxygen supply and demand may be made worse; the experimental variation of coronary A-V O_2 with MAP was consistent with this prediction. These results are of some interest. More important, though, is the insight which they give into the complex interactions that determine myocardial oxygen consumption and the supply of coronary blood flow.

The left ventricle is a pulsatile pump. The total power required to generate a given steady output is determined by the aortic input impedance and varies with SV and HR. It has been shown that the efficiency of hydraulic

power transfer is lowered under conditions of reduced peripheral loading and, for a fixed left ventricular output, the decrease in total developed power and peak left ventricular pressure with MAP was proportionately less than the reduction in MAP. While $M\dot{V}O_2$ is not well correlated with the steady power developed by the left ventricle total developed power and, more directly, peak developed pressure are both important determinants of $M\dot{V}O_2$. Thus the observed variation of $M\dot{V}O_2$ with MAP can be related to the characteristics of the hydraulic load presented to the left ventricle.

Additionally, it has been shown that the relative variation of peak left ventricular pressure and total developed power with HR becomes more pronounced under conditions of reduced peripheral loading. The increase in peak developed pressure as HR is decreased may contribute to the experimental dependence of $M\dot{V}O_2$ on HR. However, it appears that the physical constraints on left ventricular function are also an important determinant of the observed nonlinear variation of $M\dot{V}O_2$ with HR.

We recall that in these experiments left ventricular output was fixed and thus a reduction in HR led to an increase in SV. However, the ability of the left ventricle to increase SV from an enlarged end-diastolic volume becomes progressively more limited. As the limits of ventricular pumping capacity are approached very large increases in end-diastolic volume are required to produce a marginal increment in SV and, under these circumstances, developed transmural stress and per beat myocardial oxygen consumption will increase rapidly as HR is reduced.

The capacity of the left ventricle to increase SV is not determined by the end-diastolic volume alone. For a fixed level of contractile state left ventricular function is dependent on both pressure and volume loading and the nature of this dependence is clearly represented in Fig. 5.22. It can be seen that if MAP is increased a larger end-diastolic volume will be required to produce the same SV. At high levels of pressure loading this may result in left ventricular dilation and an associated reduction in the efficiency of left ventricular function. Thus, if we are correct in our analysis of the physical limitations on ventricular pumping capacity and the constraints which this imposes on cardiac performance, either increasing left ventricular output or raising MAP should lead to a more pronounced nonlinear variation of $M\dot{V}O_2$ with HR. Further, the variation of $M\dot{V}O_2$ with MAP must be more complex than the simple linear dependence presented in Figs. 5.13 and 5.14. We note that these surfaces were derived from experimental results for a restricted range of mean arterial pressures.

The myocardial oxygen consumption surfaces are also used in the composite supply and demand plots. Thus, the qualifications expressed in the previous paragraph must apply in this case too. Additionally, the supply surfaces for these plots were derived from a simple index for the effective coronary perfusion pressure and describe the haemodynamic constraints on diastolic coronary supply, only. Possible coronary supply is determined both by the arterial pressure and the impedance of the coronary circulation under conditions of maximal vasodilation. Therefore, the supply surfaces presented here may not adequately reflect the variation of possible coronary supply with HR and MAP.

For a given level of MAP, effective coronary perfusion pressure is reduced continuously as HR is increased: left ventricular output is assumed to be fixed, SV and HR are inversely related. In addition, the frequency of contraction is a primary determinant of $M\dot{V}O_2$ and normally the balance of myocardial oxygen supply demand is made worse by increasing HR. However, if the left ventricle is operating close to the limits of its pumping capacity, ventricular enlargement will lead to constriction of the coronary circulation. If HR is reduced, and the ventricle further enlarged, the increase in diastolic coronary vascular impedance may limit coronary supply despite the improvement in effective perfusion pressure. We have stated that the observed nonlinear variation of $M\dot{V}O_2$ can be related to the physical constraints on left ventricular function. It follows also that there may be a range of heart rates for which the balance of myocardial oxygen supply and demand is maximized and the experimental variation of coronary A-V O_2 with HR is consistent with this prediction.

Very similar comments apply to the relationship between MAP and the balance of myocardial oxygen supply and demand. We have shown that, if MAP is reduced below normal levels, the supply and demand balance becomes worse. If MAP is increased, though, a larger end-diastolic volume is required to generate a given SV and at some stage the limits on left ventricular pumping capacity will be reached. As this level of pressure loading is approached $M\dot{V}O_2$ will begin to increase nonlinearly with MAP, while the mechanical constriction of the coronary vascular bed, associated with ventricular enlargement, will tend to limit possible coronary supply. Again, it follows

that there may be a range of mean arterial pressures for which the balance of myocardial oxygen supply and demand is maximized.

Myocardial oxygen consumption is always reduced by lowering MAP. Clearly, therefore, our optimal systems analysis of supply and demand cannot be extended to myocardial oxygen consumption alone. We consider instead a closely related index of left ventricular performance; the efficiency of myocardial energy utilisation. This is defined as the ratio of steady output power to $M\dot{V}O_2$ and, for a fixed left ventricular pressure, steady power is directly proportional to MAP. It can be seen from our experimental results that, for reduced levels of pressure loading, the efficiency of myocardial energy utilisation is decreased by lowering MAP. We have also stated that, for high levels of pressure loading, $M\dot{V}O_2$ will increase nonlinearly with MAP and in these circumstances the efficiency of myocardial energy utilisation will be decreased by raising MAP. For a fixed MAP steady power is constant and the observed nonlinear variation of $M\dot{V}O_2$ with HR corresponds to the maximization of the efficiency of myocardial energy utilisation.

Two indices of left ventricular performance have been discussed here: the efficiency of myocardial energy utilisation and the balance of myocardial oxygen supply and demand; and we have argued that it may be possible to find different values of HR and MAP for which both are maximized. It has been shown that the possible existence of nontrivial optimal conditions is largely determined by the physical constraints on left ventricular pumping capacity. Ventricular pumping capacity reflects the functional state of the myocardium and is enhanced by an increase in inotropic level. Also, our experimental findings

confirm the established result that, under normal conditions, an increase in contractile state will lead to an increase in $M\dot{V}O_2$. Thus, the level of contractile state must also directly influence the possible optimization of left ventricular performance.

We have stated that the minimization of $M\dot{V}O_2$ with HR has not previously been demonstrated. It is essential, therefore, to critically assess the accuracy of the experimental measurements on which this result is based.

The possible sources of experimental error have already been listed and discussed. Of these, the uncertainty in the measurement of coronary A-V O_2 is clearly the most significant and this is immediately obvious if we compare the standard error of estimate for the myocardial oxygen consumption surfaces with the standard error for any other regression surface. For the experimental results presented here, coronary flow decreased monotonically and therefore the observed variation of $M\dot{V}O_2$ with HR in the range $60 < HR < 120$ beats/min was due entirely to an increase in the values of A-V O_2. In the course of two experiments seven determinations only of A-V O_2 were made in this range. The results are similar in both cases and it has been shown that the nonlinear dependence of $M\dot{V}O_2$ on HR is consistent with the variation of known determinants of $M\dot{V}O_2$. However, given the number and possible uncertainty of the significant measurements of oxygen extraction, we are forced to conclude that this result has not been established absolutely.

We have been concerned here with the investigation of different aspects of left ventricular "cost". The experimental variation of $M\dot{V}O_2$ with HR and MAP has been related both to the nature of the hydraulic load presented to the left ventricle and to the physical limits on left ventricular function. The constraints on possible coronary supply have also been considered. From this we have argued that it may be possible to find different values of HR and MAP for which the efficiency of myocardial energy utilisation and the balance of myocardial oxygen supply and demand will be maximized. It has been shown that the possible existence of nontrivial optimal conditions for these two indices of performance is due entirely to the nonlinear dependence of left ventricular pumping capacity on pressure and volume loading. If this analysis is correct then the level of contractile state must also influence the possible optimization of left ventricular performance.

The experimental results demonstrate the multi-variate character of left ventricular function. Clearly, the concepts of optimality are relevant here and to this extent we have established the feasibility of the experimental systems approach. However, this is an extremely complex problem and further work will be necessary before these ideas can be applied in any practical sense.

6. THE ANALYSIS OF LEFT VENTRICULAR STRESS

6.1 INTRODUCTION

6.2 FUNDAMENTAL EQUATIONS OF ELASTICITY

State of Stress at a Point

Strain and Displacement

Generalized Hooke's Law

The Orthogonal Curvilinear Co-ordinate System

Dyadic Notation

6.3 THE EQUATIONS OF ELASTICITY FOR A CONFOCAL PROLATE SPHEROID COORDINATE SYSTEM

The Confocal Prolate Spheroid Co-ordinate System

The Strain Tensor

The Equilibrium Equations

6.4 ELASTIC PROPERTIES OF THE MYOCARDIUM

Distribution of Fibre Angles

Elastic Properties of Cardiac Muscle

Evaluation of the Elastic Moduli

Transformation of the Elastic Moduli

Conditions for Stable Axi-symmetric Deformation

Nonhomogenous and Nonlinear Elastic Properties

6. THE ANALYSIS OF LEFT VENTRICULAR STRESS

6.1 INTRODUCTION

Myocardial oxygen consumption and the balance of oxygen supply and demand have already been considered as indices of cardiac function and their significance discussed. One important question, that remains unanswered, is whether the balance of oxygen supply and demand for the left ventricle as a whole adequately reflects the local balance at points within the myocardium. This study is directed towards answering that question.

For the left ventricle, the utilisation of oxygen and the supply of coronary blood flow are both intimately connected with the stresses developed throughout the cardiac cycle. An accurate description of the left ventricular stress distribution is therefore essential, if we are to understand the mechanisms which determine the regional balance of myocardial oxygen supply and demand.

Much work has been done on the analysis of left ventricular stress. Wong and Rautaharju (1968), Ghista and Sandler (1969), and Mirsky (1969), obtained stress distributions for the ventricle treated as a thick walled body of revolution, with isotropic and homogenous elastic properties. The myocardium, however, is neither isotropic nor homogenous. Cardiac muscle fibres have a dominant axial component of elasticity and it has been shown by Streeter and Bassett (1966) and Streeter et al (1969) that their orientation varies throughout the ventricular wall in a well defined fashion. Two essentially qualitative studies by Mirsky (1970) and Streeter et al (1970) suggest that the

location and magnitude of peak stresses are strongly influenced by this structural anisotropy. Therefore, the influence of these factors should be carefully considered before any conclusions are reached about the nature of the left ventricular stress distribution.

The left ventricle resembles a thick ellipsoid of revolution truncated at the level of the aortic and mitral valves; wall thickness varies from a maximum at the equator to a minimum at the apex. Perhaps the most accurate general model of the left ventricle is given by Dieudonné (1969). In this, the endocardium and epicardium are represented as confocal prolate spheroid surfaces, thus approximating both the ellipsoid geometry of the left ventricle and the variation in wall thickness from apex to equator.

The left ventricle is constructed of nested layers of cardiac muscle fibres and within each layer fibres tend to follow a common spiral path from the apex through the myocardium. The angle of this spiral changes as we move across the wall in a radial direction.

In the analysis of left ventricular stress which follows, we make a number of fundamental assumptions :

- the left ventricle is a thick ellipsoid of revolution, for which the endocardium and epicardium are described by confocal prolate spheroid surfaces
- the left ventricle is made up of concentric shells of muscle fibre; within each shell fibres are constrained to follow a common helicoidal path on a confocal prolate spheroid surface
- the mechanical properties of cardiac muscle are described by linear

anisotropic elasticity theory.

- the myocardium is incompressible
- the left ventricle deforms axi-symmetrically

The assumptions on the geometry and structure of the left ventricle are essentially the same as those advanced by Streeter et al. (1970) and Streeter and Hanna (1973)[1,2]. Detailed information on their accuracy is available in these papers.

The other assumptions, however, must be considered in greater depth. Implicit in the use of linear anisotropic elasticity theory, is the understanding that stress and deformation are linearly related and that only small deformations are considered. Neither is strictly true for soft biological materials. In this study, we have chosen to emphasize the structural anisotropy of the left ventricle and to also include nonlinear and large deformation theory would be far too difficult. However, a simple indirect treatment of the effects of nonlinearity is included. Using large deformation theory, Mirsky (1973) estimated the stress distribution for an isotropic spherical shell model of the left ventricle and from this work it seems likely that the use of small deformation theory leads to an underestimation of stresses in the endocardial region. For the normal physiological range of deformations, however, this effect may not be unduly important.

Soft biological tissues are generally regarded as incompressible, since volume changes are small in comparison to the magnitude of deformation. A proportion of the left ventricle is composed of blood vessels and with the onset of contraction a significant volume of blood is extruded from the myocardium. This,

it might be argued, invalidates the assumption of incompressibility during systole. The effect of relaxing the assumption of incompressibility will therefore be included in this treatment.

6.2 FUNDAMENTAL EQUATIONS OF ELASTICITY

In this section, we review those areas of linear anisotropic elasticity theory which relate to the present analysis of left ventricular stress. It is known that the elastic properties of cardiac muscle fibres are anisotropic and that their orientation varies throughout the ventricular wall. We therefore consider the way in which the elastic constants of a general anisotropic elastic body change under a rotation of co-ordinate system. In order to do this, it is first necessary to obtain the co-ordinate transformations for the components of stress and deformation. The solution of the stress equilibrium equations is a boundary value problem. If it is possible to find a co-ordinate system which is orthogonal to the surfaces for which the boundary conditions are specified, the technical complexity of solving this problem is greatly reduced. Accordingly, we review the theory of orthogonal curvilinear co-ordinate systems and reproduce expressions for the fundamental equations of elasticity with respect to such a general co-ordinate system.

What follows is drawn mainly from two sources; Chou and Pagano (1967) and Lekhnitskii (1963). No apologies are made for the mixture of tensor, vector, dyadic and matrix notation which is used here. While the exclusive use of tensor notation would have been more elegant, it is felt that the approach taken is conceptually more simple.

STATE OF STRESS AT A POINT

The state of stress at any given point in a continuous body is determined entirely by the components of stress in three mutually perpendicular planes which pass through that chosen point. Consider the infinitesimal tetrahedron OABC set up with respect to the cartesian co-ordinate system (x, y, z) and presented in Fig. 6.1; three components of stress act in each of the planes OBC, OAC and OAB. For the plane OBC, the transverse or shear components of stress are τ_{xy} and τ_{xz}, while the component of stress normal to the plane is σ_x. Similarly, the components of stress acting in OAC are τ_{yx}, τ_{yz}, σ_y and the components of stress acting in OAB are τ_{zx}, τ_{zy}, σ_z. Therefore the stress acting in any plane is a vector. It can be shown that

$$\tau_{xy} = \tau_{yx} \; ; \quad \tau_{xz} = \tau_{zx} \; ; \quad \tau_{yz} = \tau_{zy} \qquad 6.2.1.$$

and thus the nine components of stress acting at a given point constitute a symmetric second-order tensor.

$$\tau = \begin{pmatrix} \sigma_x & \tau_{xy} & \tau_{xz} \\ \tau_{xy} & \sigma_y & \tau_{yz} \\ \tau_{xz} & \tau_{yz} & \sigma_z \end{pmatrix}$$

We must determine the way in which the components of stress are transformed under a change of co-ordinate system. Consider a new cartesian co-ordinate system (x', y', z') in which the x'-axis is normal to the plane ABC in Fig. 6.1. The stress acting on this area can be represented as a vector $\vec{P}$

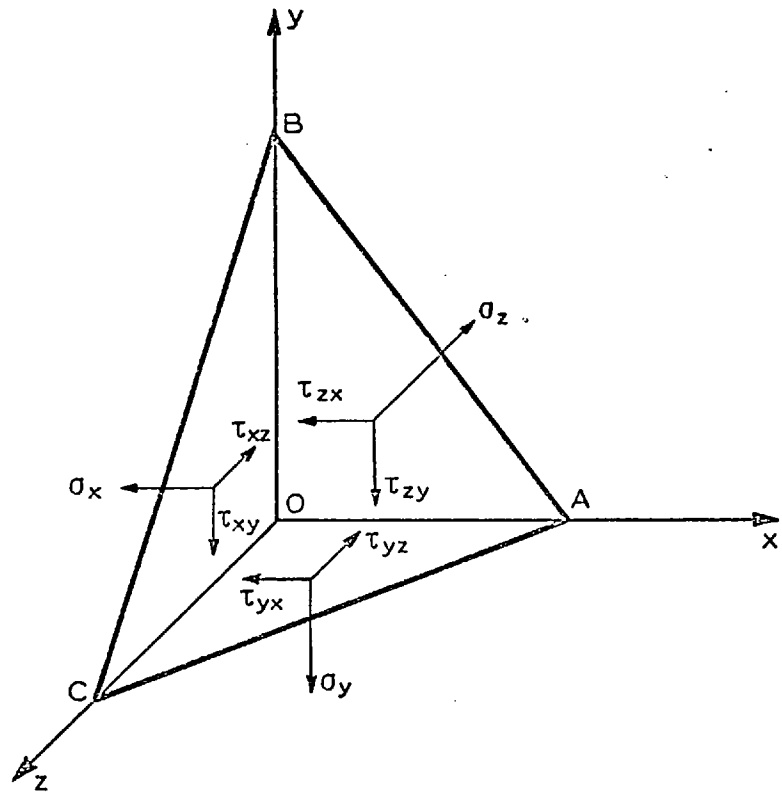

FIGURE 6·1a: State of stress at a point.

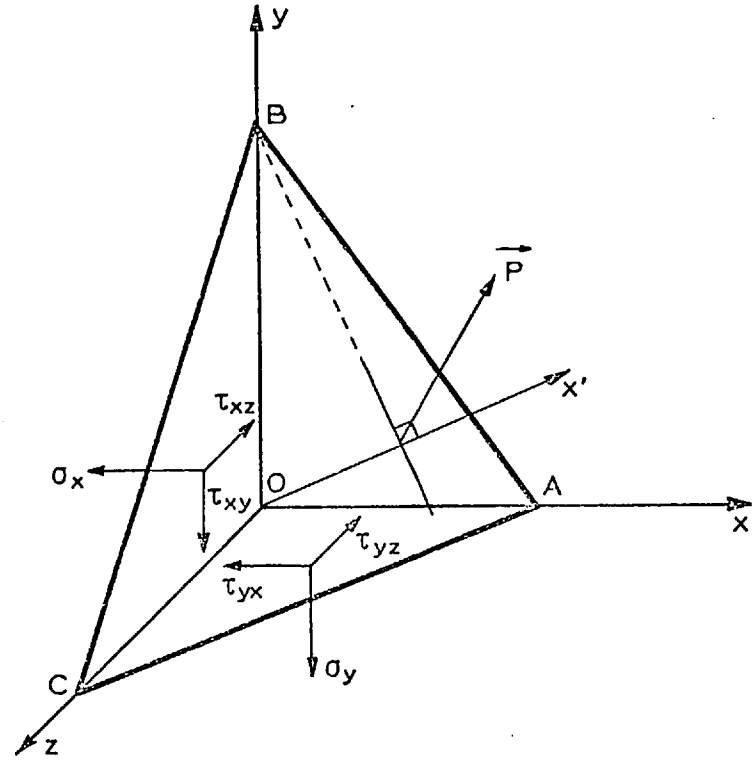

FIGURE 6·1b: Transformation of the stress components.

with components P_x, P_y, P_z in the x, y, z directions respectively. Balancing forces for the areas enclosed by the tetrahedron OABC, we obtain :

$$\begin{aligned} P_x &= \sigma_x \alpha_1 + \tau_{xy} \beta_1 + \tau_{xz} \gamma_1 \\ P_y &= \tau_{xy} \alpha_1 + \sigma_y \beta_1 + \tau_{yz} \gamma_1 \\ P_z &= \tau_{xz} \alpha_1 + \tau_{yz} \beta_1 + \sigma_z \gamma_1 \end{aligned} \qquad 6.2.2.$$

$\alpha_1, \beta_1, \gamma_1$ are the direction cosines, which give the relationship between the co-ordinate systems (x', y', z') and (x, y, z) - see Table 6.1.

	x	y	z
x'	α_1	β_1	γ_1
y'	α_2	β_2	γ_2
z'	α_3	β_3	γ_3

TABLE 6.1

$\alpha_1 = \text{Cos}(x, x')$
$\gamma_2 = \text{Cos}(x, y')$

The stress acting in the area ABC can also be resolved along the axes of the new co-ordinate system (x', y', z').

$$\begin{aligned} \sigma_{x'} &= P_x \alpha_1 + P_y \beta_1 + P_z \gamma_1 \\ \tau_{xy'} &= P_x \alpha_2 + P_y \beta_2 + P_z \gamma_2 \end{aligned} \qquad 6.2.3.$$

Substituting 6.2.2 in 6.2.3, we obtain the components of stress with respect to the co-ordinate system (x', y', z').

$$\sigma'_x = \sigma_x \alpha_1^2 + \sigma_y \beta_1^2 + \sigma_z \gamma_1^2 + 2\tau_{yz}\beta_1\gamma_1 + 2\tau_{xz}\alpha_1\gamma_1 + 2\tau_{xy}\alpha_1\beta_1$$

$$\tau_{xy'} = \sigma_x \alpha_1\alpha_2 + \sigma_y\beta_1\beta_2 + \sigma_z\gamma_1\gamma_2 + \tau_{yz}(\beta_1\gamma_2 + \beta_2\gamma_1) + \tau_{xz}(\alpha_1\gamma_2 + \alpha_2\gamma_1) + \tau_{xy}(\alpha_1\beta_2 + \alpha_2\beta_1) \qquad 6.2.4.$$

Expressions for the other components of stress have an identical form.

Conversely :

$$\sigma_x = \sigma'_x \alpha_1^2 + \sigma'_y \alpha_2^2 + \sigma'_z \alpha_3^2 + 2\tau'_{yz}\alpha_2\alpha_3 + 2\tau'_{xz}\alpha_1\alpha_3 + 2\tau'_{xy}\alpha_1\alpha_2$$

$$\tau_{xy} = \sigma'_x \alpha_1\beta_1 + \sigma'_y\alpha_2\beta_2 + \sigma'_z\alpha_3\beta_3 + \tau_{yz'}(\alpha_2\beta_3 + \alpha_3\beta_2) + \tau_{xz'}(\alpha_1\beta_3 + \alpha_3\beta_1) + \tau_{xy'}(\alpha_1\beta_2 + \alpha_2\beta_1) \qquad 6.2.5.$$

We now reproduce the equilibrium equations for a general cartesian co-ordinate system

$$\frac{\delta\sigma}{\delta x}x + \frac{\delta\tau}{\delta y}yz + \frac{\delta\tau}{\delta z}zx + F_x = 0$$

$$\frac{\delta\sigma}{\delta y}y + \frac{\delta\tau}{\delta x}xy + \frac{\delta\tau}{\delta z}zy + F_y = 0 \qquad 6.2.6.$$

$$\frac{\delta\sigma}{\delta z}z + \frac{\delta\tau}{\delta x}xz + \frac{\delta\tau}{\delta y}yz + F_z = 0$$

where F_x, F_y, F_z are the components of the body forces per unit volume.

STRAIN AND DISPLACEMENT

When forces are applied to a body the position of any point within that body is, in general, altered. The displacement of a point is defined as the vector difference between its inital and final locations.

$$\vec{U} = u\hat{i} + v\hat{j} + \omega\hat{k} \qquad 6.2.7$$

. is the displacement vector; u, v, w are the components of displacement in the x, y, z directions respectively.

If the displacement vector is not the same at each point within the body, a state of deformation is said to exist. For a continuous body, the state of deformation at any given point is completely determined by six components of strain.

In a Cartesian co-ordinate system (x, y, z), the normal components of strain ε_x, ε_y, ε_z give the relative changes in length of infinitesimally small segments, which in the undeformed state are parallel to the co-ordinate axes. The components of shear strain γ_{xy} γ_{xz} γ_{yz} give the changes in angle between these segments. Together these terms constitute the strain tensor:

$$\gamma = \begin{pmatrix} \varepsilon_x & \frac{1}{2}\gamma_{xy} & \frac{1}{2}\gamma_{xz} \\ \frac{1}{2}\gamma_{xy} & \varepsilon_y & \frac{1}{2}\gamma_{yz} \\ \frac{1}{2}\gamma_{xz} & \frac{1}{2}\gamma_{yz} & \varepsilon_z \end{pmatrix}$$

We denote the components of displacement in the x, y, z directions of a Cartesian co-ordinate system as u, v, w, respectively. For small displacements it can be shown that :

$$\varepsilon_x = \frac{\delta u}{\delta x}, \quad \gamma_{xy} = \frac{\delta u}{\delta y} + \frac{\delta v}{\delta x}$$

$$\varepsilon_y = \frac{\delta v}{\delta y}, \quad \gamma_{yz} = \frac{\delta v}{\delta z} + \frac{\delta \omega}{\delta y} \qquad 6.2.8$$

$$\varepsilon_z = \frac{\delta \omega}{\delta z}, \quad \gamma_{xz} = \frac{\delta u}{\delta z} + \frac{\delta \omega}{\delta x}$$

The strain components constitute a symmetric second-order tensor. Under a change of co-ordinate system, therefore, they transform according to the relations developed for the stress tensor. Replacing σ by ε and τ by $\frac{1}{2}\gamma$ in expressions 6.2.4 and 6.2.5, we can obtain the equivalent transformation expressions for the strain tensor.

GENERALIZED HOOKE'S LAW

It is necessary to find the relationship between the components of stress and the components of deformation. Hooke's law assumes this relationship to be linear and in its most general form is written:

$$\varepsilon_x = a_{11}\sigma_x + a_{12}\sigma_y + a_{13}\sigma_z + a_{14}\tau_{yz} + a_{15}\tau_{xz} + a_{16}\tau_{xy}$$

$$\varepsilon_y = a_{21}\sigma_x + a_{22}\sigma_y + a_{23}\sigma_z \quad \bullet \quad \bullet \quad \bullet + a_{26}\tau_{xy}$$

$$\bullet$$

$$\bullet \qquad 6.2.9$$

$$\bullet$$

$$\gamma_{xy} = a_{61}\sigma_x + a_{62}\sigma_y + a_{63}\sigma_z \quad \bullet \quad \bullet \quad \bullet + a_{66}\tau_{xy}$$

Solving this set of equations for the stress components we have:

$$\sigma_x = A_{11}\varepsilon_x + A_{12}\varepsilon_y + A_{13}\varepsilon_z + A_{14}\gamma_{yz} + A_{15}\gamma_{xz} + A_{16}\gamma_{xy}$$

$$\sigma_y = A_{21}\varepsilon_x + A_{22}\varepsilon_y + A_{23}\varepsilon_z + \quad \cdot \quad \cdot \quad \cdot \quad + A_{26}\gamma_{xy}$$

$$\cdot$$

$$\cdot \qquad\qquad\qquad\qquad\qquad\qquad\qquad\qquad\qquad\qquad 6.2.10.$$

$$\cdot$$

$$\tau_{xy} = A_{61}\varepsilon_x + A_{62}\varepsilon_y + A_{63}\varepsilon_z + \quad \cdot \quad \cdot \quad \cdot \quad + A_{66}\gamma_{xy}$$

Normally, $\sigma_{ij} = \sigma_{ji}$ and $A_{ij} = A_{ji}$

Thus for the most general case of an homogenous anisotropic body the relationship between the components of stress and the components of deformation is described by 21 independent elastic constants. If the elastic properties of a body possess symmetry of any kind the number of independent terms will be reduced.

Only in the case of an isotropic body are the constants invariant in any orthogonal co-ordinate system. It is essential, therefore, to obtain the expressions which describe the transformation of the elastic constants under a change of co-ordinate system.

Let the elastic constants of an anisotropic body be known for the coordinate system (x, y, z) and consider a new co-ordinate system (x′, y′, z′) arbitrarily set up with respect to it. The transformation between the old and new co-ordinate systems is given by the direction cosines in Table 6.1

At this point it is convenient to introduce matrix notation:

$$\begin{pmatrix} \sigma_x \\ \sigma_y \\ \cdot \\ \cdot \\ \cdot \\ \tau_{xy} \end{pmatrix} = \begin{pmatrix} A_{11} & A_{12} & A_{13} & A_{14} & A_{15} & A_{16} \\ A_{21} & A_{22} & A_{23} & \cdot & \cdot & A_{26} \\ \cdot & & & & & \\ \cdot & & & & & \\ \cdot & & & & & \\ A_{16} & A_{26} & A_{36} & \cdot & \cdot & A_{66} \end{pmatrix} \begin{pmatrix} \varepsilon_x \\ \varepsilon_y \\ \\ \\ \\ \gamma_{xy} \end{pmatrix} \qquad 6.2.11.$$

Let the matrix expression for the generalized form of Hooke's law above, be represented by

$$\sigma = A\varepsilon \qquad 6.2.12.$$

For the new coordinate system (x', y', z'), we write

$$\sigma' = A'\varepsilon' \qquad 6.2.13.$$

In the same notation, the transformation of the stress components under a change of coordinate system is represented by

$$\sigma' = R\sigma \qquad 6.2.14.$$

and for the components of deformation

$$\varepsilon' = S\varepsilon \qquad 6.2.15.$$

Also

$$\sigma = R^{-1}\sigma' \qquad 6.2.16.$$

$$\varepsilon = S^{-1}\varepsilon' \qquad 6.2.17.$$

where the components of the transformation matrices are obtained from the expressions 6.2.4 and 6.2.5. The terms R_{ij}^{-1} are given in Table 6.2.

i \ j	1	2	3	4	5	6
1	α_1^2	α_2^2	α_3^2	$2\alpha_2\alpha_3$	$2\alpha_3\alpha_1$	$2\alpha_1\alpha_2$
2	β_1^2	β_2^2	β_3^2	$2\beta_2\beta_3$	$2\beta_3\beta_1$	$2\beta_1\beta_2$
3	γ_1^2	γ_2^2	γ_3^2	$2\gamma_2\gamma_3$	$2\gamma_3\gamma_1$	$2\gamma_1\gamma_2$
4	$\beta_1\gamma_1$	$\beta_2\gamma_2$	$\beta_3\gamma_3$	$\beta_2\gamma_3+\beta_3\gamma_2$	$\beta_1\gamma_3+\beta_3\gamma_1$	$\beta_1\gamma_2+\beta_2\gamma_1$
5	$\gamma_1\alpha_1$	$\gamma_2\alpha_2$	$\gamma_3\alpha_3$	$\gamma_2\alpha_3+\gamma_3\alpha_2$	$\gamma_1\alpha_3+\gamma_3\alpha_1$	$\gamma_1\alpha_2+\gamma_2\alpha_1$
6	$\alpha_1\beta_1$	$\alpha_2\beta_2$	$\alpha_3\beta_3$	$\alpha_2\beta_3+\alpha_3\beta_2$	$\alpha_1\beta_3+\alpha_3\beta_1$	$\alpha_1\beta_2+\alpha_2\beta_1$

TABLE 6·2.

Combining 6.2.12 and 6.2.17, we have

$$\sigma = AS^{-1}\varepsilon' \qquad 6.2.18.$$

but

$$\sigma' = R\sigma = RAS^{-1}\varepsilon' \qquad 6.2.19.$$

Therefore equating 6.2.13 and 6.2.19, we obtain

$$A' = RAS^{-1} \qquad 6.2.20.$$

It is quite simple to express the components of the transformation matrix S^{-1} in terms of the coefficients R_{ij} given in Table 6.2 Application of matrix multiplication now yields the general formula for the transformation of the elastic constants

$$A'_{ij} = \frac{1}{\omega_i \omega_j} \sum_{m}^{6} \sum_{n}^{6} \omega_m \omega_n A_{mn} R_{mi}^{-1} R_{nj}^{-1}$$

where 6.2.21

$$\omega_k \begin{cases} = 1, \text{ for } k = 1, 2, 3 \\ = 2, \text{ for } k = 4, 5, 6 \end{cases}$$

THE ORTHOGONAL CURVILINEAR COORDINATE SYSTEM

We have stated that it may be convenient to develop the fundamental equations of elasticity with respect to a curvilinear co-ordinate system. It is first necessary however, to consider some of the properties of a general orthogonal curvilinear co-ordinate system.

For the cartesian co-ordinate system (x, y, z), we define three independent functions:

$$u_1 = u_1(x, y, z); \quad u_2 = u_2(x, y, z); \quad u_3 = u_3(x, y, z) \qquad 6.2.22$$

Suppose that these expressions can be solved for x, y, z in terms of u_1, u_2, u_3.

$$x_1 = x_1(u_1, u_2, u_3); \quad x_2 = x_2(u_1, u_2, u_3); \quad x_3 = x_3(u_1, u_2, u_3) \qquad 6.2.23$$

The functions above, are assumed to be single-valued and to have continuous

derivatives.

The expressions:

$$u_1(x,y,z) = d_1;\ u_2(x,y,z) = d_2;\ u_3(x,y,z) = d_3 \qquad 6.2.24$$

represent surfaces and the intersection of any pair of these surfaces forms a curve known as a co-ordinate line. If the intersection of the three co-ordinate lines is mutually perpendicular for all points the co-ordinate system is said to be orthogonal.

By definition, the Cartesian co-ordinates (x, y, z) are in units of length. However, this is not generally true of curvilinear co-ordinates. We therefore introduce the expressions :

$$dr_1 = h_1 du_1;\ dr_2 = h_2 du_2;\ dr_3 = h_3 du_3 \qquad 6.2.25$$

where $dr_1, dr_2\ dr_3$ give the incremental change in length produced by a change du_1, du_2, du_3 in the curvilinear co-ordinates. The terms h_1, h_2, h_3 are known as scale factors for the co-ordinates U_1, U_2, U_3 respectively.

Let us introduce the three unit vectors $\hat{c}_1$, $\hat{c}_2$, $\hat{c}_3$, tangent to the co-ordinate lines U_1, U_2, U_3. While the directions of a set of Cartesian unit vectors $\hat{i}, \hat{j}, \hat{k}$ remain fixed in space the directions of $\hat{c}_1$, $\hat{c}_2$, $\hat{c}_3$ vary from point to point. The derivatives of the unit vectors $\hat{c}_1$, $\hat{c}_2$, $\hat{c}_3$ with respect to changes in the co-ordinates U_1, U_2, U_3 are reproduced from Chou and Pagano (1967).

$$\frac{\delta \hat{c}_1}{\delta u_1} = -\frac{\hat{c}_2}{h_2}\frac{\delta h_1}{\delta u_2} - \frac{\hat{c}_3}{h_3}\frac{\delta h_1}{\delta u_3} \quad ; \quad \frac{\delta \hat{c}_1}{\delta u_2} = \frac{\hat{c}_2}{h_1}\frac{\delta h_2}{\delta u_1} \quad ; \quad \frac{\delta \hat{c}_1}{\delta u_3} = \frac{\hat{c}_3}{h_1}\frac{\delta h_3}{\delta u_1}$$

$$\frac{\delta \hat{c}_2}{\delta u_2} = -\frac{\hat{c}_3}{h_3}\frac{\delta h_2}{\delta u_3} - \frac{c_1}{h_1}\frac{\delta h_2}{\delta u_1} \quad ; \quad \frac{\delta \hat{c}_2}{\delta u_3} = \frac{\hat{c}_3}{h_2}\frac{\delta h_3}{\delta u_2} \quad ; \quad \frac{\delta \hat{c}_2}{\delta u_1} = \frac{\hat{c}_1}{h_2}\frac{\delta h_1}{\delta u_2}. \qquad 6.2.26$$

$$\frac{\delta \hat{c}_3}{\delta u_3} = -\frac{\hat{c}_1}{h_1}\frac{\delta h_3}{\delta u_1} - \frac{\hat{c}_2}{h_2}\frac{\delta h_3}{\delta u_2} \qquad \frac{\delta \hat{c}_3}{\delta u_1} = \frac{c_1}{h_3}\frac{\delta h_1}{\delta u_3} \quad ; \quad \frac{\delta \hat{c}_3}{\delta u_2} = \frac{\hat{c}_2}{h_3}\frac{\delta h_2}{\delta u_3}$$

DYADIC NOTATION

Dyadic notation is an extension of vector notation to cover second-order tensor quantities such as stress. Though less elegant than tensor notation, dyadic notation is used here because it is relatively simple to transform the vector operations for a general curvilinear coordinate system into the equivalent functions for a second-order tensor.

In general, any dyadic ζ is represented by :

$$\begin{aligned} \zeta = \quad & \hat{i}\hat{i}\, S_{xx} + \hat{i}\hat{j} S_{xy} + \hat{i}\hat{k} S_{xz} \\ & + \hat{j}\hat{i}\, S_{yx} + \hat{j}\hat{j} S_{yy} + \hat{j}\hat{k} S_{yz} \\ & + \hat{k}\hat{i}\, S_{zx} + \hat{k}\hat{j} S_{zy} + \hat{k}\hat{k} S_{zz} \end{aligned} \qquad 6.2.27$$

ζ may be decomposed into three vectors :

$$\zeta = \hat{i}\vec{S}_x + \hat{j}\vec{S}_y + \hat{k}\vec{S}_z \qquad 6.2.28$$

where

$$\vec{S}_x = S_{xx}\hat{i} + S_{xy}\hat{j} + S_{xz}\hat{k}$$

$$\vec{S}_y = S_{yx}\hat{i} + S_{yy}\hat{j} + S_{yz}\hat{k}$$

$$\vec{S}_z = S_{zx}\hat{i} + S_{zy}\hat{j} + S_{zz}\hat{k}$$

$$\hat{i}\hat{j} \neq \hat{j}\hat{i}$$

Thus the stress tensor can be represented as

$$\tau = \hat{i}\vec{\tau}_x + \hat{j}\vec{\tau}_y + \hat{k}\vec{\tau}_z \qquad 6.2.29$$

where

$$\vec{\tau}_x = \sigma_x\hat{i} + \tau_{xy}\hat{j} + \tau_{xz}\hat{k} \quad \text{etc.}$$

The equilibrium equations 6.2.6 can be written in the condensed form

$$\text{div}\,\tau + \vec{F} = 0 \qquad 6.2.30$$

where

$$\text{div}\,\tau = \frac{\delta}{\delta x}\vec{\tau}_x + \frac{\delta}{\delta y}\vec{\tau}_y + \frac{\delta}{\delta z}\vec{\tau}_z$$

Similarly, for the strain tensor

$$E = \hat{i}\vec{e}_x + \hat{j}\vec{e}_y + \hat{k}\vec{e}_z \qquad 6.2.31$$

where

$$\vec{e}_x = \varepsilon_x \hat{i} + \frac{1}{2}\gamma_{xy}\hat{j} + \frac{1}{2}\gamma_{xz}\hat{k} \qquad \text{etc.}$$

But from 6.2.8

$$\vec{e}_x = \frac{\delta u \hat{i}}{\delta x} + \frac{1}{2}\left(\frac{\delta v}{\delta x} + \frac{\delta u}{\delta y}\right)\hat{j} + \frac{1}{2}\left(\frac{\delta \omega}{\delta x} + \frac{\delta u}{\delta z}\right)\hat{k} \qquad 6.2.32$$

Combining the expressions for the strain components we write

$$E = \frac{1}{2}\left(\nabla\vec{U} + \vec{U}\nabla\right) \qquad 6.2.33$$

where $\vec{U}$ is the displacement vector

$$\nabla\vec{U} = \hat{i}\frac{\delta\vec{U}}{\delta x} + \hat{j}\frac{\delta\vec{U}}{\delta y} + \hat{k}\frac{\delta\vec{U}}{\delta z}$$

and

$$\vec{U}\nabla = \frac{\delta\vec{U}}{\delta x}\hat{i} + \frac{\delta\vec{U}}{\delta y}\hat{j} + \frac{\delta\vec{U}}{\delta z}\hat{k}$$

The dyadic operators which describe the strain tensor and the stress equilibrium equations can be obtained for a general orthogonal curvilinear co-ordinate system by extending the equivalent vector functions.

Thus

$$\nabla\cdot\zeta = \frac{1}{h_1 h_2 h_3}\sum_{i=1}^{3}\frac{\delta}{\delta U_i}\left(h_1 h_2 h_3 \frac{\vec{S}_i}{h_i}\right) \qquad 6.2.34$$

$$\nabla\vec{A} = \sum_{i=1}^{3}\frac{\hat{c}_i}{h_i}\frac{\delta\vec{A}}{\delta U_i} \qquad 6.2.35$$

$$\vec{A}\nabla = \sum_{i=1}^{3} \frac{1}{h_i} \frac{\delta \vec{A}}{\delta U_i} \hat{c}_i \qquad 6.2.36$$

where U_i is one of the set of co-ordinate variables, $\hat{c}_i$ is a unit vector and h_i is the scale factor for the variable U_i

We note that

$$\frac{\delta \vec{A}}{\delta U_1} = \frac{\delta}{\delta U_1} (A_1 \hat{C}_1 + A_2 \hat{C}_2 + A_3 \hat{C}_3)$$

$$= \frac{\delta A_1}{\delta U_1} \hat{C}_1 + \frac{\delta A_2}{\delta U_1} \hat{C}_2 + \frac{\delta A_3}{\delta U_1} \hat{C}_3$$

$$+ A_1 \frac{\delta \hat{C}_1}{\delta U_1} + A_2 \frac{\delta \hat{C}_2}{\delta U_1} + A_3 \frac{\delta \hat{C}_3}{\delta U_1}$$

Thus to evaluate the differential operators 6.2.34, 6.2.35 and 6.2.36 for the strain and equilibrium equations, with respect to a general orthogonal curvilinear co-ordinate system, we must first specify the scale factors and then use 6.2.26 to obtain the derivatives of the unit vectors with respect to changes in the co-ordinate variables.

6.3 THE EQUATIONS OF ELASTICITY FOR A CONFOCAL PROLATE SPHEROID COORDINATE SYSTEM

THE CONFOCAL PROLATE SPHEROID COORDINATE SYSTEM

For a confocal prolate spheroid co-ordinate system (ξ, η, Φ) we have :

$$x = a \sinh \xi \sin \eta \cos \Phi, \quad y = a \sinh \xi \sin \eta \sin \Phi, \quad z = a \cosh \xi \cos \eta \qquad 6.3.1$$

where a is defined as the focal length of the system and

$$\xi \geq 0, \qquad 0 \leq \eta \leq \pi, \quad 0 \leq \Phi \leq 2\pi$$

The scale factors are :

$$h_\xi = h_\eta = a(\sinh^2 \xi + \sin^2 \eta)^{1/2}, \quad h_\Phi = a \sinh \xi \sin \eta \qquad 6.3.2$$

and the set of unit vectors is $(\hat{C}_\xi, \hat{C}_\eta, \hat{C}_\Phi)$

The principal radii of curvature at any point are given by :

$$\frac{1}{R_1} = \frac{1}{a(\sinh^2 \xi + \sin^2 \eta)^{1/2} \tanh \xi}$$

$$\frac{1}{R_2} = \frac{\sinh \xi \cosh \xi}{a(\sinh^2 \xi + \sin^2 \eta)^{3/2}} \qquad 6.3.3$$

In Fig. 6.2, we represent the left ventricle as a truncated confocal prolate spheroid shell. The endocardial surface is described by the rotation of the co-ordinate line $\xi = \xi_1$ around the z-axis. Similarly, the epicardial surface is specified by the co-ordinate $\xi = \xi_2$

Z_1 and Z_2 are the endocardial and epicardial major semi-axes; X_1 and X_2 are the minor semi-axes.

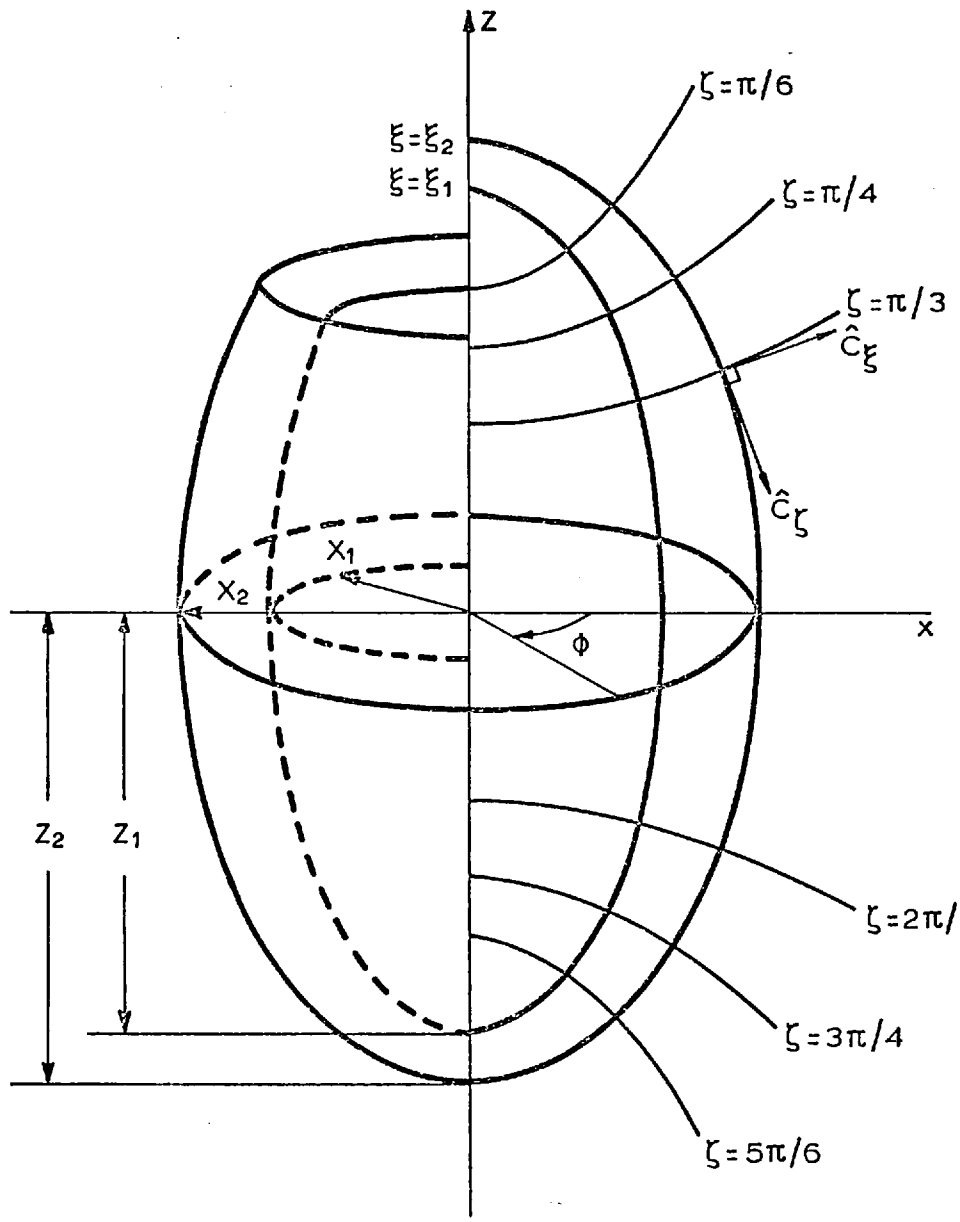

FIGURE 6·2: Confocal prolate spheroid representation of the left ventricle.
X_1 and Z_1 are the endocardial minor and major semi-axes; X_2 and Z_2 are the epicardial minor and major semi-axes.

We note that

$$a^2 = Z_i^2 - X_i^2 \qquad i = 1,2 \qquad 6.3.4$$

THE STRAIN TENSOR

In a confocal prolate spheroid co-ordinate system the displacement vector is given by

$$\vec{U} = U\hat{c}_\xi + V\hat{c}_\eta + \omega\hat{c}_\phi \qquad 6.3.5$$

and for deformation to be axi-symmetric, the following must hold:

$$U = U(\xi,\eta), \quad V = V(\xi,\eta), \quad \omega = 0 \qquad 6.3.6$$

For this co-ordinate system the dyadic representation of the strain tensor is

$$E = \hat{c}_\xi \vec{e}_\xi + \hat{c}_\eta \vec{e}_\eta + \hat{c}_\phi \vec{e}_\phi \qquad 6.3.7$$

where

$$\vec{e}_\xi = \varepsilon_\xi \hat{c}_\xi + \frac{1}{2}\gamma_{\xi\eta}\hat{c}_\eta + \frac{1}{2}\gamma_{\xi\phi}\hat{c}_\phi$$

But we have stated that

$$E = \frac{1}{2}(\nabla\vec{U} + \vec{U}\nabla)$$

The scale factors for the confocal prolate spheroid co-ordinate system are given in 6.3.2; we use 6.2.35, 6.2.36 and the methods outlined in the previous section to evaluate the strain tensor for this co-ordinate system.

The components of strain are :

$$\varepsilon_\xi = \frac{1}{T}\frac{\delta u}{\delta \xi} + \frac{v}{S_2}$$

$$\varepsilon_\eta = \frac{1}{T}\frac{\delta v}{\delta \eta} + \frac{u}{R_2} \qquad 6.3.8$$

$$\varepsilon_\phi = \frac{u}{R_1} + \frac{v}{S_1}$$

$$\gamma_{\xi\eta} = \frac{1}{T}\left(\frac{\delta u}{\delta \eta} + \frac{\delta v}{\delta \xi}\right) - \frac{u}{S_2} - \frac{v}{R_2}$$

where

$$\frac{1}{S_1} = \frac{\sin\eta\cos\eta}{a\,(\sinh^2\xi + \sin^2\eta)^{3/2}}$$

$$\frac{1}{S_2} = \frac{1}{a\,(\sinh^2\xi + \sin^2\eta)^{1/2}\tan\eta} \qquad 6.3.9$$

$$\frac{1}{T} = \frac{1}{a(\sinh^2\xi + \sin^2\eta)^{1/2}}$$

THE EQUILIBRIUM EQUATIONS

The dyadic representation of the stress tensor in the coordinate system (ξ, η, ϕ) is

$$\tau = \hat{c}_\xi \vec{\tau}_\xi + \hat{c}_\eta \vec{\tau}_\eta + \hat{c}_\phi \vec{\tau}_\phi \qquad 6.3.10$$

where

$$\vec{\tau}_\xi = \sigma_\xi \hat{c}_\xi + \tau_{\xi\eta} \hat{c}_\eta + \tau_{\xi\phi} \hat{c}_\phi$$

etc.

In the absence of body forces, the equilibrium equation 6.2.30 reduces to

$$\text{div } \tau = 0$$

For a body of revolution, which deforms axi-symmetrically, the components of stress are independent of the coordinate ϕ .

Also

$$\tau_{\xi\phi} = \tau_{\eta\phi} = 0 \qquad 6.3.11$$

We evaluate the equilibrium equations using 6.2.34 and the approach outlined earlier.

$$\frac{1}{T}\left(\frac{\delta\sigma}{\delta\xi}\xi + \frac{\delta\tau}{\delta\eta}\xi\eta\right) + \frac{1}{R_1}(\sigma_\xi - \sigma_\phi) + \frac{1}{R_2}(\sigma_\xi - \sigma_\eta) + \left(\frac{1}{S_1} + \frac{2}{S_2}\right)\tau_{\xi\eta} = 0 \qquad 6.3.12$$

$$\frac{1}{T}\left(\frac{\delta\sigma_\eta}{\delta\eta} + \frac{\delta\tau}{\delta\xi}\xi\eta\right) + \frac{1}{S_1}(\sigma_\eta - \sigma_\phi) + \frac{1}{S_2}(\sigma_\eta - \sigma_\xi) + \left(\frac{1}{R_1} + \frac{2}{R_2}\right)\tau_{\xi\eta} = 0$$

6.4 ELASTIC PROPERTIES OF THE MYOCARDIUM

DISTRIBUTION OF FIBRE ANGLES

The left ventricle is constructed of nested layers of cardiac muscle fibres. Within each layer, fibres tend to describe a common spiral path from the apex through the myocardium. The angle of this spiral changes from layer to layer as we move across the ventricular wall in a radial direction.

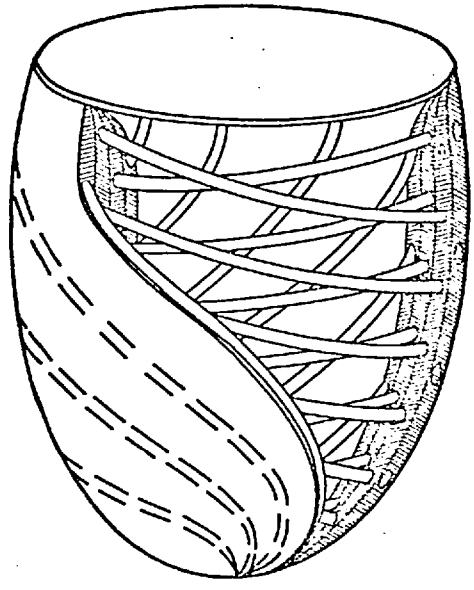

Figure 6.3: Distribution of muscle fibres in the left ventricle *(After Streeter and Hanna, 1973).*

Consider a fibre constrained to follow a helical course on a confocal prolate spheroid surface, given by $\xi = c$, $\xi_1 \leqslant c < \xi_2$. The trajectory of the fibre at any point on this surface is completely specified by the distance Δz moved by the fibre in the direction of the z - axis, as it travels through an infinitesimally small angle $\Delta \phi$ about that axis. Thus, the helical path followed by the fibre can be described by

$$\frac{\Delta Z}{\Delta \phi} = F(\eta) \qquad 6.4.1$$

Also, the orientation of the fibre at any point, with respect to the coordinate system (ξ, η, ϕ), is given by a simple rotation. Let α be the angle of fibre orientation; it can be seen from Fig. 6.4, that

$$\text{Tan } \alpha = \frac{\Delta z}{R \Delta \phi \cos \gamma} \qquad 6.4.2$$

It can be shown that

$$\text{Tan } \gamma = -\text{Tanh} \xi \cot \eta$$

and

$$R = a \sinh \xi \sin \eta$$

Combining these expressions, we obtain

$$\text{Tan } \alpha = \frac{F(\eta) \cdot (1 + \cot^2 \eta \tanh^2 \xi)^{1/2}}{a \sinh \xi \sin \eta} \qquad 6.4.3$$

The distribution of fibre angles at the equator is well established and Fig. 6.5 is based on the published data of Streeter and Bassett (1966) and Streeter et al (1969). We have considered the variation of fibre angles to be a continuous function of the radial coordinate. If an assumption is made about the nature of the path followed by the fibres, the angle of fibre orientation for any point in the myocardium can be predicted from the equatorial distribution of fibre angles using 6.4.3.

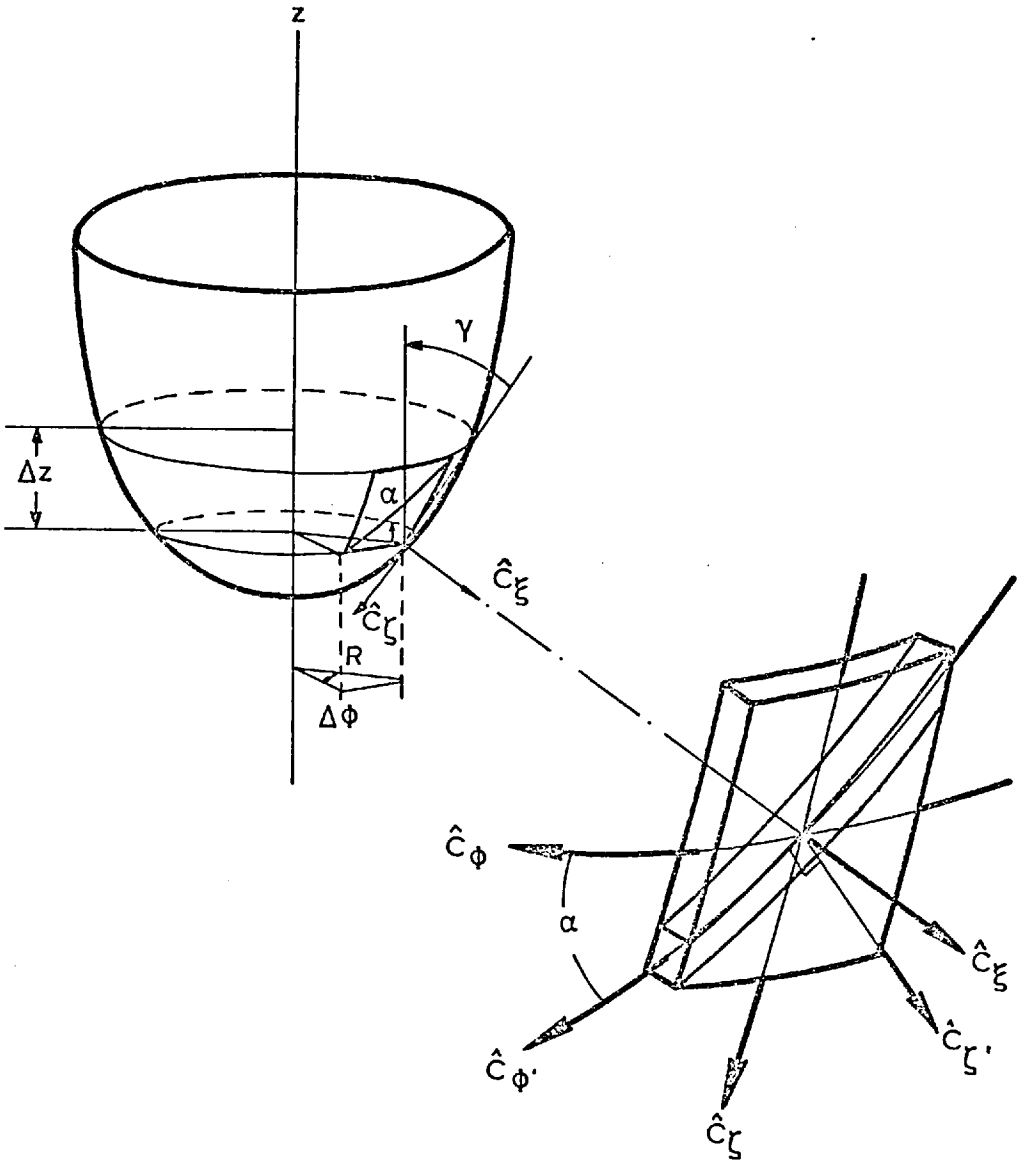

FIGURE 6.4: Myocardial structure and the course of fibre orientation.

The simplest such assumption is that

$$F(\eta) = K, \quad K \text{ is a constant}$$

The projection of this path onto a concentric cylinder is a circular helix of constant pitch. Streeter and Hanna (1973)[2] obtained good agreement with measured fibre angles in the equatorial region using this approach. At the apex, however, they predicted fibre angles of $\pm 90^{o}$ for the inner and outer halves of the ventricular wall respectively. The observed fibre orientation here is circumferential and it is clear, therefore, that the constant pitch helix assumption breaks down in the apical region.

We propose instead that :

$$F(\eta) = \begin{cases} K, & \frac{\pi}{4} \leq \eta \leq \frac{\pi}{2} \\ K \sin^3 2\eta, & 0 \leq \eta \leq \frac{\pi}{4} \end{cases} \qquad 6.4.4$$

Thus for the surface $\xi = \xi_i$ we have

$$\operatorname{Tan}\alpha_i = \begin{cases} \dfrac{\operatorname{Tan}\alpha_{i,\frac{\pi}{2}}\,(1+\tanh^2\xi_i \cot^2\eta)^{1/2}}{\sin\eta}, & \frac{\pi}{4} \leq \eta \leq \frac{\pi}{2} \\ \dfrac{\operatorname{Tan}\alpha_{i,\frac{\pi}{2}} \sin^3 2\eta\,(1+\tanh^2\xi_i \cot^2\eta)^{1/2}}{\sin\eta}, & 0 \leq \eta \leq \frac{\pi}{4} \end{cases} \qquad 6.4.5$$

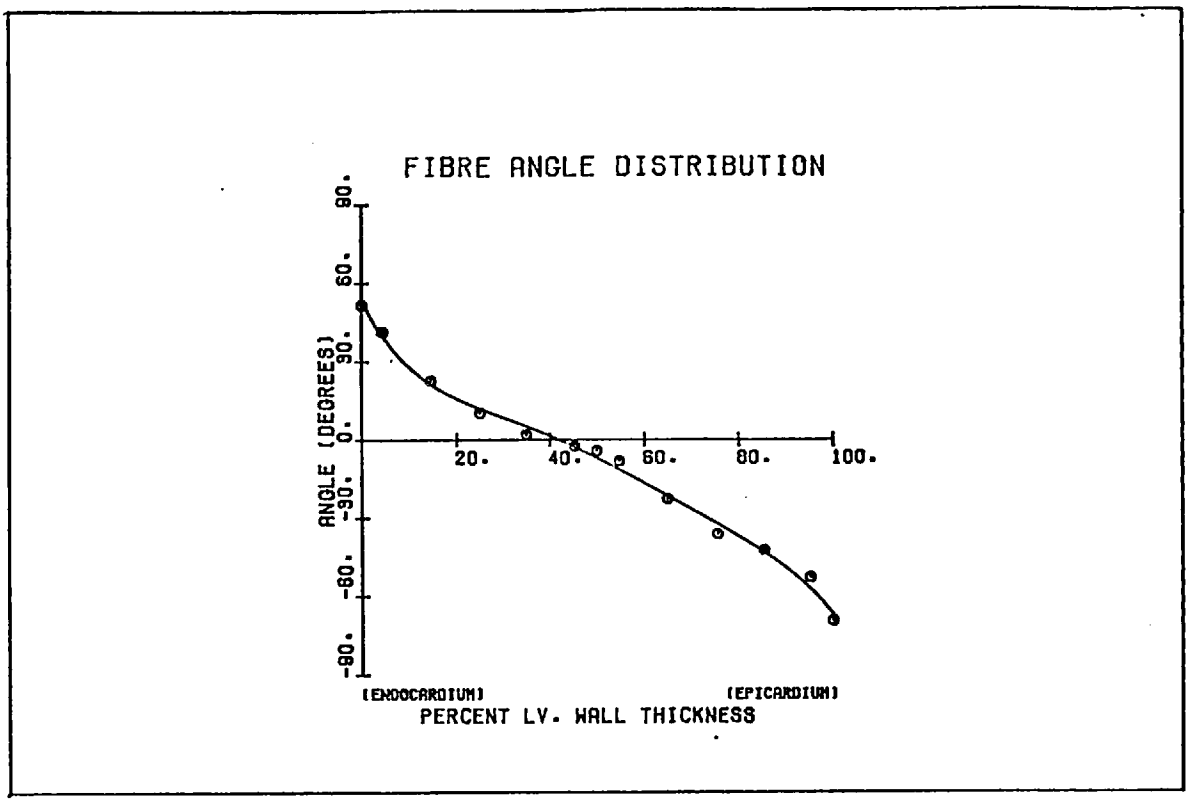

FIGURE 6.5: TRANSMURAL DISTRIBUTION OF FIBRE ANGLES AT THE EQUATOR; (AFTER STREETER ET AL, 1970)

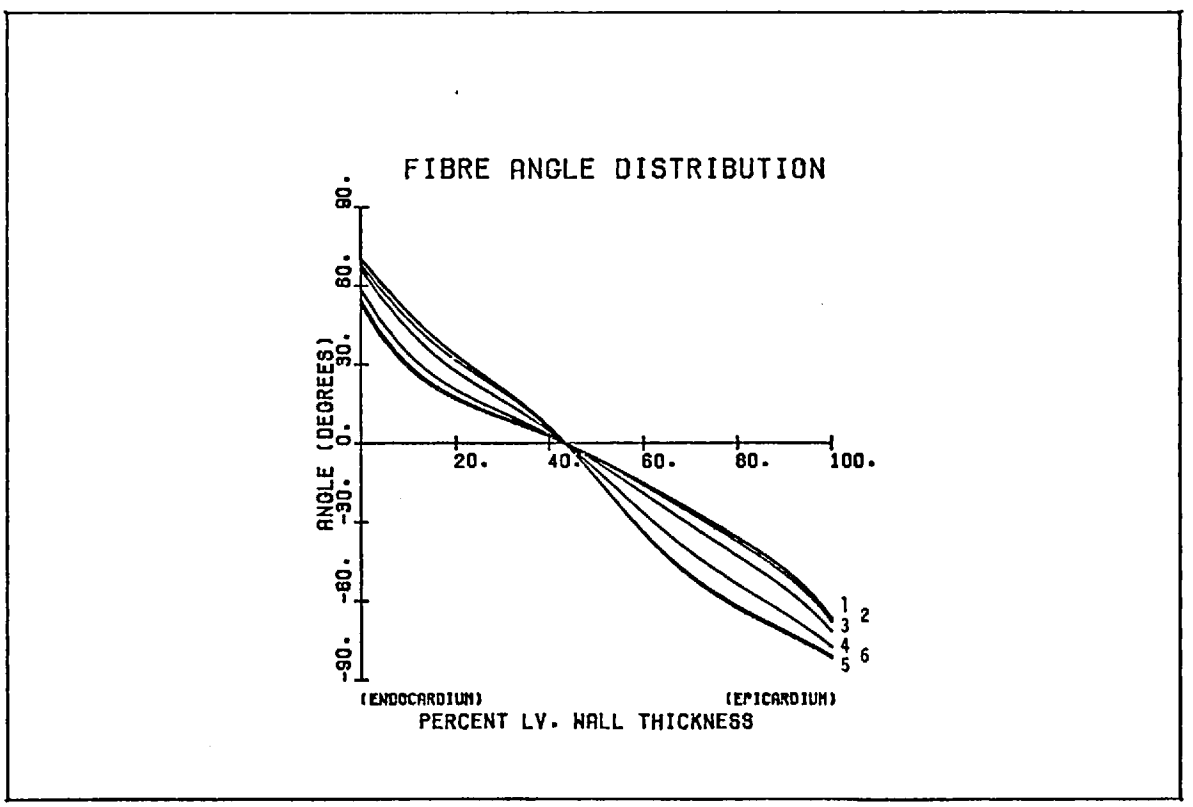

FIGURE 6.6: PREDICTED TRANSMURAL DISTRIBUTION OF FIBRE ANGLES AT DIFFERENT VALUES OF THE MERIDIONAL CO-ORDINATE η
1. $\eta = 90^{\circ}$, 2. $\eta = 75^{\circ}$, 3. $\eta = 60^{\circ}$, 4. $\eta = 45^{\circ}$, 5. $\eta = 30^{\circ}$, 6. $\eta = 15^{\circ}$,

where $\mathrm{Tan}\,\alpha_{i,\frac{\pi}{2}}$ gives the equatorial fibre angle for this surface. It can be seen from Fig. 6.6. that this assumption retains agreement with the experimental results in the equatorial region, but produces sensible predictions in the limit of the apex.

ELASTIC PROPERTIES OF CARDIAC MUSCLE

The mechanical behavior of isolated heart muscle has been exhaustively studied in both the passive and active states. In the passive state the properties of cardiac muscle resemble those of most biological soft tissues. The mechanical behavior in the active state, however, contains an additional and highly complex dynamic component. We consider here only the passive state and the isometric phase of the active state. In Fig. 6.7 typical "length-tension" curves are presented for these two cases.

Despite the obvious differences some features are common to the elastic properties of both these states. Cardiac muscle, like striated muscle, has a continuous fibre structure and tends to carry load along the axes of these fibres. The elastic properties are also extremely nonlinear, although the nature of this nonlinearity is different in the active and passive states.

Clearly, both these factors will be important in the analysis of left ventricular stresses. In this approach, however, we have chosen to emphasize the anisotropy of cardiac muscle fibres and to also include an exact treatment of nonlinearity would be very difficult. A quasi-linear approximation is therefore adopted and the effects of nonlinearity are introduced indirectly.

Visco-elastic features such as hysterisis, relaxation and fatigue are not considered.

In Fig. 6.4 we set up a curvilinear coordinate system (ξ', η', ϕ'), which is orthogonal to the fibre axis. The elastic properties of cardiac muscle are considered to be transversally isotropic with respect to this axis.

$$\varepsilon_{\xi'} = \frac{1}{E}\sigma_{\xi'} - \frac{\nu}{E}\sigma_{\eta'} - \frac{\nu'}{E'}\sigma_{\phi'}$$

$$\varepsilon_{\eta'} = -\frac{\nu}{E}\sigma_{\xi'} + \frac{1}{E}\sigma_{\eta'} - \frac{\nu'}{E'}\sigma_{\phi'}$$

$$\varepsilon_{\phi'} = -\frac{\nu'}{E'}\sigma_{\xi'} - \frac{\nu'}{E'}\sigma_{\eta'} + \frac{1}{E'}\sigma_{\phi'} \qquad 6.4.6$$

$$\gamma_{\eta\phi'} = \frac{1}{G'}\tau_{\eta\phi'}$$

$$\gamma_{\xi\phi'} = \frac{1}{G'}\tau_{\xi\phi'}$$

$$\gamma_{\xi\eta'} = \frac{2(1+\nu)}{E}\tau_{\xi\eta'}$$

where E, E' are the Young's moduli for the directions lying in the plane of isotropy and the direction perpindicular to it respectively; ν, ν' are the Poisson coefficients; G, G' are the shear moduli for the planes normal and parallel to the plane of isotropy.

Solving this set of equations we obtain :

$$\sigma_{\xi'} = A'_{11}\varepsilon_{\xi'} + A'_{12}\varepsilon_{\eta'} + A'_{13}\varepsilon_{\phi'}$$

$$\sigma_{\eta'} = A'_{12}\varepsilon_{\xi'} + A'_{11}\varepsilon_{\eta'} + A'_{13}\varepsilon_{\phi'}$$

$$\sigma_{\phi'} = A'_{13}\varepsilon_{\xi'} + A'_{13}\varepsilon_{\eta'} + A'_{33}\varepsilon_{\phi'}$$

$$\tau_{\eta\phi'} = A'_{44}\gamma_{\eta\phi'} \qquad 6.4.7$$

$$\tau_{\xi\phi'} = A'_{44}\gamma_{\xi\phi'}$$

$$\tau_{\xi\eta'} = \frac{1}{2}(A'_{11} - A'_{12})\gamma_{\xi\eta'} = A'_{66}\gamma_{\xi\eta'}$$

where

$$A'_{11} = \frac{E}{1+\nu}\,\frac{1 - \nu'^2\frac{E}{E'}}{1 - \nu - 2\nu'^2\frac{E}{E'}}$$

$$A'_{12} = \frac{E}{1+\nu}\,\frac{\nu - \nu'^2\frac{E}{E'}}{1 - \nu - 2\nu'^2\frac{E}{E'}}$$

$$A'_{13} = \frac{E\nu'}{1 - \nu - 2\nu'^2\frac{E}{E'}} \qquad 6.4.8$$

$$A'_{33} = \frac{E'(1-\nu)}{1 - \nu - 2\nu'^2\frac{E}{E'}}$$

$$A'_{44} = G'$$

$$A'_{66} = \frac{E}{2(1+\nu)}$$

For the "quasi-linear" approximation the Young's moduli are functions of the local components of deformation.

EVALUATION OF THE ELASTIC MODULI

To evaluate the elastic moduli the assumption of incompressibility is used. The relative change in volume accompanying a deformation is given by the dilatation ε , where

$$\varepsilon = \varepsilon_x + \varepsilon_y + \varepsilon_z \qquad 6.4.9$$

This expression is invariant in all coordinate systems and thus for cardiac muscle we have from 6.4.6 and 6.4.9

$$\varepsilon = \frac{1}{E}\left(1 - \nu - \nu'\frac{E}{E'}\right)\sigma_{\xi'} + \frac{1}{E}\left(1 - \nu - \nu'\frac{E}{E'}\right)\sigma_{\eta'} + \frac{1}{E'}(1 - 2\nu')\sigma_{\phi'} \qquad 6.4.10$$

For an incompressible body $\varepsilon = 0$

The condition of incompressibility must be independent of the applied stresses. This will be true only if

$$1 - 2\nu = 0 \qquad 6.4.11$$

$$1 - \nu - \nu'\frac{E}{E'} = 0$$

For this case, however, it can be shown that the elastic moduli are indeterminate. We therefore evaluate the elastic moduli in the limit

$$\lim_{\delta \to 0} \begin{cases} 1 - 2\nu' = \delta \\ \\ 1 - \nu - \dfrac{\nu'}{\beta} = \delta \end{cases} \qquad 6.4.12$$

where $\beta = \frac{E'}{E}$ is defined as the anisotropy parameter.

We assume throughout that $A'_{44} = A'_{66}$. Thus if a value is chosen for the anisotropy parameter β, it is possible to evaluate the relative magnitudes of the elastic moduli 6.4.8, with respect to the Young's modulus E.

TRANSFORMATION OF THE ELASTIC MODULI

The elastic moduli of cardiac muscle have been evaluated with respect to the fibre axis. It has been shown, however, that the angle of fibre orientation varies throughout the myocardium and to determine the elastic moduli for the confocal prolate spheroid coordinate system (ξ, η, Φ) we use the transformation expressions developed in a previous section.

We consider that the orientation of a fibre at any point, with respect to the coordinate system (ξ, η, Φ), is given by a simple rotation. Thus the relationship between the coordinate system (ξ', η', Φ') orthogonal to the fibre axis and the coordinate system (ξ', η', Φ') is described by Table 6.3

	ξ'	η'	ϕ'
ξ	1	0	0
η	0	$\cos\alpha$	$-\sin\alpha$
ϕ	0	$\sin\alpha$	$\cos\alpha$

TABLE 6·3

It is quite straightforward to obtain the terms R_{ij} for the transformation matrix 6.2.14, from Table 6.2. Using expression 6.2.21 we can, therefore, evaluate the elastic moduli with respect to the coordinate system (ξ, η, Φ).

$$A_{11} = A'_{11}$$

$$A_{12} = A'_{12}\cos^2\alpha + A'_{13}\sin^2\alpha$$

$$A_{13} = A'_{13}\cos^2\alpha + A'_{12}\sin^2\alpha$$

$$A_{14} = (A'_{13} - A'_{12})\sin\alpha\cos\alpha$$

6.4.13

$$A_{22} = A'_{11}\cos^4\alpha + A'_{33}\sin^4\alpha + 2(A'_{13}+2A'_{44})\sin^2\alpha\cos^2\alpha$$

$$A_{23} = A'_{13}(\cos^4\alpha + \sin^4\alpha) + (A'_{11} + A'_{33} - 4A'_{44})\sin^2\alpha\cos^2\alpha$$

$$A_{24} = A'_{33}\sin^3\alpha\cos\alpha - A'_{11}\sin\alpha\cos^3\alpha + (A'_{13}+2A'_{44})\sin\alpha\cos\alpha\,(\cos^2\alpha - \sin^2\alpha)$$

$$A_{33} = A'_{33}\cos\alpha + A'_{11}\sin\alpha + 2(A'_{13}+2A'_{44})\sin^2\alpha\cos^2\alpha$$

$$A_{34} = A'_{33}\sin\alpha\cos^3\alpha - A'_{11}\sin^3\alpha\cos\alpha - (A'_{13}+2A'_{44})\sin\alpha\cos\alpha\,(\cos^2\alpha-\sin^2\alpha)$$

$$A_{44} = A'_{44} + (A'_{11}+A'_{33}-2(A'_{13}+2A'_{44}))\sin^2\alpha\cos^2\alpha$$

$$A_{55} = A'_{44}\cos^2\alpha + A'_{66}\sin^2\alpha$$

$$A_{56} = (A'_{66}-A'_{44})\sin^2\alpha\cos^2\alpha$$

$$A_{66} = A'_{66}\cos^2\alpha + A'_{44}\sin^2\alpha$$

CONDITIONS FOR STABLE AXI-SYMMETRIC DEFORMATION

A fundamental assumption of this work is that the left ventricle deforms as a body of revolution. An isotropic body always remains a body of revolution under deformation; that is it deforms axi-symmetrically. For a body with anisotropic elastic properties, however, this will be true only in certain cases.

Consider the confocal prolate spheroid representation of the left ventricle. For axi-symmetric deformation to take place the displacement components must satisfy the requirement :

$$u = u(\xi,\eta) \quad v = v(\xi,\eta) \quad \omega = 0$$

And thus

$$\gamma_{\xi\phi} = \gamma_{\eta\phi} = 0 \qquad 6.4.14$$

Such a deformation will be stable only if :

$$\tau_{\xi\phi} = \tau_{\eta\phi} = 0 \qquad 6.4.15$$

For a thick ellipsoid shell orthogonally anisotropic or orthotropic elastic properties are the most general that are consistent with the requirements for stable axi-symmetric deformation.

The relationships between stress and strain for orthogonal anisotropy are given by :

$$\begin{Bmatrix} \sigma_\xi \\ \sigma_\eta \\ \sigma_\phi \\ \tau_{\eta\phi} \\ \tau_{\xi\phi} \\ \tau_{\xi\eta} \end{Bmatrix} = \begin{bmatrix} A_{11} & A_{12} & A_{13} & & & \\ A_{12} & A_{22} & A_{23} & & & \\ A_{13} & A_{23} & A_{33} & & & \\ & & & A_{44} & & \\ & & & & A_{55} & \\ & & & & & A_{66} \end{bmatrix} \begin{Bmatrix} \varepsilon_\xi \\ \varepsilon_\eta \\ \varepsilon_\phi \\ \gamma_{\eta\phi} \\ \gamma_{\xi\phi} \\ \gamma_{\xi\eta} \end{Bmatrix} \qquad 6.4.16$$

We have derived expressions for the elastic constants of the left ventricular myocardium and these are listed in 6.4.13. Clearly, these elastic properties are not consistent with the conditions for stable axi-symmetric deformation and in the present analysis, we neglect the terms A_{14}, A_{24}, A_{34}, A_{56}. While the magnitudes of these elastic constants are much less than those for A_{11}, A_{12}, A_{13}, A_{22}, A_{23}, A_{33}, they do give rise to significant circumferential shear forces. If the equilibrium equations are developed for the most general case, however, it can be shown that inclusion of these shear terms would only marginally alter the stress distributions obtained in the present analysis.

The apex must be considered as a special case.

At this point $R_1 = R_2$ and $\varepsilon_\eta = \varepsilon_\phi$

For stable deformation, therefore, the following must hold

$$\sigma_\eta = \sigma_\phi$$

but this will be true only if $A_{13} = A_{12}$, $A_{22} = A_{33}$, $A_{55} = A_{66}$

Thus at the apex the most general elastic properties consistent with stable deformation are those of transverse isotropy with respect to the radial direction. In reality, muscle fibres are circumferentially oriented in this region. The stability condition is therefore not satisfied and for this reason the left ventricle deforms inwards at the apex, giving rise to the so-called apical "dimple" or "vortex".

NONHOMOGENOUS AND NONLINEAR ELASTIC PROPERTIES

The myocardium is an heterogenous medium comprising not just muscle fibres, but also an extensive network of blood vessels. For this composite structure the elastic moduli must be less than those evaluated for cardiac muscle alone. We assume that the reduction in compliance is uniform; that the Young's moduli E and E' are decreased equally.

The proportion of the total volume occupied by blood vessels increases toward the endocardium. At any point in the myocardium, therefore, the elastic moduli should be considered as functions of the spatial co-ordinates.

Typically

$$E = E_o G(\xi,\eta), \qquad E' = E'_o G(\xi,\eta). \tag{6.4.17}$$

the anisotropy parameter β is constant.

In this study the Young's moduli are assumed to be linear functions of the radial coordinate alone.

Consider now the mechanical properties for isolated cardiac muscle presented in Fig. 6.7. These results were obtained under conditions of axial loading: $\sigma_{\xi'} = \sigma_{\eta'} = 0$; as before, the co-ordinate system (ξ', η', ϕ') is orthogonal to the fibre axis.

Thus by definition

$$\sigma_{\phi'} = E'\varepsilon_{\phi'} \tag{6.4.18}$$

Clearly, the Young's modulus E' for the axial direction is a function of axial strain and to a reasonable approximation

$$\sigma_{\phi'} = E'_1\varepsilon_{\phi'} + E'_2\varepsilon^2_{\phi'} \tag{6.4.19}$$

Two separate cases must be considered here; for the passive state $E'_2 > 0$ and for the active state $E'_2 < 0$. The Young's modulus E in the transverse plane is assumed to be independent of the magnitude of local strain.

Therefore, the anisotropy parameter β exactly reflects the variation of the Young's modulus E'

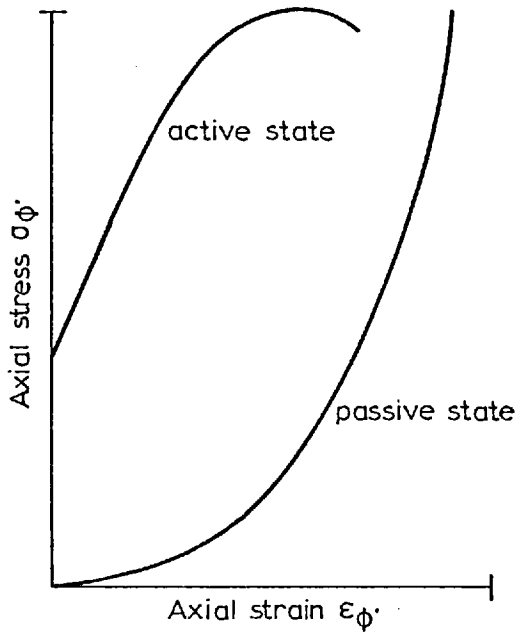

FIGURE 6.7 : The mechanical properties of isolated cardiac muscle.

The transformation expressions for the elastic constants developed previously, apply in the linear case only. However, we introduce the effects of nonlinear elasticity indirectly, as an extension of the treatment for nonhomogeneity. If the axial strain distribution is known exactly, it is possible to obtain the anisotropy parameter β for different values of the radial co-ordinate using the expression

$$E' = E'_1 + E'_2 \varepsilon_{\phi'} \qquad 6.4.20$$

This may then be used to solve the left ventricular stress distribution. A formal, quasi-linear iterative technique can be based on this approach.

6.5 SOLUTION OF THE EQUILIBRIUM EQUATIONS

EQUATORIAL SOLUTION

At the equator, displacement takes place in the radial direction only. Thus $\tau_{\xi\eta} = 0$ and the equilibrium equations 6.3.12 reduce to

$$\frac{d\sigma}{d\xi}_{\xi} + (\sigma_{\xi} - \sigma_{\eta}) \operatorname{Tanh}\xi + (\sigma_{\xi} - \sigma_{\phi}) \operatorname{Coth}\xi = 0 \qquad 6.5.1$$

Using 6.3.8 and 6.4.16, we obtain the equilibrium equation 6.5.1 in terms of the displacement component U

$$\frac{d^2U}{d\xi^2} + \operatorname{Coth}\xi \frac{dU}{d\xi} + \frac{1}{A_{11}} \left[\begin{array}{l} 2(A_{12} - A_{23}) + A_{13} - (A_{12} + A_{22}) \operatorname{Tanh}^2\xi - A_{33} \operatorname{Coth}^2\xi \\ \\ + A_{66} \operatorname{Sech}^2\xi + \frac{\delta A_{12}}{\delta \xi} \operatorname{Tanh}\xi + \frac{\delta A_{13}}{\delta \xi} \operatorname{Coth}\xi \end{array} \right] U = 0 \qquad 6.5.2$$

A_{11}, A_{12} etc. are the transformed elastic moduli.

It is assumed that the ventricle supports hydrostatic pressure only and that the epicardial pressure is negligible. The boundary conditions at the endocardium and epicardium, respectively, are:

$$\sigma_{\xi} = -P, \quad \xi = \xi_1 \quad \text{and} \quad \sigma_{\xi} = 0, \quad \xi = \xi_2$$

where P is the intraventricular pressure.

This is a closed form of the boundary value problem, which can be solved using conventional numerical techniques. An initial value is chosen for the displacement at the endocardium and the first derivative is calculated to satisfy the endocardial boundary condition. The magnitude of the radial stress at the epicardium is then determined from these values using a fourth-order Runge-Kutta estimator and this is used to correct the initial guess. In this way, a solution which satisfies the boundary conditions at both the endocardium and the epicardium is rapidly converged upon. If we introduce the variable transformation

$$U' = \frac{E}{P} U \qquad 6.5.3$$

it is possible to obtain the normalised transmural stress distribution without evaluating the Young's modulus E.

APICAL SOLUTION

The physical reasons for the existence of an apical "dimple" or "vortex" were considered previously. We do not, however, include this feature in the solution of the stress distribution at the apex.

The most general elastic properties consistent with stable deformation at the apex are those of transverse isotropy with respect to the radial direction. It can be shown, that the stress distribution for this case is identical to that for the isotropic case. We therefore present the solution of the apical stress distribution for isotropic elastic properties only.

At the apex, as with the equator, it follows from symmetry that displacement

occurs in the radial direction only. For a stable axi-symmetric deformation we require that $\sigma_\eta = \sigma_\phi$ The equilibrium equations 6.3.12 therefore reduce to

$$\frac{d\sigma}{d\xi}\xi + 2(\sigma_\xi - \sigma_\phi)\,\mathrm{Coth}\xi = 0 \qquad 6.5.4$$

Expressed in terms of the displacement component U the equilibrium equation is

$$\frac{d^2U}{d\xi^2} + \mathrm{Coth}\xi\,\frac{dU}{d\xi} + \frac{2A_{12} - 2(A_{11}+A_{12})\,\mathrm{Coth}^2\xi - (A_{11}-A_{12})\,\mathrm{Cosech}^2\xi}{A_{11}}\,U = 0 \qquad 6.5.5$$

The boundary conditions and mathematical techniques used here are identical to those for the equator.

GENERAL SOLUTION

In general, the displacement vector at any point within the ventricular wall will have both radial and meridional components. If we express the equilibrium equations 6.3.12 in terms of the displacement components U and V, we obtain two linked second order partial differential equations of the form :

$$A_1\frac{\delta^2U}{\delta\xi^2} + B_1\frac{\delta^2U}{\delta\xi\delta\eta} + C_1\frac{\delta^2U}{\delta\eta^2} + D_1\frac{\delta U}{\delta\xi} + E_1\frac{\delta U}{\delta\eta} + F_1U$$
$$+ a_1\frac{\delta^2V}{\delta\xi^2} + b_1\frac{\delta^2V}{\delta\xi\delta\eta} + c_1\frac{\delta V}{\delta\eta^2} + d_1\frac{\delta V}{\delta\xi} + e_1\frac{\delta V}{\delta\eta} + f_1V = 0 \qquad 6.5.6$$

At the endocardium and epicardium, respectively, the following boundary conditions hold:

$$\sigma_\xi = -P,\ \tau_{\xi\eta} = 0\ ; \quad \sigma_\xi = 0,\ \tau_{\xi\eta} = 0$$

The equilibrium equations and boundary expressions can be converted into a set of simultaneous linear equations using a finite difference scheme. It is then feasible, though extremely tedious, to obtain solutions for U and V using an iterative relaxation technique, such as the Gauss Seidal method.

However, the use of confocal prolate spheroid notation means that we can solve a much simpler expression with only a marginal loss of accuracy. It has been shown by Dieudonné (1969) and Streeter and Hanna (1973)[1] that, for the confocal prolate spheroid representation of the left ventricle, the focal length a remains remarkably constant over a wide range of deformation.

This will be true only if $V \ll U$.

We therefore neglect the meridional component of displacement and the equilibrium equations 6.3.12 reduce to

$$\frac{d^2U}{d\xi^2} + \mathrm{Coth}\xi \frac{dU}{d\xi} \qquad 6.5.7$$

$$+ \frac{1}{A_{11}} \left[A_{13} - A_{33}\,\mathrm{Coth}^2\xi + \frac{\delta A_{13}}{\delta \xi}\mathrm{Coth}\xi \right.$$

$$\left. + \frac{2(A_{12}-A_{23})\mathrm{Cosh}^2\xi + A_{12}\mathrm{Sinh}^2\xi - A_{66}(2\mathrm{Cos}^2\eta - \mathrm{Sin}^2\eta) + \frac{\delta A}{\delta \xi}_{13}\mathrm{Sinh}\xi\mathrm{Cosh}\xi}{\mathrm{Sinh}^2\xi + \mathrm{Sin}^2\eta} \right.$$

$$\left. - \frac{(A_{22}+2A_{12})\,\mathrm{Sinh}^2\xi\mathrm{Cosh}^2\xi + A_{66}\,\mathrm{Sin}^2\eta\,\mathrm{Cos}^2\eta}{(\mathrm{Sinh}^2\xi + \mathrm{Sin}^2\eta)^2} \right] U=0$$

For any meridional co-ordinate η we obtain the transmural stress distribution using the methods already described for the apex and equator.

6.6 RESULTS

The numerical values used here for left ventricular wall geometry and fibre distribution are taken from averaged data for the canine heart, arrested at end-diastole. This was published by Streeter et al (1970) and Streeter and Hanna (1973)[1, 2].

	ENDOCARDIUM	EPICARDIUM
X cm.	1.91 ± 0.10	2.84 ± 0.10
Z cm.	4.18 ± 0.26	4.74 ± 0.23

TABLE 6.4

X is the minor semi-axis

Z is the major semi-axis

See Fig. 6.2

From these values for the major and minor semi-axes we obtained a confocal prolate spheroid representation for the left ventricle. The focal length a was estimated from both endocardial and epicardial co-ordinates using the expression 6.3.4 and the averaged result is $a = 3.74 \pm 0.1$ cm. Co-ordinates ξ_1, ξ_2 specifying the endocardial and epicardial surfaces, respectively, were then obtained from

$$\xi_i = \sinh^{-1}\frac{X_i}{a} \qquad i = 1, 2$$

An expression for the equatorial distribution of fibre angles was determined by fitting a polynomial to measured values of fibre orientation given by

Streeter et al (1970); the best fit polynomial and the experimental data on which it is based are presented in Fig. 6.5

ANISOTROPY AND FIBRE DISTRIBUTION

We consider first the isotropic homogenous model of the left ventricle and the equatorial stress distribution for this case is given in Fig. 6.8. Mirsky (1969), presented very similar results for the isotropic left ventricle and discrepancies between the stresses predicted in these two studies reflect the different geometrical models used.

If the muscle fibres are assumed to be transversally isotropic and circumferentially oriented with respect to the axis of rotation for the left ventricle, we obtain the results given in Fig. 6.9. While mean circumferential stress is increased and mean meridional stress is decreased with increasing values of the anisotropy parameter β , the transmural stress distribution here is not markedly different to the isotropic result. Further, it can be seen from Fig. 6.11 that for values of the anisotropy parameter $\beta > 5$ the stress distribution tends towards a limiting case. Again, the results compare very closely to those given by Mirsky (1970) for a study based on similar assumptions.

When the description of the elastic properties of myocardium includes the variable orientation of cardiac muscle fibres the nature of the stress distribution is radically altered; see Fig. 6.10. As before, however, mean circumferential stress increases and mean meridional stress is reduced as the values of β are increased. We note from Fig. 6.11 that there is a limiting stress distribution in this case also. The results in Fig. 6.10 superficially

resemble those presented by Streeter et al (1970) for an analysis based on an identical distribution of fibre angles. There are, however, significant differences between them. In the present study peak circumferential stress is located between the subendocardial and midwall regions; Streeter et al found peak circumferential stress at the midwall. Additionally, the estimates of peak and mean circumferential stress are about 20% greater for the former case than for the latter. These differences are almost certainly due to the qualitative nature of the approach used by Streeter et al (1970). Simplifications adopted by them include: the treatment of the ventricle as a set of interconnected shells, the use of the thin shell equilibrium equation and the assumption that each muscle fibre carries the same axial load.

Using the transformation expressions given in Table 6.2, it is possible to find the stresses acting in the direction of the fibre axes at the equator from the circumferential and meridional stress distributions. In Fig. 6.12 results are presented for the equatorial distributions of both axial stress and the stress acting perpendicular to the fibre axis. We also reproduce experimental results for average equatorial sarcomere lengths measured at different sites across the ventricular wall; Yoran et al (1973), Fig. 6.13. The very close correlation of the axial stress distributions obtained in the present analysis and experimentally determined values for axial fibre deformation is of some interest and this result has not previously been demonstrated.

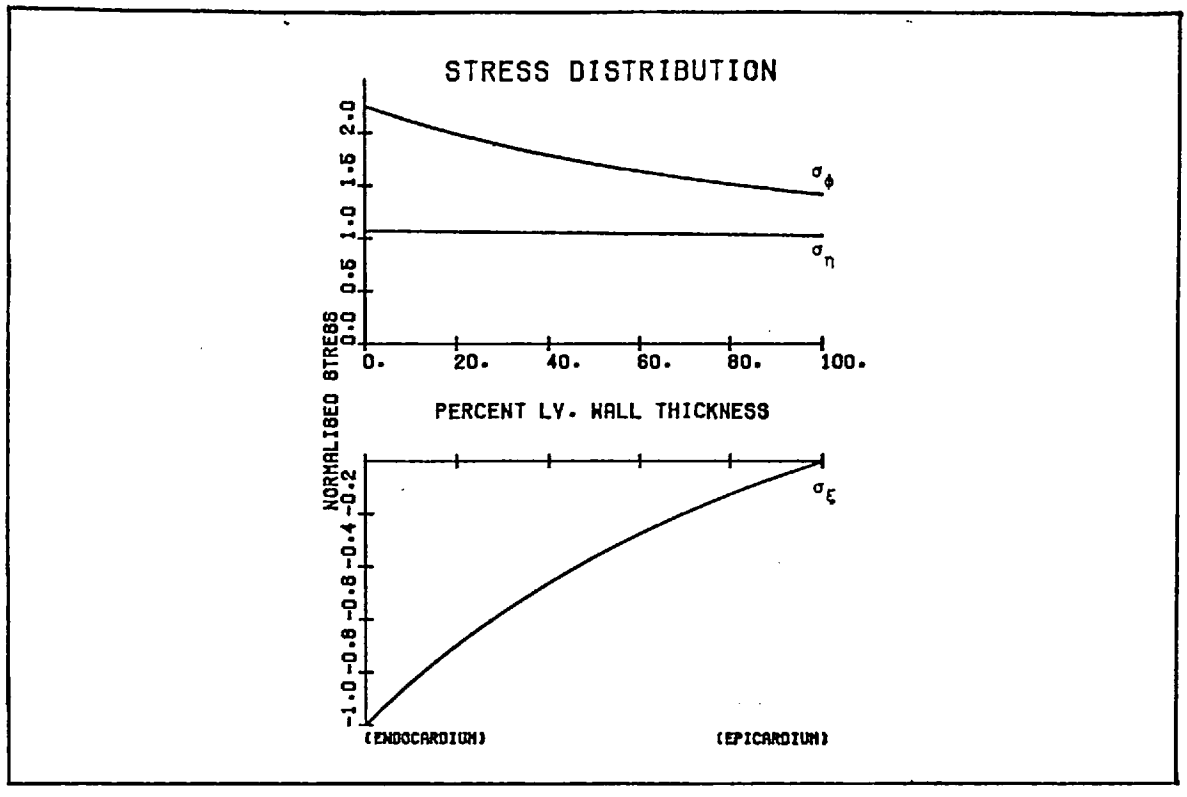

FIGURE 6.8: STRESS DISTRIBUTION AT THE EQUATOR; ISOTROPIC ELASTIC PROPERTIES

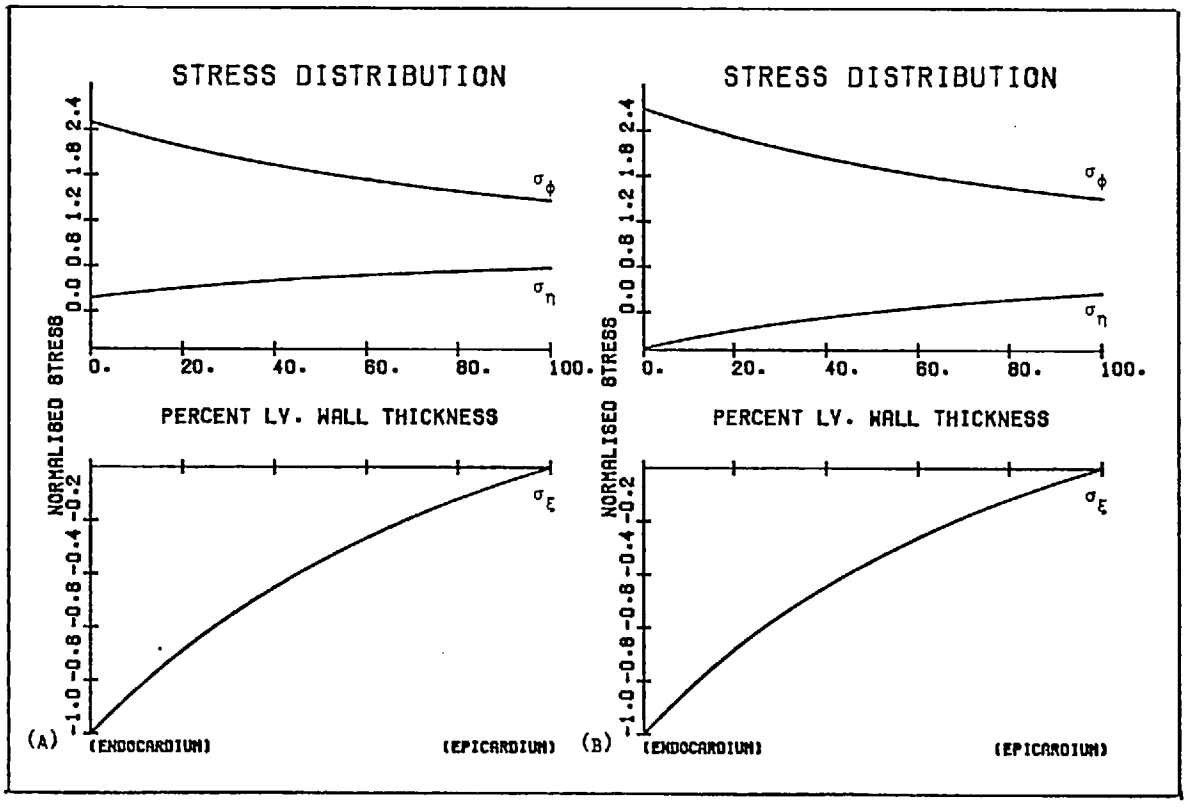

FIGURE 6.9: STRESS DISTRIBUTION AT THE EQUATOR; ANISOTROPIC ELASTIC PROPERTIES, CIRCUMFERENTIAL FIBRE ORIENTATION
(A) $\beta = 2$, (B) $\beta = 5$

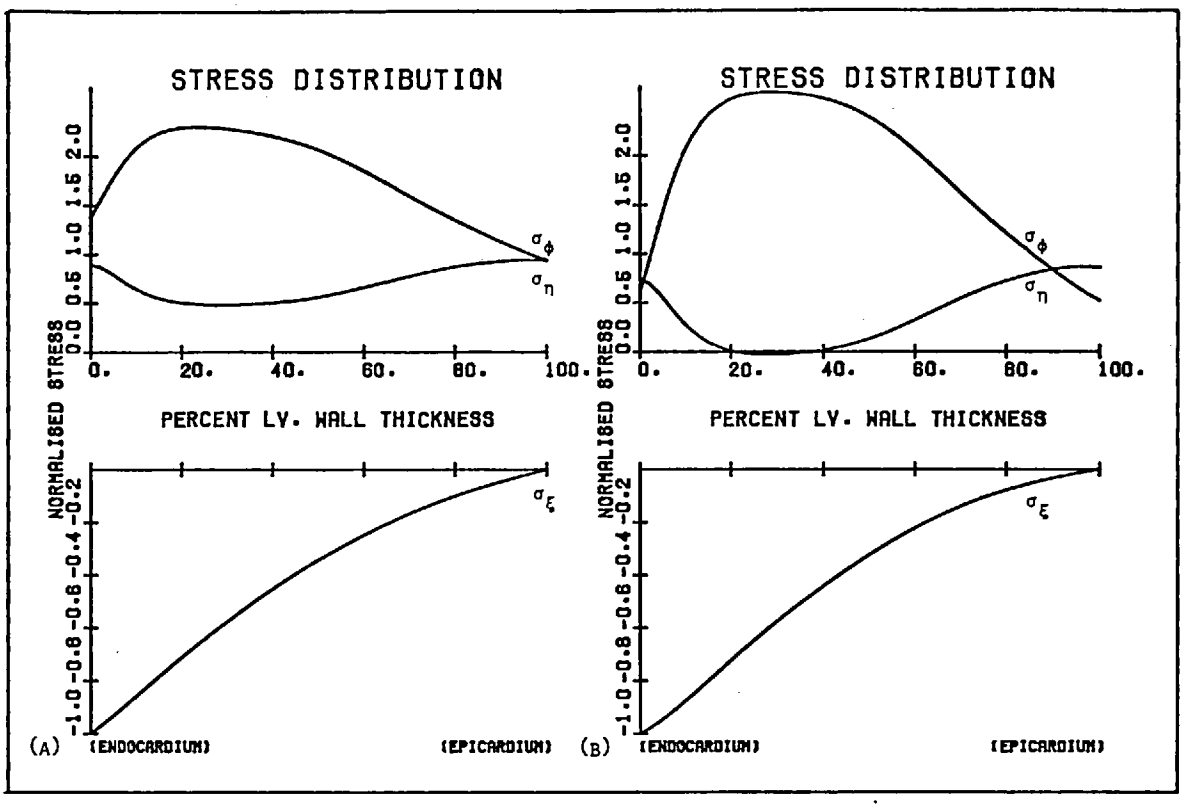

FIGURE 6.10: STRESS DISTRIBUTION AT THE EQUATOR; ANISOTROPIC ELASTIC PROPERTIES, VARIABLE FIBRE ORIENTATION
(A) $\beta = 2$, (B) $\beta = 5$

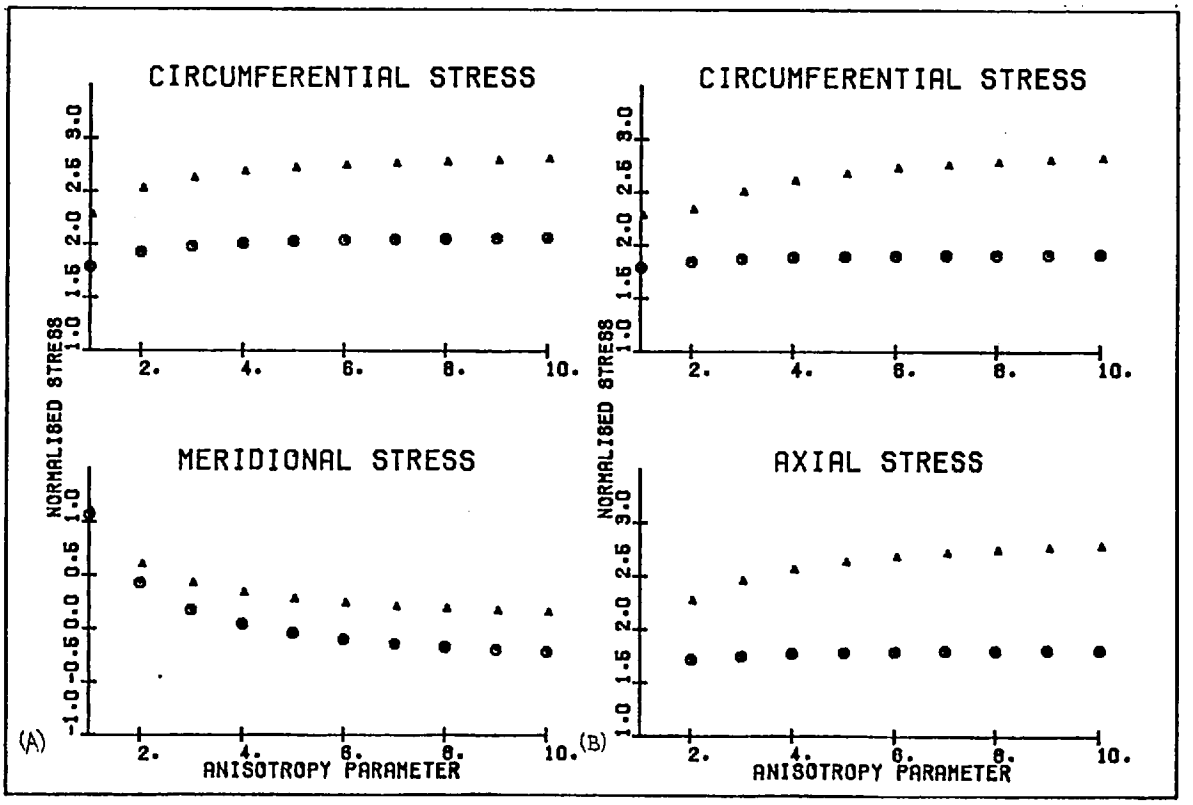

FIGURE 6.11: VARIATION OF STRESSES AT THE EQUATOR WITH INCREASING ANISTROPY PARAMETER β ;
▲ MAXIMUM STRESS, ⊙ MEAN STRESS
(A) CIRCUMFERENTIAL FIBRE ORIENTATION
(B) VARIABLE FIBRE ORIENTATION

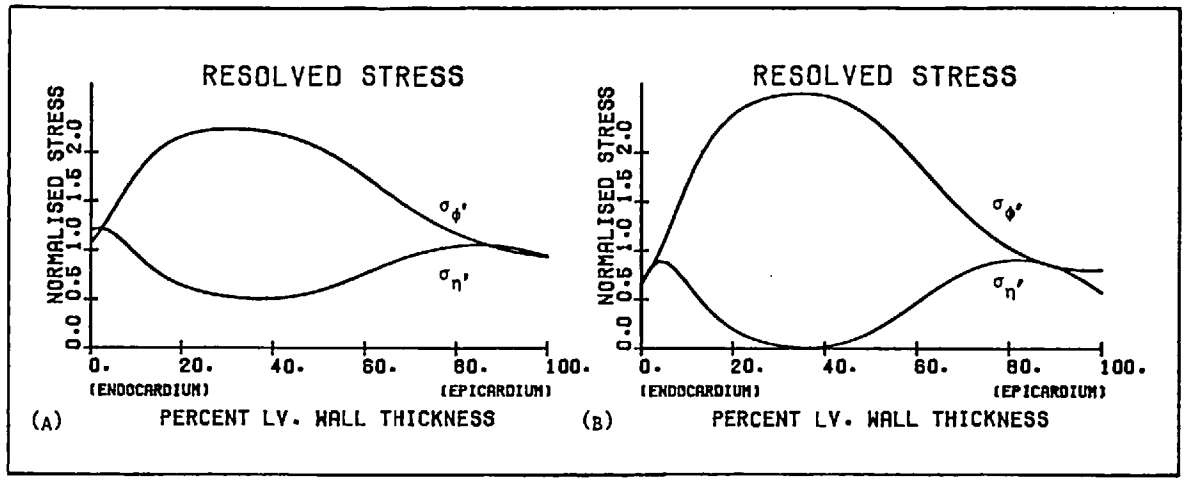

FIGURE 6.12: AXIAL AND TRANSVERSE FIBRE STRESS AT THE EQUATOR; ANISOTROPIC ELASTIC PROPERTIES, VARIABLE FIBRE ORIENTATION
(A) $\beta = 2$, (B) $\beta = 5$

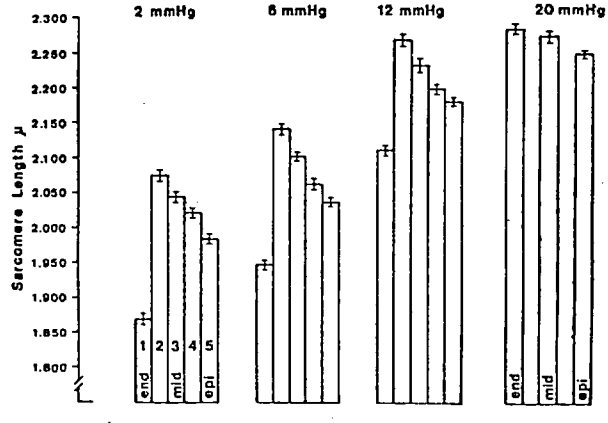

FIGURE 6.13: SARCOMERE LENGTHS AND DISTRIBUTIONS ACROSS THE LEFT VENTRICULAR WALL AT FILLING PRESSURES OF 2, 6, 12 AND 20 MM HG; (FROM YORAN ET AL, 1973)
SITE 1 (END) IS THE SUBENDOCARDIAL LAYER, SITE 2 (MID) IS THE MIDWALL LAYER, SITE 3 (EPI) IS THE SUBEPICARDIAL LAYER
SITE 2 IS MIDWAY BETWEEN SITES 1 AND 3, SITE 4 IS MIDWAY BETWEEN SITES 3 AND 6

VARIATION OF LEFT VENTRICULAR DIMENSIONS

As the left ventricle is enlarged endocardial and epicardial dimensions are increased and wall thickness is reduced. It has been stated that the left ventricle deforms as a confocal prolate spheroid shell; we consider, separately, the effect on the equatorial stress distribution of changes in the endocardial minor semi-axis X_1 and the wall thickness H.

In Fig. 6.14 the results for peak and mean circumferential and meridional stresses at a constant wall thickness H^o are plotted for different values of the normalised surface parameter X_1 / X_1^o. The same indices of stress are also presented in Fig. 6.15 as functions of the normalised wall thickness parameter H^0 / H and in this case the endocardial minor semi-axis is fixed at the value X_1^0. It should be noted that $H^0 = X_2^0 - X_1^0$, where X_1^0, X_2^0 are the experimental minor semi-axes given in Table 6.4. We also compare these results with estimates of mean circumferential and meridional stress based on the Laplace approximation for an ellipsoid shell; the expressions used here were taken from Mirsky (1969).

It can be seen that, under variation of both the surface parameter and the wall thickness parameter, the values of mean circumferential stress determined using the present model lie between the Laplace estimates for thin walled ellipsoid shells with endocardial and midwall dimensions. The rate of change of mean stress with variations in ventricular dimension does not, however, correlate well with either of the thin shell results. Neither is mean meridional stress predicted by these approximations.

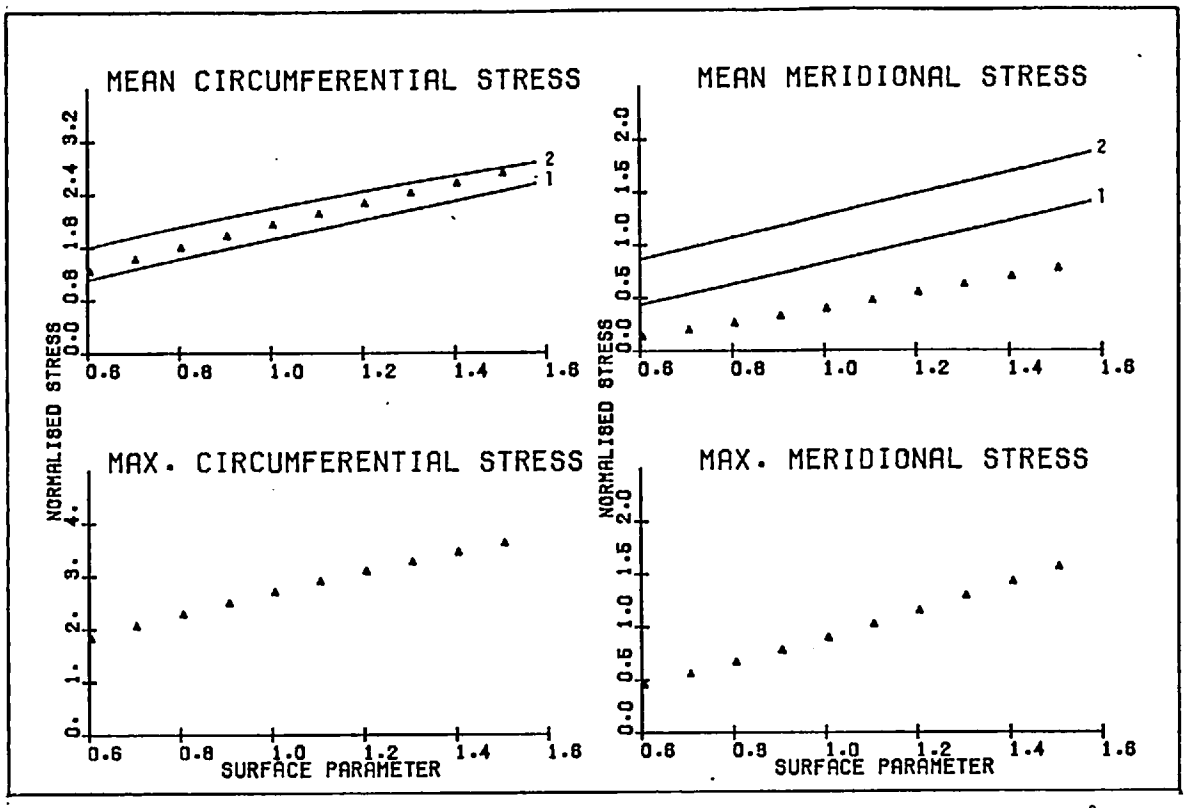

FIGURE 6.14: VARIATION OF STRESSES AT THE EQUATOR WITH INCREASING SURFACE PARAMETER X_1/X_1^0 AND FIXED WALL THICKNESS H^0;
ANISOTROPIC ELASTIC PROPERTIES $\beta = 5$, VARIABLE FIBRE ORIENTATION
1 AND 2 ARE LAPLACE ESTIMATES FOR MEAN STRESSES IN THIN ELLIPSOID SHELLS WITH ENDOCARDIAL AND MIDWALL CO-ORDINATES RESPECTIVELY

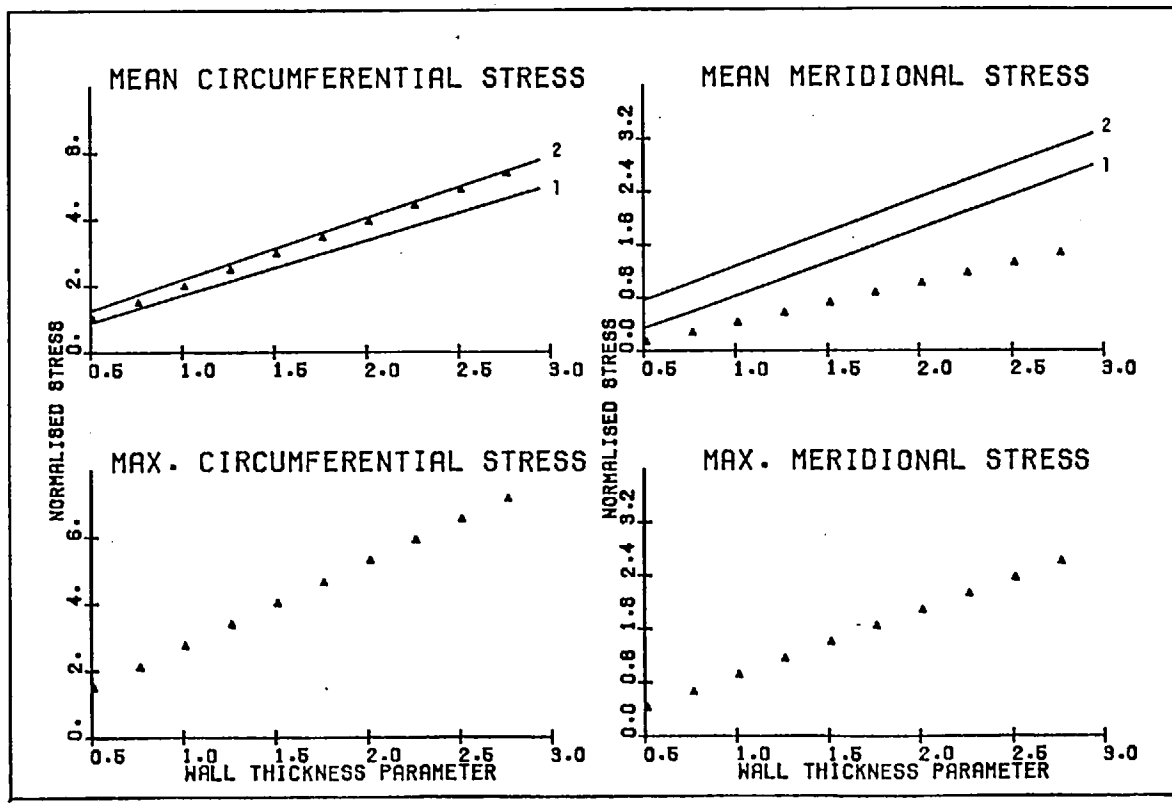

FIGURE 6.15: VARIATION OF STRESSES AT THE EQUATOR WITH INCREASING WALL THICKNESS PARAMETER H^0/H AND FIXED ENDOCARDIAL MINOR SEMI-AXIS X_1^0; AS ABOVE

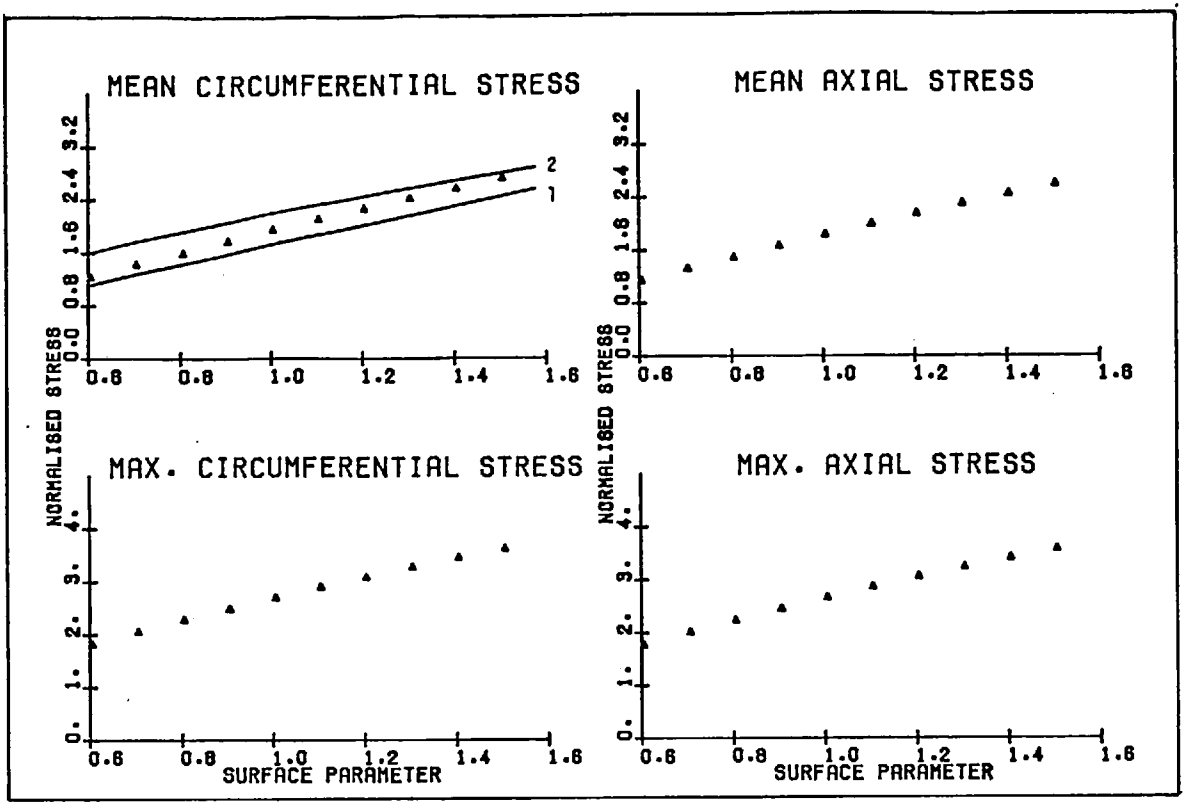

FIGURE 6.16: COMPARISON OF CIRCUMFERENTIAL AND AXIAL STRESS AT THE EQUATOR AS THE SURFACE PARAMETER X_1/X_1^0 IS INCREASED AT A FIXED WALL THICKNESS H^0;
ANISOTROPIC ELASTIC PROPERTIES $\beta = 5$, VARIABLE FIBRE ORIENTATION
1 AND 2 ARE LAPLACE ESTIMATES FOR MEAN STRESSES IN THIN ELLIPSOID SHELLS WITH ENDOCARDIAL AND MIDWALL CO-ORDINATES RESPECTIVELY

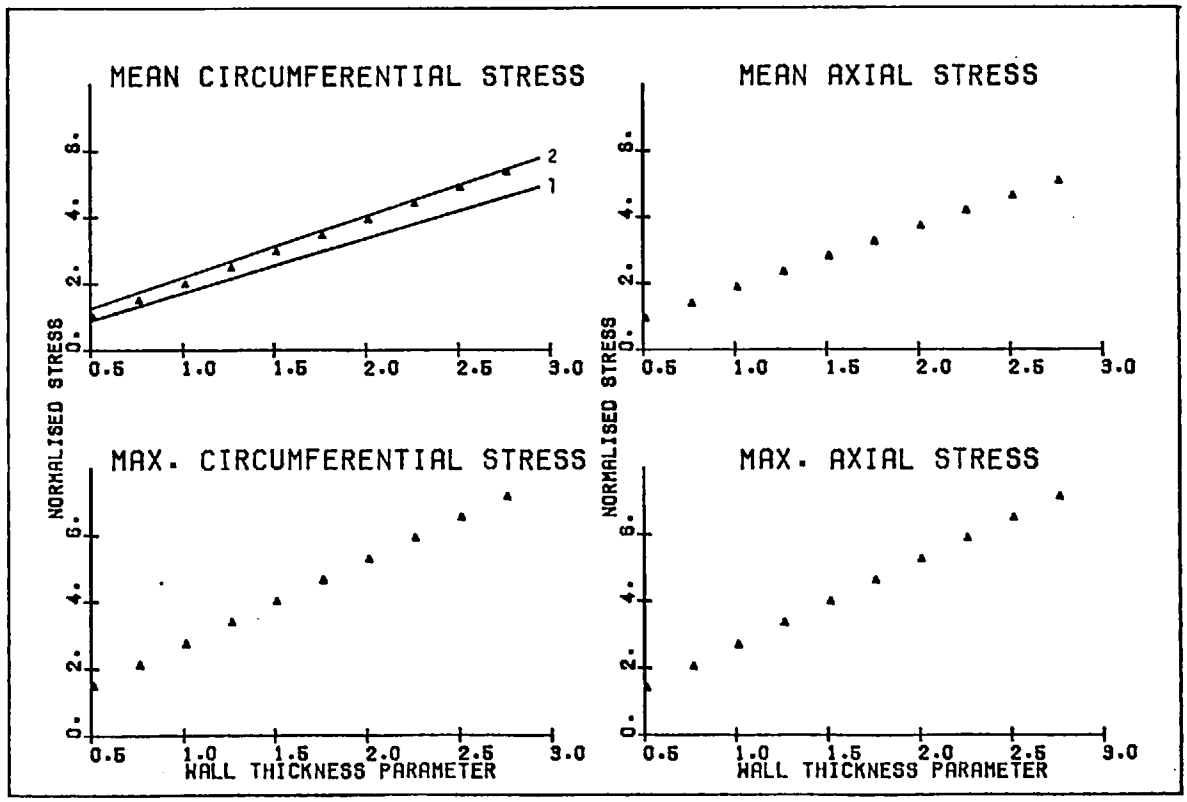

FIGURE 6.17: COMPARISON OF CIRCUMFERENTIAL AND AXIAL STRESS AT THE EQUATOR AS THE WALL THICKNESS PARAMETER H^0/H IS INCREASED AT A FIXED ENDOCARDIAL MINOR SEMI-AXIS X_1^0;
AS ABOVE

McHale and Greenfield (1973) directly measured mean circumferential stresses at the equator for canine hearts in a variety of haemodynamic states. These were compared with estimates of mean circumferential stress based on a number of simple models of the left ventricle. They found that a thin walled ellipsoid shell model with midwall dimensions gave the closest estimate for the magnitude of mean circumferential stress, but that it underestimated the rate of change of stress with variations in ventricular dimension. These results agree quite closely with those of the present study.

The results presented in Figs. 6.16 and 6.17 are also of interest. It can be seen that peak and mean values of circumferential and axial stress are identical under changes in ventricular dimension. From this, it follows that the average stress developed or supported by muscle fibres at the equator can be estimated with reasonable accuracy using a thin walled ellipsoid shell model based on midwall dimensions.

NONHOMOGENEITY AND NONLINEARITY

We now consider the effects of nonhomogenous and nonlinear elastic properties on the equatorial distribution of left ventricular stress. It has been stated that myocardium is an heterogenous medium; the Young's moduli E and E' are considered to vary linearly across the left ventricular wall, such that the anisotropy parameter β remains constant. The magnitudes of the Young's moduli are assumed to be smallest at the endocardium and the absolute variation in the magnitude of E and E' from endocardium to epicardium is 40%

of the midwall value. From Fig. 6.18 it can be seen that the inclusion of this nonhomogeneity results in a skewing of the stress distribution with respect to the homogenous case and also leads to a significant increase in the values of peak and mean circumferential stress.

The treatment of nonlinearity described here is essentially qualitative, although the quasi-linear approach used could be extended to obtain more rigorous solutions. We treat the anisotropy parameter β as a simple function of axial strain; two separate cases are distinguished and these correspond to the mechanical properties of isolated cardiac muscle in the passive and active states.

We recall that in the passive state the Young's modulus E' for the axial direction increases with axial deformation. For the results presented in Fig. 6.19 the transmural variation of the anisotropy parameter reflects these nonlinear elastic properties. It can be seen that the inclusion of nonlinearity produces increased values of peak circumferential stress, but that mean stress and the location of peak circumferential stress are not changed.

The results for the active state are quite different. In this case the Young's modulus E' remains essentially constant for small deformations, but is reduced progressively as the axial deformation is increased beyond this range. Again, the analysis is based on a distribution of values for the anisotropy parameter, which reflects these nonlinear elastic properties. We note from Fig. 6.19, that the location of peak circumferential stress moves closer to the endocardium and that stresses are increased in both the subendocardial region and the outer half of the ventricular wall.

As left ventricular volume increases the effects of nonlinear elastic

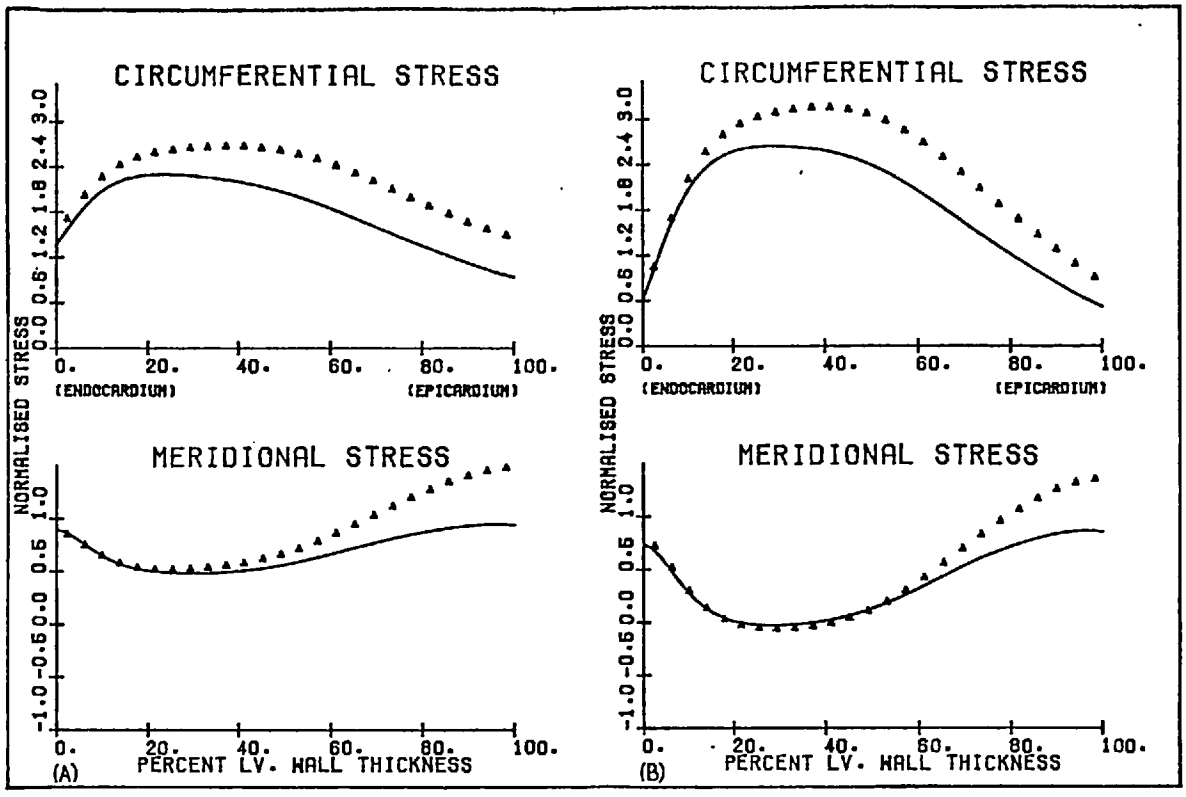

FIGURE 6.18: EFFECT OF NONHOMOGENEITY ON THE STRESS DISTRIBUTION AT THE EQUATOR; ANISOTROPIC ELASTIC PROPERTIES, VARIABLE FIBRE ORIENTATION
— HOMOGENOUS CASE, ▲ NONHOMOGENOUS CASE
(A) $\beta = 2$, (B) $\beta = 5$

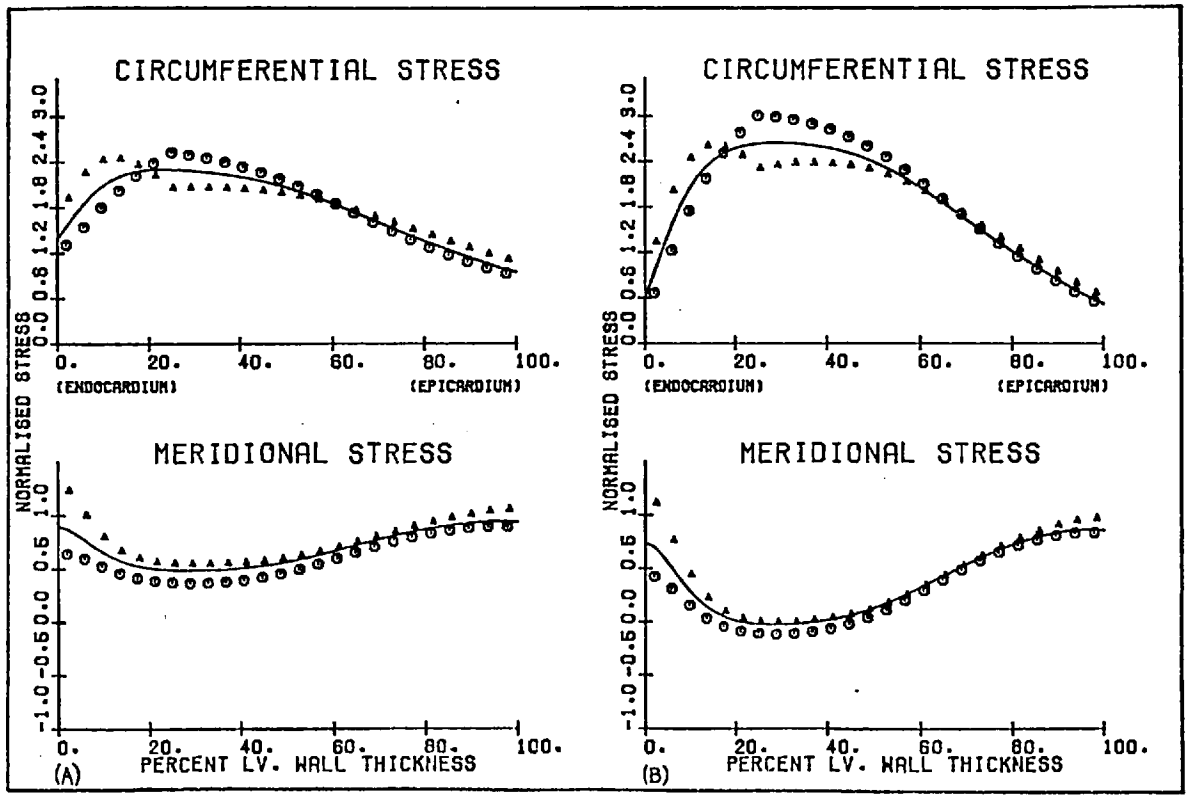

FIGURE 6.19: EFFECT OF NONLINEARITY ON STRESS DISTRIBUTION AT THE EQUATOR; ANISOTROPIC ELASTIC PROPERTIES, VARIABLE FIBRE ORIENTATION
— LINEAR CASE, ▲ "ACTIVE" AND ⊙ "PASSIVE" CASES
(A) $\beta = 2$, (B) $\beta = 5$

properties become more pronounced. From the results presented, it may be inferred that during diastole the distribution of circumferential stress in the dilated left ventricle is increasingly concentrated in the region between the endocardium and midwall. Similarly, it seems likely that for the isovolumic phase of systole, at least, ventricular enlargement is associated with the intensification of stresses in both the subendocardial and subepicardial regions.

INCOMPRESSIBILITY

We determine the equatorial stress distribution as the condition of incompressibility is approached, using two different paths.

These are :

$$\lim_{\delta \to 0} \begin{cases} 1 - 2\nu' = \delta \\ 1 - \nu - \nu'/\beta = \delta \end{cases}$$

and

$$\lim_{\delta \to 0} \begin{cases} 1 - 2\nu' = \delta \\ 1 - \nu - \nu'/\beta = 0 \end{cases}$$

The incompressibility parameter is defined as $2/\delta$

It can be seen from the results in Fig. 6.20 that the peak and mean values of circumferential and meridional stress are independent of the limiting path and also independent of the degree of incompressibility for values of $0.45 \leq \nu' < 0.5$ Therefore, it follows that the methods used to evaluate the elastic moduli here are quite adequate. Further, the extrusion of blood from the myocardium during systole would appear to have an insignificant effect on the stress distribution.

APICAL STRESS DISTRIBUTION

We have shown that the equilibrium equation for the apex can be satisfied only if the elastic properties at this point are isotropic, or transversally isotropic, with respect to the radial direction. At the apex a confocal prolate spheroid approaches spherical symmetry very closely and in Fig. 6.21, the apical stress distribution is compared with the stress distribution for a thick walled sphere. Isotropic elastic properties are assumed; the internal radius of curvature and wall thickness are the same in both cases. For a confocal prolate spheroid, however, the radius of curvature at the apex is not a linear function of the radial co-ordinate and thus we would expect circumferential stress here to be marginally greater than the circumferential stress supported by a sphere. From Fig. 6.21 it can be seen that this is so.

The peak and mean values of circumferential stress at the apex are less than those obtained by Mirsky (1969), but again this reflects the difference in the geometrical models used. In the present study, however, we are unable to include either the circumferential orientation of fibres at the apex, or the apical dimple, which this causes. It seems likely, therefore, that the circumferential stress at the apex is significantly underestimated in this analysis.

GENERAL STRESS DISTRIBUTION

Finally, we consider the transmural stress distribution for different meridional co-ordinates between the apex and equator. Two cases are analysed here: isotropic elastic properties and variable anisotropic elastic properties.

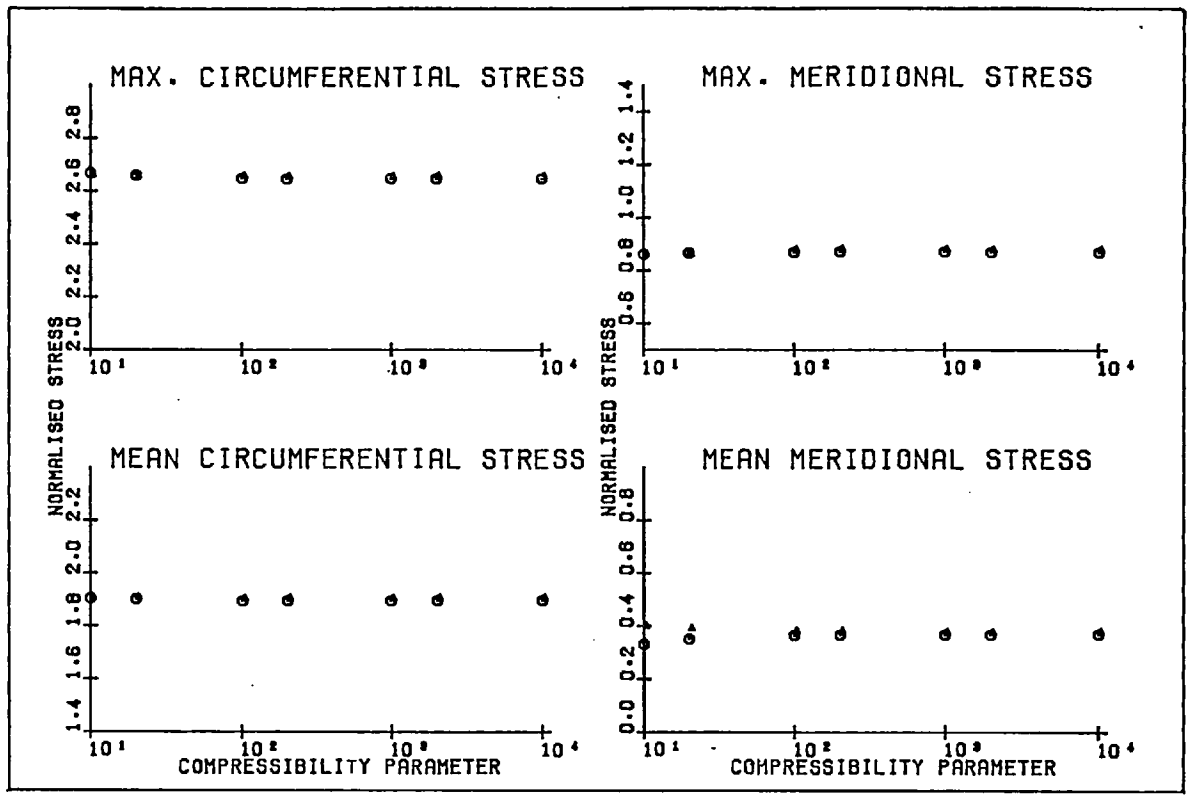

FIGURE 6.20: VARIATION OF STRESSES AT THE EQUATOR WITH INCREASING COMPRESSIBILITY PARAMETER $2/\delta$; ANISOTROPIC ELASTIC PROPERTIES $\beta = 5$, VARIABLE FIBRE ORIENTATION
▲ LIMIT PATH 1, ⊙ LIMIT PATH 2

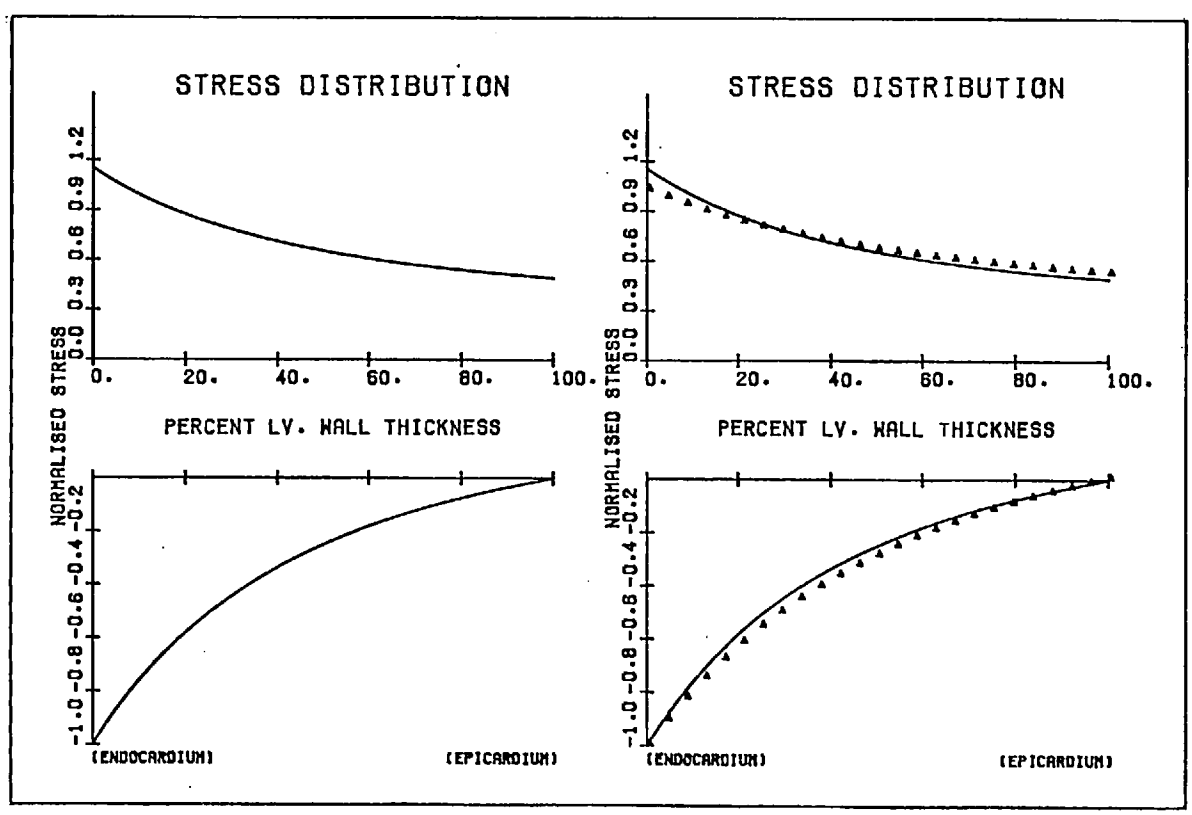

FIGURE 6.21: STRESS DISTRIBUTION AT THE APEX; ISOTROPIC ELASTIC PROPERTIES
▲ STRESS DISTRIBUTION FOR SPHERICAL SHELL WITH IDENTICAL WALL THICKNESS AND INTERNAL RADIUS OF CURVATURE

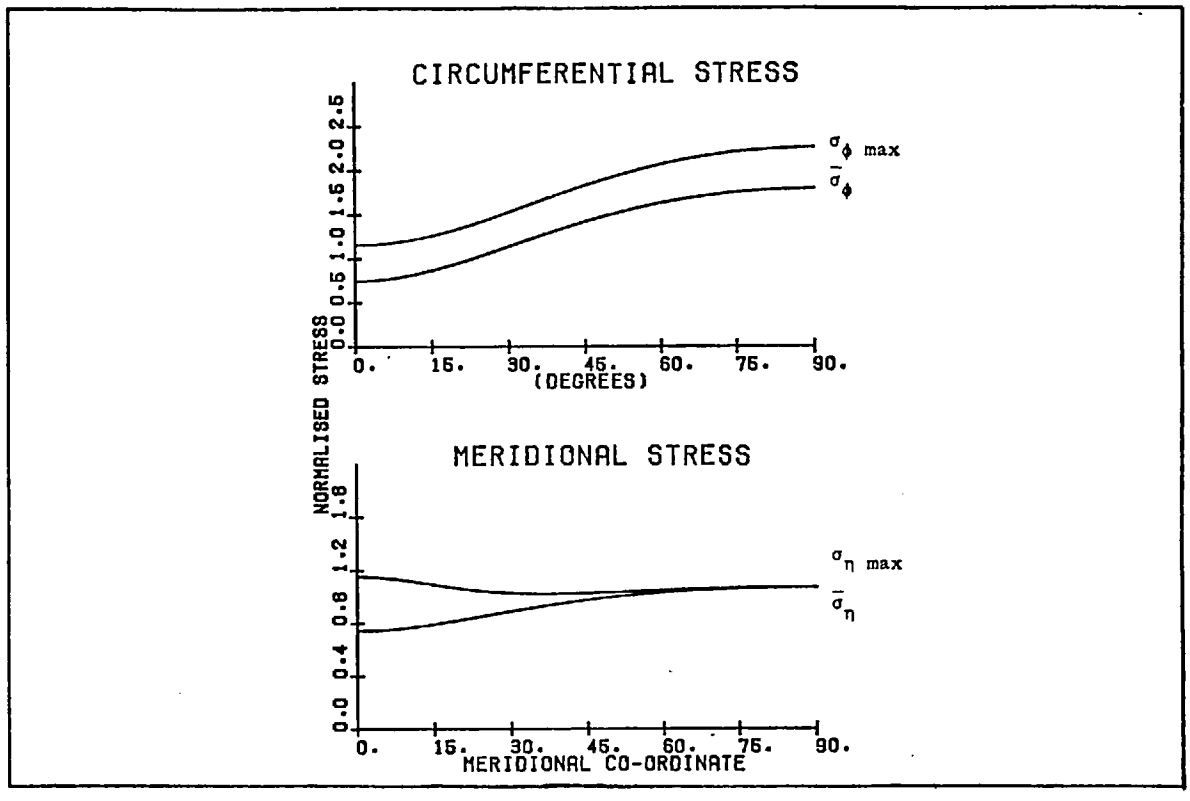

FIGURE 6.22: VARIATION OF CIRCUMFERENTIAL AND MERIDIONAL STRESSES WITH THE MERIDIONAL CO-ORDINATE η; ISOTROPIC ELASTIC PROPERTIES

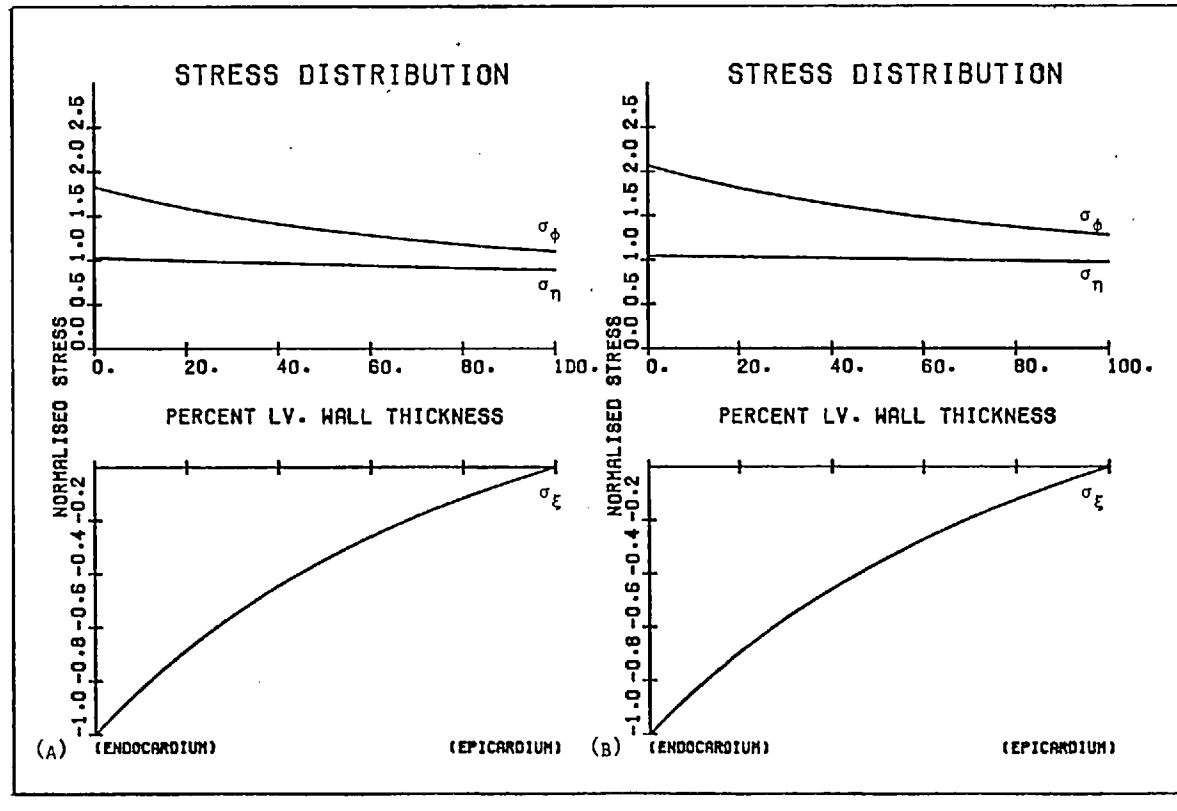

FIGURE 6.23: STRESS DISTRIBUTION AT DIFFERENT MERIDIONAL LOCATIONS; ISOTROPIC ELASTIC PROPERTIES
(A) $\eta = 30°$, (B) $\eta = 45°$

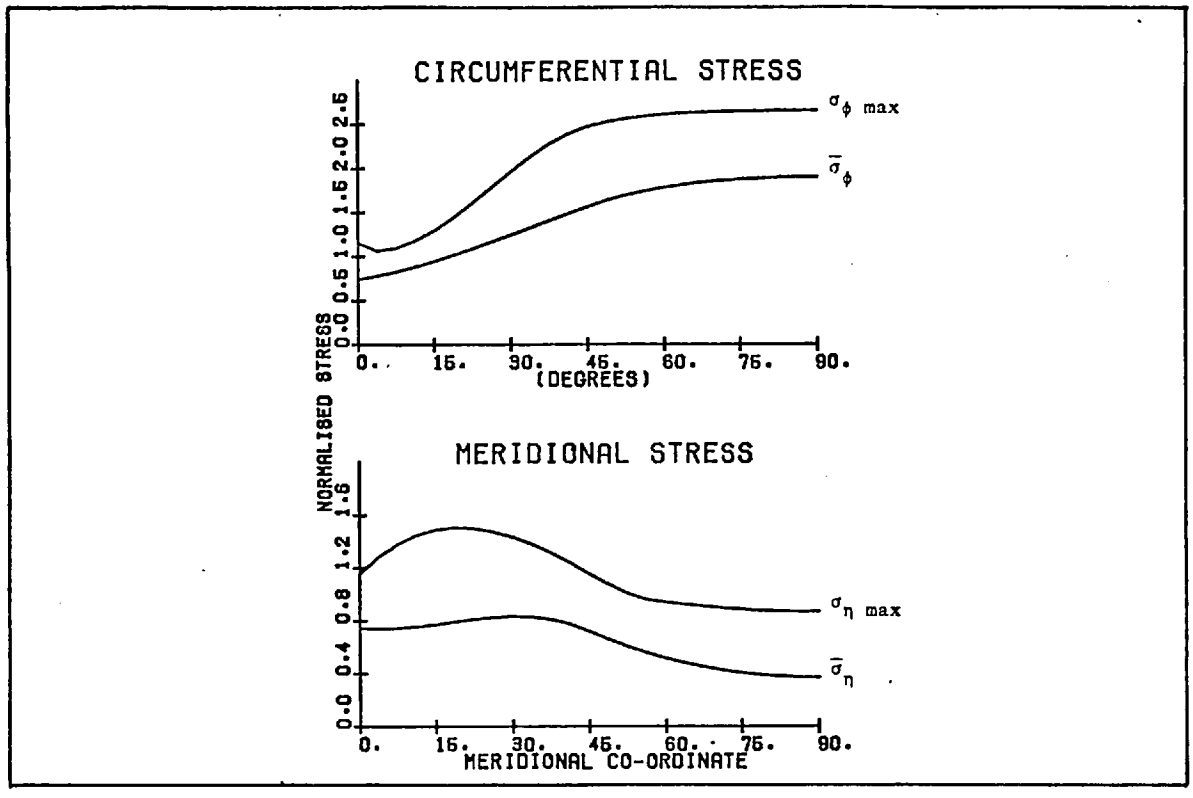

FIGURE 6.24: VARIATION OF CIRCUMFERENTIAL AND MERIDIONAL STRESSES WITH MERIDIONAL CO-ORDINATE η; ANISOTROPIC ELASTIC PROPERTIES, VARIABLE FIBRE ORIENTATION

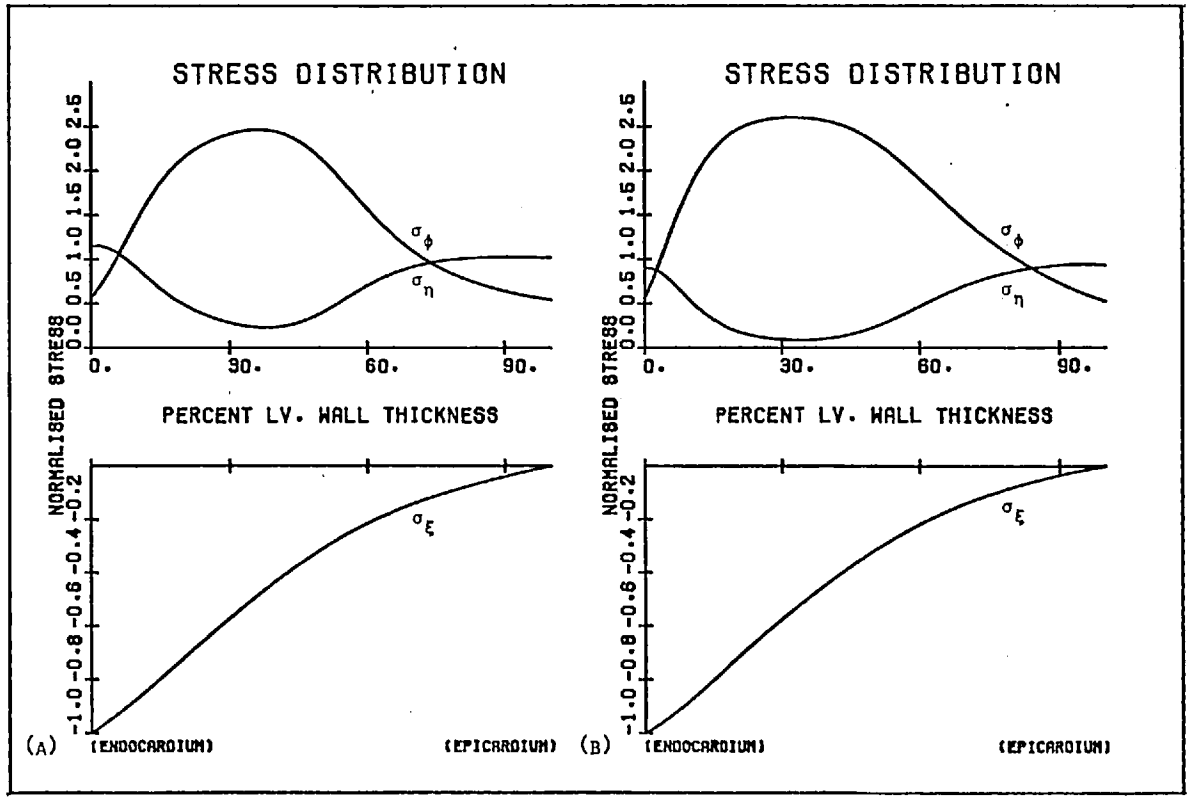

FIGURE 6.25: STRESS DISTRIBUTION AT DIFFERENT MERIDIONAL LOCATIONS; ANISOTROPIC ELASTIC PROPERTIES, VARIABLE FIBRE ORIENTATION
(A) $\eta = 30°$, (B) $\eta = 45°$

The results for the isotropic case are presented in Figs. 6.22 and 6.23 and the distribution of circumferential and meridional stresses, as a function of the meridional co-ordinate η , closely resembles the result obtained by Mirsky (1969). Evidently the assumption that displacement occurs in the radial direction only introduces very little error here.

For the anisotropic case we assume that the anisotropy parameter varies continuously with the meridional co-ordinate from $\beta = 5$ at the equator, to $\beta = 1$ at the apex. In Fig. 6.24 we present peak and mean values of circumferential and meridional stress as functions of the meridional co-ordinate. Differences between these results and those for the isotropic case are largely due to the variation in the fibre angle distribution with meridional co-ordinate; see Fig. 6.6. From our previous discussion it is clear that the results for the apical region must be treated with some skepticism. However, it appears that the transmural stress distribution at the equator accurately reflects the stresses acting over a large proportion of the ventricular wall and this a most interesting result.

6.7 DISCUSSION

The aim of the work described in this chapter was to set up a realistic model for the analysis of left ventricular stress. Development of such a model was seen as an important step towards understanding the factors which determine the balance of oxygen supply and demand at points within the myocardium.

The present study is based on two theoretical innovations. We used a description for the elastic properties of the ventricular myocardium, which includes the anisotropy and variable orientation of cardiac muscle fibres; the fundamental equations of elasticity were developed with respect to a confocal prolate spheroid co-ordinate system. It has been stated that the confocal prolate spheroid representation gives reasonably accurate descriptions of left ventricular geometry over a wide range of loading conditions and thus the present analysis can be applied in a general sense. Further, using the confocal prolate spheroid co-ordinate system, it was possible to reduce the complexity of the stress equilibrium equations and obtain solutions for the stress distribution at meridional co-ordinates between the apex and equator.

We now summarize the relative importance of different features included in this model. The variation of fibre orientation across the ventricular wall was found to be the most important determinant of the left ventricular transmural stress distribution. Obviously, the variation of fibre angles would not be significant if the fibres did not also have anisotropic elastic properties; however, for values of the anisotropy parameter $\beta > 4$ the nature of the stress distribution was not much altered by increases in the magnitude of anisotropy. The influence of nonhomogenous and nonlinear elastic properties was also considered. It was shown that if the nonhomogeneity of the myocardium is not taken into account peak and mean values of circumferential stress could be significantly underestimated. The results also suggest that for large values of deformation the left ventricular stress distribution is increasingly influenced by nonlinear elastic properties; two separate cases must be distinguished here

and these correspond to the active and passive states of isolated cardiac muscle. Finally, it was found that the mean values of the circumferential and axial stress acting over a large proportion of the ventricular wall can be accurately predicted using the Laplace approximation for a thin walled ellipsoid shell with midwall dimensions.

At present, direct experimental results for the distribution of stresses in the left ventricle are scarce and unreliable. This reflects the fact that most techniques for measuring intramyocardial stress significantly alter the stress distribution itself. In assessing the accuracy of the present analysis we are, therefore, forced to rely on indirect evidence. Such evidence includes the observed deformation of the left ventricle under pressure loading, the experimental measurement of mean stresses and the distribution of axial strain, determined from muscle sarcomere lengths at sites across the ventricular wall. Janz and Grimm (1973) have shown that the gross deformation of the left ventricle is accurately predicted using nonlinear isotropic elasticity theory. It is unlikely that deformation behavior will provide any additional information as to the accuracy of a model, which also includes anisotropic elastic properties and variable fibre orientation. We do, however, obtain excellent predictions for both mean circumferential stress and the detailed distribution of axial strain.

From these results it is possible to draw some simple conclusions about the balance of oxygen supply and demand at different points within the myocardium. We assume that the utilisation of oxygen by the left ventricle is related to the forces developed during systole. Apparently, therefore, requirements for oxygen vary considerably across the ventricular wall, with demand most pronounced in the

regions between the subendocardium and the midwall. We have shown that the mean values of the axial and circumferential stress acting over a large proportion of the ventricular wall are identical and can be predicted using a thin shell approximation. This suggests that the use of the Laplace estimate for mean circumferential stress as an index of total myocardial oxygen consumption has a firm theoretical basis.

Coronary blood vessels penetrate the ventricular wall radially and are therefore acted upon by circumferential and meridional components of stress. The extent to which these stresses impede the distribution of coronary flow, during diastole, is not immediately obvious from this analysis. In the normal state the magnitude of the forces involved is small and thus the influence on coronary supply is probably marginal. For the dilated ventricle, however, the increased concentration of stresses between the subendocardial and midwall regions may effect the supply of blood to the subendocardium. Further, we have shown that for the enlarged left ventricle the stress distribution during systole is changed, with a greater proportion of the force being developed fibres in the subendocardium, potentially the worst supplied region. Clearly, these mechanisms could be significant in the failing heart.

Subject to the assumptions and approximations made, three facts stand out from the present study:

- the mean values of stress for the left ventricular wall do not adequately reflect the transmural distribution of stresses; by implication, therefore, the balance of oxygen supply and demand for the left ventricle as a whole probably does not reflect the regional balance of myocardial oxygen supply and demand

- if this is so, the most critical region for supply and demand balance is located near the subendocardium
- the balance of myocardial oxygen supply and demand in this region is made worse by dilation of the left ventricle.

7. CONCLUSIONS

7.1 SUMMARY OF THE RESEARCH

7.2 DISCUSSION

7.3 PROPOSALS FOR FUTURE RESEARCH

7. CONCLUSIONS

7.1 SUMMARY OF THE RESEARCH

This thesis is concerned with the feasibility of applying multi-variate optimization theory to specific aspects of cardiac function. It was felt that such a systems approach might provide additional insight into the mechanisms which determine normal cardiovascular responses. Also, the concepts of optimization and "cost" were seen to be directly relevant to particular clinical problems.

The research which is described is divided into two parts:

- a systems analysis of quasi-static left ventricular function based on a digital simulation and experimental studies
- a theoretical analysis of the distribution of left ventricular transmural stress

We will consider the relationship of these different areas of study and their wider significance in the final sections of this chapter.

The left ventricle was characterized as a multi-variate pump, the output of which is determined by four fundamental system parameters: end-diastolic volume, aortic input impedance, contractile state and heart rate; the generation of flow was treated as a primary system constraint.

Two steps were seen to be central to an optimal systems approach within this context. These were the identification of relevant indices of left ventricular function or "cost" and the quantitative description of these "cost" indices as

multi-variate functions of the system parameters. The present study essentially relates to these two problems.

A digital model was used to investigate the possible existence of optimal conditions for myocardial oxygen consumption and the balance of myocardial oxygen supply and demand. At a fixed level of cardiac output and mean arterial pressure the values of myocardial oxygen consumption, predicted for different heart rates on the basis of two simple estimates, exhibited a shallow minimum at a low heart rate. The location of this minimum was found to shift to a higher heart rate when cardiac output was increased or mean arterial pressure was lowered. It was shown that these results reflected the interaction of increased stroke volume at low heart rates with the hydraulic load presented to the left ventricle; the results were, however, also strongly dependent on the empirical method used to estimate myocardial oxygen consumption.

Considerable effort was spent in an attempt to develop a general method both to obtain experimental "cost" surfaces for the left ventricle and to investigate the underlying factors which determine those surfaces. It was hoped that this approach might provide a basis for the analysis of left ventricular function in a wide range of normal and pathological conditions. Additionally, we wished to check the predictions of the simple digital model with respect to myocardial oxygen consumption and the balance of myocardial oxygen supply and demand.

The method applied may be useful in other biomedical applications. Physiological data is often determined by more than one variable and, in general, it is difficult to control these variables as strictly as would be possible in a technological system. In such cases, regression analysis can be used to find the

multi-variate relationship underlying the data and thus reduce the apparent variability of the results. There are well established statistical methods for assessing the significance of the relationships so determined. The efficient use of multi-variate regression analysis imposes some requirements on the way in which the system variables are sampled and this provides a rational basis for the specification of experimental design and the planning of experimental protocol.

In this study the approach was based on the bi-variate analysis of experimental data with respect to heart rate and mean arterial pressure, at different levels of contractile state and left ventricular output. Changes in contractile state were discriminated using left ventricular function curves and nonlinear regression surfaces were fitted to the experimental results, to establish their dependence on heart rate and mean arterial pressure.

Six experiments were analysed and "cost" surfaces were obtained for myocardial oxygen consumption, coronary venous flow, coronary reserve and hydraulic power transfer. For low heart rates myocardial oxygen consumption was found to vary nonlinearly with heart rate in a way which suggested the existence of a minimum. It was shown that the observed variation of myocardial oxygen consumption with heart rate and mean arterial pressure could be related to the nature of the aortic input impedance and to the physical constraints on left ventricular pumping capacity. The effect of changing contractile state was also considered. Unfortunately, low heart rates were obtained in only two experiments and thus the existence of an optimal heart rate was not considered to have been established absolutely. However, it was established that, under normal conditions, the balance of myocardial oxygen supply and demand is made worse by reducing mean arterial pressure or increasing heart rate.

An accurate description of the left ventricular stress distribution was seen to be an important step towards understanding the mechanisms which determine the regional balance of oxygen supply and demand within the myocardium. Our approach was based on linear elastic theory, but included two useful theoretical innovations. A description for the elastic properties of myocardium which takes into account the anisotropy and the variable orientation of cardiac muscle fibres was proposed. Also, the fundamental equations of elasticity were developed for a confocal prolate spheroid co-ordinate system. The use of this co-ordinate system allowed the analysis to be applied in a very general sense, since the left ventricle can be accurately described as a truncated confocal prolate spheroid shell for a wide range of deformations. Solutions for the left ventricular stress distribution were obtained for the equator, the apex and for the meridional co-ordinates between those limits. The influence of geometrical variation on the stress distribution was considered, as were the relative importance of nonhomogeneity, nonlinearity and variations of anisotropy.

It was found that the mean value for the stress acting in the direction of the muscle fibres could be estimated with reasonable accuracy using the Laplace approximation for a thin walled ellipsoid shell with dimensions based on the midwall co-ordinates. However, the distribution of stresses was shown to be strongly influenced by the structural properties of the myocardium, with peak circumferential and fibre stresses concentrated between the subendocardium and the midwall. The results also suggest that in dilation the left ventricular stress distribution is increasingly influenced by the nonlinear elastic properties of cardiac muscle. From these results it was inferred that the balance of myocardial oxygen supply

and demand for the left ventricle as a whole does not adequately reflect the regional balance at points within the myocardium.

7.2 DISCUSSION

Perhaps the most striking feature of the experimental results is the apparent existence of a heart rate for which myocardial oxygen consumption is minimized. We have argued that the observed variation of myocardial oxygen consumption with heart rate and mean arterial pressure reflects the nature of the aortic input impedance and the physical constraints on left ventricular pumping capacity.

In exercise left ventricular output is increased and peripheral resistance is reduced. Normally, requirements for increased flow are met by a raised heart rate and a slightly enlarged stroke volume. It follows from our analysis of myocardial oxygen consumption in relation to ventricular pumping capacity that an increase in left ventricular output will lead to a more pronounced nonlinear variation of myocardial oxygen consumption with heart rate. Also, we have shown that under conditions of reduced peripheral loading, the dependence of hydraulic power transfer efficiency on heart rate is increased. Thus, it can be inferred that the normal exercise response is consistent with the optimization of myocardial oxygen consumption and the efficiency of hydraulic power transfer in the face of changed loading conditions.

These predictions are in apparent agreement with the results of the simple optimal model, but the correspondence is misleading. For the digital

simulation stroke volume was assumed to be a linear function of end-diastolic volume only. In reality, ventricular pumping capacity is a complex function of pressure and volume loading and we have emphasized that this may be an important determinant of the experimental variation of myocardial oxygen consumption with heart rate. Thus, at most, the results of the simulation give some insight into the relative efficiency with which the circulatory load is matched to the left ventricle under different physiological conditions. For this reason no attempt was made to relate the experimental findings and the results of the digital simulation in any formal sense.

Our analysis of the experimental results also suggests that it may be possible to find values of heart rate and mean arterial pressure for which the efficiency of myocardial energy utilisation is maximized. The efficiency of myocardial energy utilisation is defined as the ratio of steady output power to myocardial oxygen consumption. It has been shown that the possible existence of nontrivial optimal conditions here is due entirely to the nonlinear dependence of ventricular pumping capacity on pressure and volume loading. But left ventricular pumping capacity is determined by the contractile state of the myocardium. Thus, inotropic level must also influence the possible optimization of left ventricular performance.

We have obviously simplified the very complex mechanisms of left ventricular function in this discussion. For instance, the role of contractile state has not been considered in any detail. However, it appears that optimal criteria involving the minimization of energy "costs" do influence the control of the cardiovascular system under normal conditions.

Consider now the pathology of acute myocardial infarction and associated left ventricular failure. When a coronary blood vessel is suddenly occluded the area of the myocardium perfused by it becomes ischaemic and normal myocardial function in this region is compromised. If coronary supply is not restored irreversible cell damage - myocardial infarction, will occur.

The process of left ventricular failure is progressive; impaired myocardial function leads to reduced cardiac output and a drop in mean arterial pressure. In general, the right ventricle is marginally effected by the infarction and it continues to function normally. However, the "Frank-Starling" mechanism no longer balances the outputs of the right and left hearts, blood pools in the pulmonary circuit and the elevated filling pressure causes the left ventricle to dilate. These conditions contribute further to the imbalance of oxygen supply and demand in the region of the infarction. Thus the area of myocardial ischaemia and impaired myocardial function spreads steadily.

It is now accepted that if steps are taken to reduce myocardial oxygen demand and increase coronary supply, it may be possible to limit and perhaps reverse the progression from myocardial ischaemia to tissue damage and death. The primary aims of clinical management are therefore to restore the balance of myocardial oxygen supply and demand in the ischaemic region, while maintaining or improving cardiac output.

In an earlier chapter we stated that there are values of heart rate and mean arterial pressure for which the balance of myocardial oxygen supply and

demand is maximized. Again, the possible existence of nontrivial optimal conditions was seen to reflect the physical constraints on ventricular pumping capacity.

The composite supply and demand plots presented in this thesis do not accurately represent the variation of possible coronary supply and myocardial oxygen demand under all conditions. Further, we have shown that the balance of oxygen supply and demand for the left ventricle as a whole does not reflect the balance at points within the myocardium and this is especially true for the failing left ventricle. Despite these qualifications the experimental supply and demand surfaces provide some insight into the possible goals of clinical intervention. They suggest that the balance of myocardial oxygen supply and demand will be improved if mean arterial pressure is increased and heart rate is reduced. For the failing heart, however, any attempt to increase mean arterial pressure without also augmenting left ventricular function will, in general, lead to a reduction in stroke volume and greater ventricular dilation. Similarly, a reduced heart rate may lead to a reduced cardiac output and once again to further ventricular distension. The administration of a positive inotropic agent will augment myocardial function, but in excess may lead to increased oxygen demand and a higher heart rate.

It is obvious that, even within the constraints of what is clinically possible, conditions for the optimal management of left ventricular failure exist. However, these conditions cannot be directly related to normal cardiac function and probably differ from patient to patient. Given the complex interactions which must be taken into consideration it seems unlikely that a

truly optimal clinical treatment can be based on the empirical approach at present used. The multi-variate techniques developed in this thesis have been shown to provide a practical basis for the analysis of normal cardiac function. We contend that the extension of these methods could lead to a rational and quantitative approach to the problem of optimal management of the failing heart.

7.3 PROPOSALS FOR FUTURE RESEARCH

It is suggested that experimental work should be continued along the lines described, both to confirm results already obtained and to determine left ventricular "cost" surfaces for a wider range of normal conditions. Ideally, a comprehensive set of different levels of cardiac output and contractile state would be considered.

Before this is done, however, some features of the experimental preparation should be improved. A more reliable method to lower the intrinsic heart rate must be found. One possibility here is the surgical induction of complete heart block followed by coupled atrial and ventricular pacing. An experimental technique should also be developed to increase the level of mean arterial pressure without changing the physiological character of the aortic input impedance. The determination of oxygen content was time consuming and despite careful analysis and the duplicate checking of results, more subject to error than any other experimental measurement. Addition of a system for continuously monitoring arterial and coronary venous oxygen partial pressures would probably improve measurement and sampling accuracy.

From our previous discussion it is clear that regression surfaces for coronary reserve and myocardial oxygen consumption obtained under normal conditions cannot be directly related to the failing heart. It is proposed that the experimental approach outlined in this thesis should be extended to include this specific pathological state. The parallel development of a computer model to simulate the function of the failing left ventricle is also seen to be extremely

useful. This would be utilized both in the interpretation of experimental results and to predict the effects of possible clinical interventions on the balance of myocardial oxygen supply and demand. Obviously, such a pathological model would need to be considerably more sophisticated than the simulation presented in this study (though, arguably, not to the extent of including cardiac muscle mechanics). Both the impairment of myocardial efficiency associated with infarction and the interaction of right and left ventricular function are extremely important within this context and their effects must be included. The minimum requirement therefore is probably an unconstrained closed loop simulation of the cardiovascular system which accurately reflects the influence of ventricular dimension, hydraulic input impedance, contractile state and heart rate on cardiac function, coronary supply and myocardial oxygen consumption.

For the failing dilated left ventricle, the stress analysis presented in this thesis suggests that the balance of myocardial oxygen supply and demand is most critical for the subendocardial region. It seems important therefore to extend the analysis and to consider the factors which determine the supply of blood to this region. Ideally, one should attempt to define an index of subendocardial supply and demand as a function of external haemodynamic and mechanical parameters.

APPENDICES

A. INSTRUMENTATION

To perform the experiments described in this thesis it was necessary to extend the instrumentation available. This involved some mechanical construction and the development of several simple electronic circuits. In this appendix we give details of the methods used to measure coronary venous flow and blood temperature.

A.1 THE MEASUREMENT OF CORONARY VENOUS FLOW

The development of a rapid and accurate method to determine coronary venous flow was an essential prerequisite of our experimental work. A simple and potentially very accurate approach to this problem is to use the method of timed collection; the time taken to fill a known volume. Typically, a single measurement cylinder is used and the time taken for a column of blood to pass between two spaced electrodes is determined electronically. This method has some disadvantages though. If the measurement column is filled from the top instability of the blood surface and the formation of froth may lead to spurious electrode contact and inaccurate timing. However, if the column is filled from the bottom the hydraulic load presented to the inflowing blood varies throughout the timing interval and this may influence the flow measurement.

A system which overcomes these problems was developed from a suggestion by R. Challis, Engineer, Department of Clinical Physiology, Guys Hospital. It is based on the equalisation of fluid columns in a U-tube and a

diagram is given in Fig. A.1. Coronary venous blood flows from the right ventricle to the top of the left hand column against a small fixed hydraulic head. If the outlet to the U-tube is not clamped the blood runs through it into the venous reservoir - see also Fig. 4.1. When the outlet is clamped blood rises equally in both columns, but surface instability and frothing are largely confined to the left hand side. An digital counter-timer is started and stopped as the right hand blood column makes contact with electrodes 2 and 3, respectively, and when the clamp is released the blood empties rapidly into the venous reservoir.

An adjustible mounting, developed from an Ontos universal vice and fixed to the operating table, was used for perpendicular alignment of the columns and to alter the hydrostatic head presented to coronary flow. To improve accuracy flow was integrated over several respiratory cycles and for the normal range of experimental coronary flows the timing interval was 20 - 30 seconds. It was possible to make at least one flow determination per minute and repeatibility was, in general, better than 1%.

An electronic circuit was developed to start and stop the counter-timer and a diagram is given in Fig. A.2. This device also produced a voltage step during the timing interval, which served as an event marker for the recording apparatus.

The Wein bridge oscillator A continuously excites terminals 2 and 3 at 5 KHz; this frequency was chosen to minimize electrode polarisation. The signals at these two points are rectified, smoothed and applied to the Schmidt triggers B and C. Normally, the impedance from earth to terminals 2 and 3, respectively, is high and the outputs of the Schmidt triggers are held in the

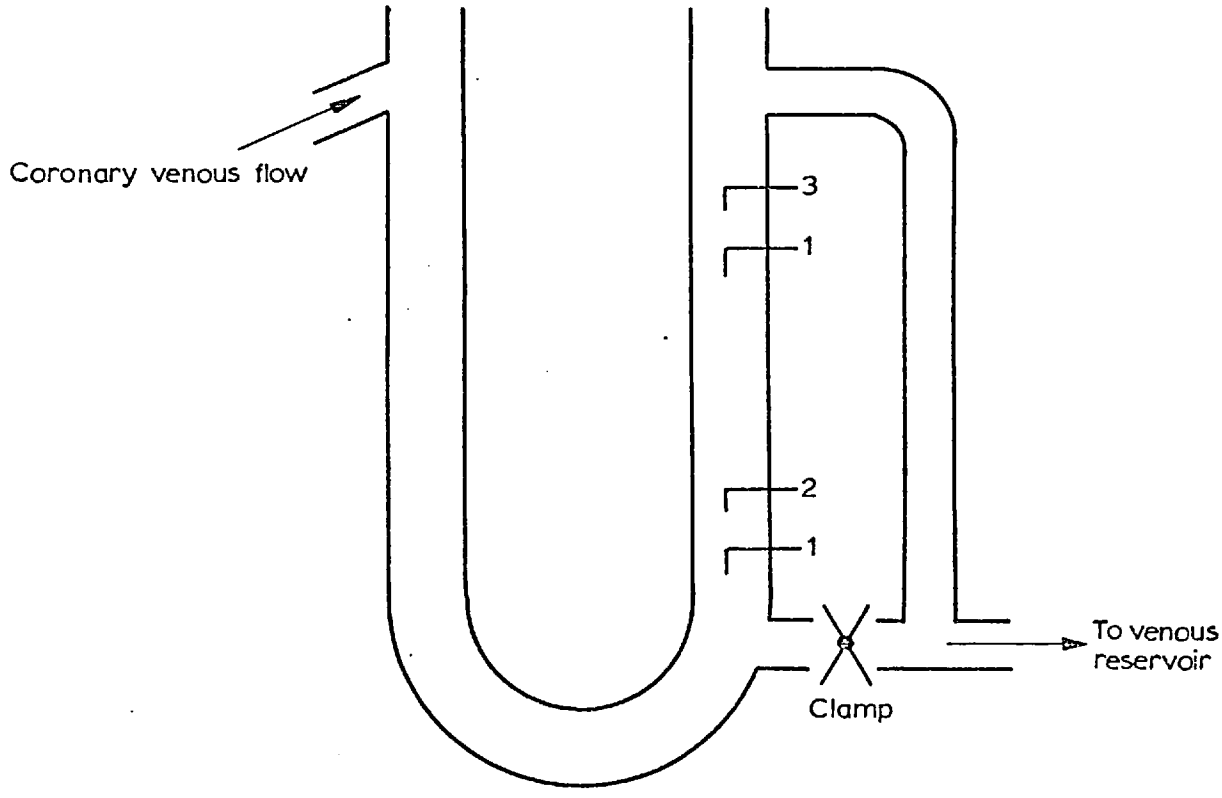

FIGURE A.1: Coronary flow timing cell.

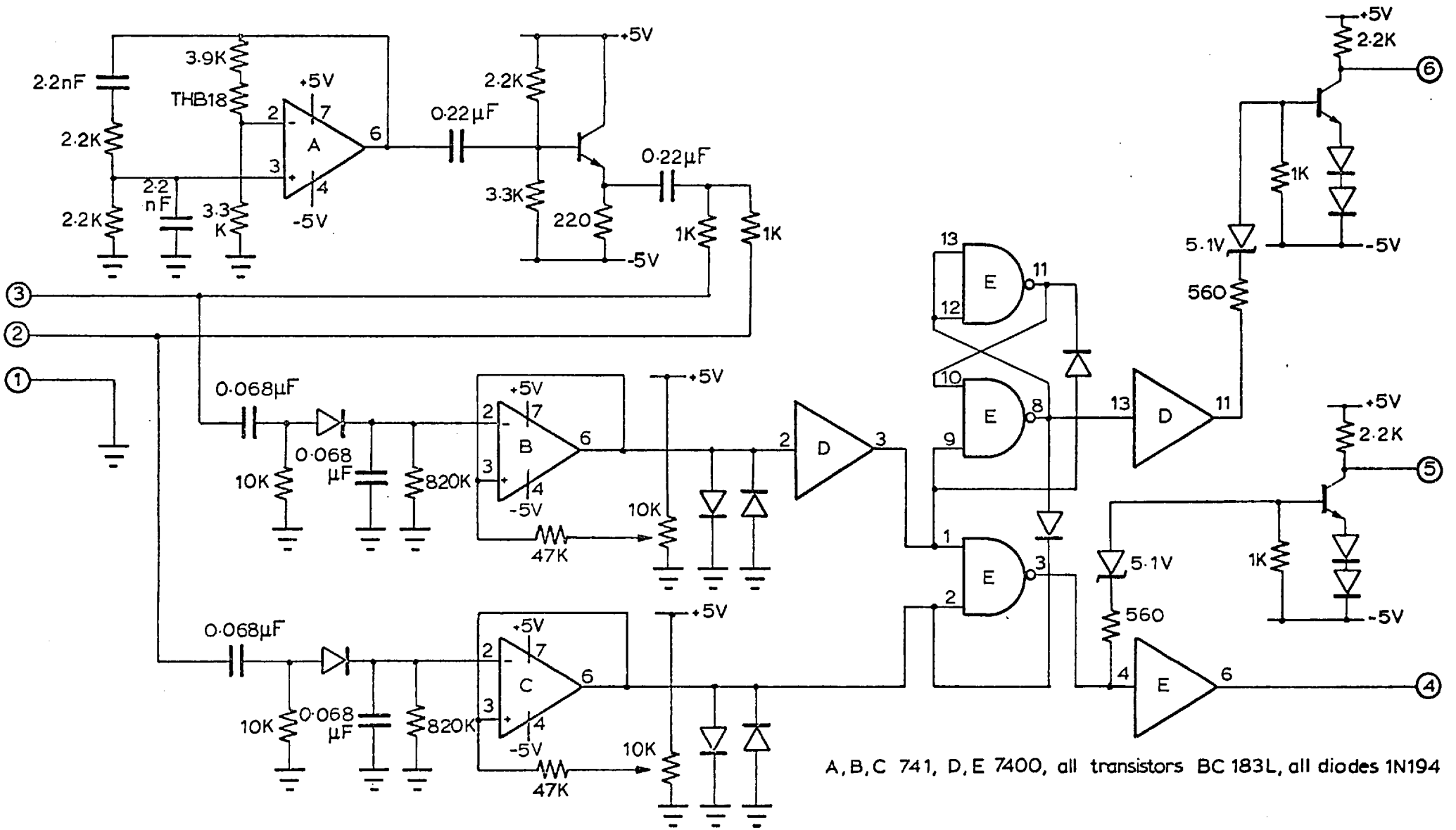

FIGURE A.2. Flow timing circuit

negative state. When the column of blood contacts electrode 2, however, a low impedance path to earth is provided at this point and the corresponding Schmidt trigger changes state producing a "start" pulse for the timer at terminal 5. Similarly, the timer is stopped by a pulse at terminal 6 when the blood column reaches electrode 3. The logic elements E and D generate a voltage step at terminal 4 during the timing interval and the bistable configuration ensures that this terminal remains in the negative state when the measuring columns are drained. Threshold and detection levels for the Schmidt triggers are adjusted to give some discrimination against interference and spurious electrode contact. The output transistors for terminals 5 and 6 transform the timing pulses to the voltage range compatible with the Venner TSA 3436 digital counter-timer.

A.2 THE MEASUREMENT OF BLOOD TEMPERATURE

Blood temperature was monitored with a Devices thermistor probe and it was necessary to develop and construct a calibrated amplifier in order to use this transducer. Typical instrumentation specifications applied here for a low drift DC. amplifier with linearity better than 1% of FSD. It was intended that this device should interface directly with the recording appuratus and this imposed some additional constraints. For both off-line data analysis and on-line use of the temperature chart record, preset voltage levels were required for calibration purposes. Further, it was decided that the span and DC. offset should be adjustible so that the calibrated output range could be matched to the

desired chart record spacing.

The circuit design is based on a bridge amplifier - see Fig. A. 3. The bridge must be supplied by a stabilized voltage source and diodes are included as an additional safety factor to limit voltage. Since the impedance of the thermistor was low, it was possible to use the simple differential configuration A without compromising the drift requirements. The DC. level at the output can be altered by adjusting potentiometer R_4; the centre-tap to earth here attenuates the effect of supply voltage fluctuation. Output gain can be adjusted using potentiometer R_5 and the DC. level is independent of gain variation. For the three way switch represented in Fig. A. 3 position 1 connects the thermistor to the input of the bridge, while switch positions 3 and 2 give the calibration levels for 30^{o} C and 40^{o} C, respectively.

A description of the calibration process follows. Initially, switch position 3 is chosen and the output of amplifier A is nulled using R_3. The switch is then reset at position 1, with the thermistor immersed in a water bath at a constant temperature of 30^{o}C and the output voltage for amplifier A is once more set to zero, this time by adjusting the precision potentiometer R_2. We increase the temperature of the water bath to 40^{o}C and note the output voltage at A. Switch position 2 is then set and the precision potentiometer R_1 adjusted until the output voltage at A exactly matches the reference setting.

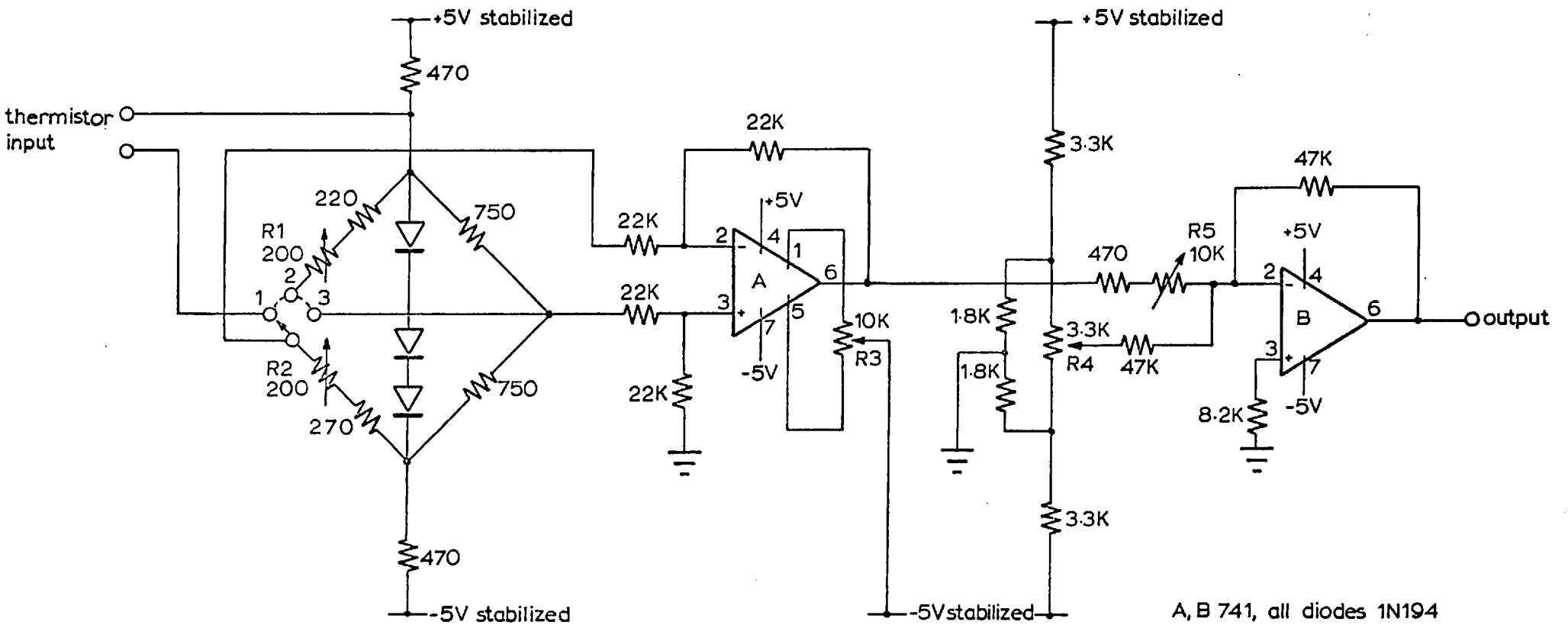

FIGURE A.3: Temperature measurement circuit.

B. COMPUTER PROGRAMS

In this appendix we describe some aspects of the programs used to analyse the experimental data. Large amounts of data were obtained for a series of different experiments and it was essential that these programs should be organized into a comprehensive and flexible processing scheme. Existing programs were used wherever possible, but it was necessary to write a number of special purpose programs and subroutines. This formed a significant proportion of the work done for this project.

B.1 DATA PROCESSING PROCEDURE

The important steps in the processing scheme have been outlined in Chapter 4. and are represented schematically in Fig. 4.2. First, specific sections of the analogue record were digitized and stored on magnetic tape. Reduction of the experimental data was performed in three stages: the location of characteristic points within the cardiac cycle, evaluation of indices of cardiac function for successive heart beats, the calculation of simple confidence limits for these indices. In general, this reduction sequence was repeated many times for a given experimental record. The results were then stored, sorted into related groups and subjected to nonlinear bi-variate regression analysis.

Processing was necessarily sequential. In addition, considerable emphasis was placed on the visual checking of results at critical stages of the analysis. Within these constraints programs were organized for maximum flexibility and

the system of program control by high level data words; Stagg (1970), was extensively used. The aim here was to perform the most comprehensive range of functions possible in any single processing run; this approach was particularly useful in the analysis of long sections of magnetic tape.

These considerations determine the program organization represented in Fig. B. 1. For digitization, editing and preprocessing, in which facilities for A-D interfacing, interactive programming and visual display were required, the IBM computer in the Engineering in Medicine Laboratory was used. All other processing was carried out on the CDC 6400 and Cyber computers in the Imperial College Computer Centre. The computer generated plots presented in this thesis were obtained using a Kingmatic flat-bed drafting machine and a Calcomp microfilm plotter.

B. 2 MAIN PROGRAMS

Extensive use was made of routines contributed by other members of the laboratory. ADC is a general purpose analogue to digital conversion program. It was used here to convert six channel analogue data into multiplexed integer words of 11 bit precision and these were written on magnetic tape in blocks of 1200 words. In addition, a number of general purpose subroutines were used. With the exception of ADC, however, all main programs were specially written and Fortran was used exclusively as the programming language. We now give some details of the data analysis programs; a brief description of the programs used for graphical presentation of the results is also included.

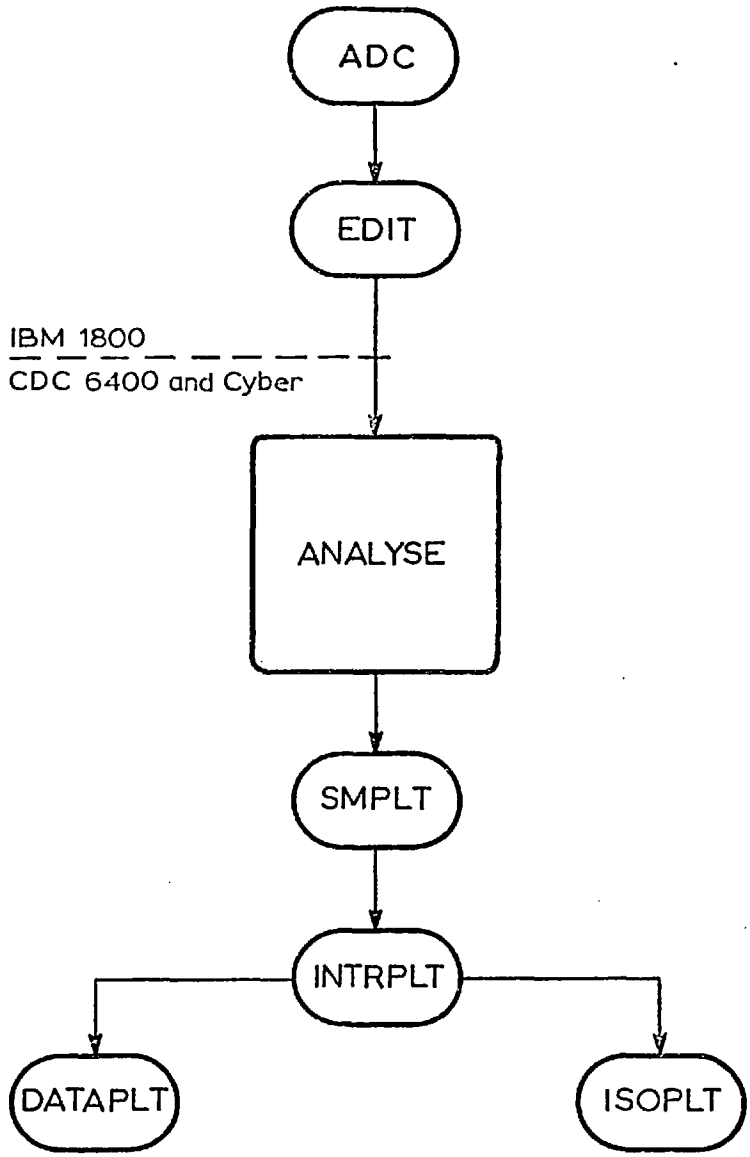

FIG.B.1: Program sequence for data processing.

EDIT; was used to edit and preprocess the experimental data stored on magnetic tape.

The program is controlled by a system of process interrupts. Options include: rapid scanning oscilloscope display of any two channels, print out of the magnitude, first derivative and location of any point displayed and preliminary processing of the digital record. This last option is used to generate data which controls the main reduction program ANALYSE. For a specified length of the experimental record each cardiac cycle is characterized by identifying three points: left ventricular end-diastolic pressure, the onset of ejection and the finish of ejection. The left ventricular pressure, aortic flow and aortic pressure records are visually checked and the locations of the selected points can, if necessary, be corrected by the operator. Information specifying the tape positions of these characteristic points is stored as a file of punched binary cards.

The preprocessing sequence is an important step in the scheme of data analysis and we shall consider it in further detail. Seven blocks of data are read from magnetic tape, demultiplexed and scaled; left ventricular pressure, aortic flow and aortic pressure records are stored in separate arrays. First, the left ventricular pressure array is scanned to locate the onset of ventricular contraction for each cardiac cycle; a simple running difference algorithm is used here. Sections of the left ventricular record are displayed on the oscilloscope with the selected location of end-diastolic pressure brightened. The next stage of the program is then initiated.

For each cardiac cycle the onset and finish of ejection are identified from the aortic flow record or the aortic pressure record; simple difference algorithms are used here also. Sections of both records are simultaneously displayed with the selected points for the onset and finish of systole brightened. A single record of binary cards is punched and the sequence is repeated until the required section of the digital record has been preprocessed. An end of file card is then appended to the set of binary data cards.

In this way it was possible to rapidly preprocess and visually check each of the files of a typical digitized experimental record.

ANALYSE; was used to reduce the experimental data stored on magnetic tape.

The program is divided into three parts: initialisation, reduction and simple statistical analysis; processing is controlled by a multi-file input of data cards. A record of coded data words is appended to each of the files of binary cards produced by EDIT and during the initialisation stage, this record is read and decoded. The data words correspond to specific commands through which it is possible to set up processing options, to evaluate calibration factors, to enter data etc. Control is then transferred to the next part of the program.

Each file of binary cards contains preprocessed data relating to a specific section of the magnetic tape and this information is used to control the reduction sequence. The binary cards are read one record at a time. Seven blocks of multiplexed data corresponding to this record are read from magnetic tape, demultiplexed, calibrated and stored in six separate arrays. For each

cardiac cycle the left ventricular pressure, aortic flow and aortic pressure waveforms are reduced to a set of indices of left ventricular function and these results are successively added to separate storage arrays. The reduction process continues until an end of file card is read; control is then transferred to the final stage of the program.

The stored indices of left ventricular function are subjected to simple statistical analysis. For each, mean value, standard deviation and maximum deviation are tabulated and written on disk. Analysis of further sections of the digital record is determined by the files of "control" cards which follow.

In this way a great deal of flexibility was retained in processing of each section of the experimental record and yet it was possible to reduce a multi-file magnetic tape in a single run.

INTRPLT; was used for interpolation and regression analysis of irregularly spaced data points.

Processing is controlled by a record of coded data cards. Experimental values for specific indices of left ventricular function; ANALYSE, are read from disk and stored. The corresponding values for heart rate HR and mean arterial pressure MAP are also stored as independent variable pairs. Using the least squares criterion, a simple two dimensional polynomial is fitted to the data points; coefficients for the best fit polynomial and statistical indices for the regression surface are tabulated. Included in the latter are the interpolated values for the experimental data points and the adjusted values for the standard

error of estimate and the index of correlation. A 10 level contour plot is also produced using the line printer and grey scale routines.

This sequence was repeated for other stored indices of left ventricular function. It was possible to change the order of the fitted polynomial and to discard experimental results from the pool of data points in each case.

SMPLT; produced a two dimensional representation for the locations of experimental (HR, MAP) data pairs, using the line printer

ISOPLT; produced isometric plots of the three dimensional left ventricular function surfaces.

DATAPLT; was a general plotting routine for the presentation of the experimental results.

C. MULTIVARIATE REGRESSION ANALYSIS

Regression analysis is an attempt to establish the functional relationship between a dependent variable and one or more independent variables from a finite number of observations of those variables. In this appendix we consider the statistical basis for the indices of multi-variate regression which were used in the analysis of the experimental data. Much of what follows is drawn from Ezekial and Fox (1959).

Consider the set of N experimental observations $\{x_n, y_n, z_n\}$: z_n the dependent variable is subject to random errors of observation; x_n and y_n are the independent variables and are accurately determined. We assume that the functional relationship between these variables is described by the general polynomial

$$Z' = C_o + C_1 x + C_2 y + C_3 x^2 + C_4 xy + C_6 y^2 - - - \qquad C.1$$

For each data point the difference between the experimental and the estimated value of the dependent variable is given by

$$\begin{aligned} \Delta Z_n &= Z_n - Z_n' \\ &= Z - (C_o + C_1 x_n + C_2 y_n + C_3 x^2 + C_4 xy + C_5 y^2 - - -) \end{aligned} \qquad C.2$$

ΔZ_n is defined as the residual.

To obtain the best fit polynomial we must choose C_0, C_1, .. such that the total magnitude of the residual terms is minimized. The least squared error criterion is used here.

$$\frac{\delta}{\delta C_i}\left(\sum_{n=1}^{N} \Delta Z_n^2\right) = 0 \qquad i = 0, 1, 2, 3, 4, 5, - - - \qquad \text{C.3}$$

Substituting C.1 and C.2 into C.3, we have:

$$\begin{aligned}
&NC_o + \sum_{n=1}^{N} x_n C_1 + \sum_{n=1}^{N} y_n C_2 + \sum_{n=1}^{N} x_n^2 C_3 + \sum_{n=1}^{N} x_n y_n C_4 + \sum_{n=1}^{N} y_n^2 C_5 \; - - - \; = \sum_{n=1}^{N} z_n \\
&\qquad\qquad\qquad\qquad\qquad\qquad\qquad\qquad\qquad\qquad\qquad\qquad\qquad\qquad\qquad\qquad\qquad\qquad \text{C.4} \\
&\sum_{n=1}^{N} y_n^2 C_o + \sum_{n=1}^{N} x_n y_n^2 C_1 + \sum_{n=1}^{N} y_n^3 C_2 + \sum_{n=1}^{N} x_n^2 y_n^2 C_3 + \sum_{n=1}^{N} x_n y_n^3 C_4 + \sum_{n=1}^{N} y_n^4 C_5 \; - - - \; = \sum_{n=1}^{N} z_n y_n^2
\end{aligned}$$

This set of equations can now be solved for C_0, C_1, .. etc. Z' is a bi-variate regression surface and C_0, C_1, .. are defined as regression co-efficients.

The polynomial function was used as an example here for convenience only. This approach is completely general and can be applied to any well defined function. Clearly, therefore, it is essential to find measures of the accuracy with which the assumed function reflects the underlying relationship between the experimental observations. Two statistical indices are commonly used for this purpose: S the standard error of estimate and R the index of correlation.

The standard error of estimate is defined as

$$S^2 = \frac{1}{N}\sum_{n=1}^{N} \Delta Z_n^2 \qquad \text{C.5}$$

Consider the standard deviation for the residuals

$$S^2_{\Delta Z} = \frac{1}{N}\sum_{n=1}^{N} (\overline{\Delta Z} - \Delta Z_n)^2 \qquad C.6$$

For a regression surface fitted by the least squared error criterion the mean value of the residuals is zero thus

$$\varsigma = S_{\Delta Z} \qquad C.7$$

Therefore, the standard error of estimate can be interpreted in the same way as a standard deviation. It is, however, a standard deviation not about a mean value, but about a surface.

The index of correlation measures the relative closeness of the observed values of the dependent variable and the values estimated from the independent variables. It is defined by

$$R^2 = \frac{S^2_{z'}}{S^2_z} \qquad C.8$$

where S_z and $S_{z'}$ are the standard deviations for the observed and the estimated values of the dependent variable, respectively.

It can be shown that

$$S^2_{\Delta z} = S^2_z - S_{z'}$$

and thus

$$R^2 = 1 - \frac{\varsigma^2}{S^2_z} \qquad C.9$$

In most cases regression analysis is based on observations which conform to some predetermined scheme. We must consider the effect which non-random selection of the independent variables has on the standard error of estimate and

the index of correlation. Implicit in this approach is the assumption that the error of observation for the dependent variable is random and not affected by the choice of independent variables. If this is true the residuals will tend to be normally distributed and the standard error of estimate should not be influenced by the non-random selection of the independent variables. It can be seen from C. 9, though, that the index of correlation R is determined by the standard error of estimate S and the standard deviation S_Z . While the non-random selection of the independent variables does not alter the standard error of estimate, it does, in general, change the distribution of the dependent variable and thus its standard deviation. It can be seen that any selection of the independent variables which increases the standard deviation S_Z will also increase R and vice verse. The index of correlation therefore has absolute significance only if the independent variables are randomly selected. For non-random selection it is possible to attach conditional significance to the index of correlation where the distribution of the dependent variable is approximately normal or where regression surfaces based on identical values for the independent variables are compared.

The standard error of estimate calculated for a small sample is, on average, smaller than that which would be obtained from a larger sample. Under these conditions the index of correlation is, in general, overestimated. Similarly, if we increase the order of the surface which is fitted to a limited set of experimental observations, the number of independent samples is effectively reduced and the surface will tend to follow the random fluctuations of the dependent variable. Although the standard error of estimate will be decreased here and

the index of correlation will be increased, this apparent improvement in accuracy is clearly not significant.

An expression for the unbiassed value of the standard error of estimate is given below

$$\bar{S}^2 = \frac{NS^2}{N-M} \qquad C.10$$

where N is the number of observations and M is the number of co-efficients in the regression equation. $\bar{S}$ is the adjusted standard error of estimate. Similarly, the adjusted index of correlation is given by

$$\bar{R}^2 = 1 - (1 - R^2)\left(\frac{N-1}{N-M}\right) \qquad C.11$$

This approach is based on the assumption that errors occur with equal probability for all observations of the dependent variable. Random errors of observation tend to lower the index of correlation and to increase the standard error of estimate. However, if the uncertainty is associated with dependent variable only and there are enough observations to balance out the errors, the regression surface should not be influenced.

Thus the methods of regression analysis provide a powerful quantitative basis for investigating the underlying relationship reflected by multi-variate experimental data.

REFERENCES

Beneken, J. E. W. (1965)
A mathematical approach to cardiovascular function
Ph. D. Thesis, Utrecht

Bergel, D. H. and Gessner, U. (1966)
The electromagnetic flowmeter
Methods in Medical Research, Vol. 11, 70

Boerth, R. C., Covell, J. W., Pool, P. E., Ross, J. (1969)
Increased myocardial oxygen consumption with increased heart rate in dogs
Circulation Research, Vol. 24, 725

Borst, C. (1972)
Optimal control of left ventricular function in angina pectoris
D. I. C. Dissertation, Imperial College, London

Braunwald, E. and Maroko P. R. (1974)
Protection of the ischemic myocardium
in The Myocardium: Failure and Infarction, edited by E. Braunwald
H. P. Publishing Co., New York

Burton, A. C. (1957)
The importance of the shape and size of the heart
American Heart Journal, Vol. 54, 801

Burton, A. C. (1972)
Physiology and Biophysics of the Circulation
Year Book Medical Publishers, Chicago

Cheung, D. C. W., Chamberlain, J. H., Seed, R. C. F. L. (1974)
Effect of haemodynamic changes on maximum blood flow acceleration in the anaesthetised open chest dog
Cardiovascular Research, Vol. 8, 362

Chou, P. C. and Pagano, N. J. (1967)
Elasticity: Tensor, Dyadic and Engineering Approaches
Van Nostrand, Princeton, New Jersey

Dieudonné, J. (1969)
The left ventricle as confocal prolate spheroids
Bulletin of Mathematical Biophysics, Vol. 31, 433

Elzinga, G. and Westerhof, N. (1973)
Pressure and flow generated by the left ventricle against different impedances
Circulation Research, Vol. 32, 178

Ezekial, M. and Fox, K.A. (1959)
Methods of Correlation and Regression Analysis Linear and Curvilinear
John Wiley and Sons, New York

Folkow, B. and Neil, E. (1971)
Circulation
Oxford University Press, London

Fusako, K., Butts, W.C., Ruff, W.L. (1973)
Superior analytical performance by electrolytic cell analysis of blood oxygen content
Journal of Applied Physiology, Vol. 35, 299

Gabe, I.T. (1972)
Pressure measurement in experimental physiology
in Cardiovascular Fluid Dynamics, edited by D.H. Bergel
Academic Press, London

Gessner, U. (1972)
Vascular input impedance
in Cardiovascular Fluid Dynamics, edited by D.H. Bergel
Academic Press, London

Ghista, D.N. and Sandler, H. (1969)
An analytical elastic-viscoelastic model for the shape and the forces in the left ventricle
Journal of Biomechanics, Vol. 2, 35

Goodman, A.H. (1966)
Electronic dynamic calibration of electromagnetic flowmeters
Journal of Applied Physiology, Vol. 21, 933

Graham, T.P., Covell, J.W., Sonnenblick, E.H., Ross, J., Braunwald, E. (1968)
Control of myocardial oxygen consumption: Relative influence of contractile state and tension development
Journal of Clinical Investigation, Vol. 47, 375

Grossman, W., Brooks, H., Meister, S., Sherman, H., Dexter, L. (1971)
New technique for determing instantaneous myocardial force-velocity relations in the intact heart
Circulation Research, Vol. 28, 290

Herndon, C.W. and Sagawa, K. (1969)
Combined effects of aortic and right atrial pressure on aortic flow
American Journal of Physiology, Vol. 217, 65

Hill, A.V. (1911)
The position occupied by the production of heat, in the chain of process constituting a muscular contraction
Journal of Physiology, Vol. 42, 1

Janz, R.F. and Grimm, A.F. (1973)
Deformation of the diastolic left ventricle
I. Nonlinear elastic effects
Biophysical Journal, Vol. 13, 689

Lekhnitskii, S.G. (1963)
Theory of Elasticity of an Anisotropic Elastic Body
Holden Day, San Fransisco

Levy, M.N., Iano, T., Zieske, H. (1972)
Effects of repetitive bursts of vagal activity on heart rate
Circulation Research, Vol. 30, 186

Mills, C.J. (1972)
Measurement of pulsatile flow and flow velocity
in Cardiovascular Fluid Dynamics, edited by D.H. Bergel
Academic Press, London

Mirsky, I. (1969)
Left ventricular stresses in the intact human heart
Biophysical Journal, Vol. 9, 189

Mirsky, I. (1970)
Effects of anistropy and nonhomogeneity on left ventricular stresses in the intact heart
Bulletin of Mathematical Biophysics, Vol. 32, 197

Mirsky, I. (1973)
Ventricular and arterial wall stresses based on large deformation analysis
Biophysical Journal, Vol. 13, 1141

Moir, T.W. (1972)
Subendocardial distrubution of coronary blood flow and the effect of antianginal drugs
Circulation Research, Vol. 30, 621

McDonald, R.H., Taylor, R.R., Cingolani, H.E. (1966)
Measurement of myocardial developed tension and its relation to oxygen consumption
American Journal of Physiology, Vol. 211, 667

McHale, P.A. and Greenfield, J.C. (1973)
Evaluation of several geometric models for estimation of left ventricular circumferential wall stress
Circulation Research, Vol. 33, 303

Noble, I.M., Trenchard, D., Guz, A. (1966)
Left ventricular ejection in conscious dogs
I. Measurement and significance of the maximum acceleration of blood from the left ventricle
Circulation Research, Vol. 19, 139

O'Rourke, M.F. and Taylor, M.G. (1967)
Input impedance of the systemic circulation
Circulation Research, Vol. 20, 365

O'Rourke, M.F. (1970)
Arterial hemodynamics in hypertension
Circulation Research, Vol. 27, 11-123

Rodbard, S.R., Williams, C.B., Rodbard, D., Berglund, E. (1964)
Myocardial tension and oxygen uptake
Circulation Research, Vol. 14, 139

Sagawa, K. (1967)
Analysis of the ventricular pumping capacity as a function of input and output pressure loads
in Physical Bases of Circulatory Transport: Regulation and Exchange, edited by E.B. Reeve and A.C. Guyton
W.B. Saunders Co., Philadelphia

Sarnoff, S.J., Braunwald, E., Welsh, E.H., Stainsbury, W.N, Case, W.B., Macruz, E. (1958)
Hemodynamic determinants of the oxygen consumption of the heart with special reference to the tension-time index
American Journal of Physiology, Vol. 192, 148

Sarnoff, S.J., Brockman, S.K., Gilmore, J.P., Linden, R.J., Mitchell, J.H. (1960)
Regulation of ventricular contraction: Influence of cardiac sympathetic and vagal nerve stimulation an atrial and ventricular dynamics
Circulation Research, Vol. 8, 1108

Scher, A.M. and Young, A.C. (1963)
Servoanalysis of carotid sinus reflex effects on peripheral resistance
Circulation Research, Vol. 12, 152

Skelton, C.L. and Sonnenblick, E.H. (1974)
Myocardial energetics
in Cardiac Mechanics: Physiological, Clinical and Mathematical Considerations, edited by I. Mirsky, D.N. Ghista, H. Sandler
John Wiley and Sons , New York.

Sonnenblick, E.H., Ross, J., Cavell, J.W., Kaiser, G.A., Braunwald, E. (1965)
Velocity of contraction as a determinant of myocardial oxygen consumption
American Journal of Physiology, Vol. 209, 919

Sonnenblick, E.H., Ross, J., Braunwald, E. (1968)
Oxygen consumption of the heart: Newer concepts of its multifactoral determination
American Journal of Cardiology, Vol. 22, 328

Stagg, D.T. (1970)
The control of mammalian muscle spindles studied by analysis of neuroelectric signals
Ph.D. Thesis, London

Streeter, D.D. and Bassett, D. (1966)
An engineering analysis of myocardial fibre orientation in pig's left ventricle in systole
Anatomical Record, Vol. 145, 503

Streeter, D.D., Henry, S.M., Spotnitz, H.M., Patel, D.J., Ross, J., Sonnenblick, E.H. (1969)
Fibre orientation in the canine left ventricle during diastole and systole
Circulation Research, Vol. 24, 339

Streeter, D.D., Vaishnav, R.N., Patel, D.J., Spotnitz, H.M., Ross, J., Sonnenblick, E.H. (1970)
Stress distribution in the canine left ventricle during diastole and systole
Biophysical Journal, Vol. 10, 345

Streeter, D.D. and Hanna, W.T. (1973)[1]
Engineering mechanics for successive states in canine left ventricular myocardium
I. Cavity and wall geometry
Circulation Research, Vol. 33, 639

Streeter, D.D., and Hanna, W.T., (1973)[2]
Engineering mechanics for successive states in canine left ventricular myocardium
II. Fibre angle and sarcomere length
Circulation Research, Vol. 33, 656

Taylor, M.G. (1964)
Wave travel in arteries and the design of the cardiovascular system
in Pulsatile Blood Flow, edited by E.O. Attinger
McGraw Hill, New York

Topham, W.S. and Warner, H.R. (1967)
The control of cardiac output during exercise
in Physical Bases of Circulatory Transport: Regulation and Exchange,
edited by E.B. Reeve and A.C. Guyton
W.B. Saunders Co., Philadelphia

Van Slyke, D.D. and Neill, J.M. (1924)
Determination of gases in blood and other solutions
by vacuum extraction and manometric measurement
Journal of Biological Chemistry, Vol. 61, 523

Wong, A.Y.K. and Rautaharju, P.M. (1968)
Stress distribution within the left ventricular wall approximated as a
thick ellipsoid shell
American Heart Journal, Vol. 75, 649

Yoran, C., Covell, J.W., Ross, J. (1973)
Structural basis for the ascending limb of left ventricular function
Circulation Research, Vol. 32, 297